Probing the Intrinsic Ability of Particles to Generate Reactive Oxygen Species and the Effect of Physiologically Relevant Solutes

Part I: Results from Field Campaigns

FINAL REPORT

Contract No. 10-314

Prepared for:

California Air Resources Board

Prepared by:

Dr. S.E. Paulson, Dr. A. Hasson and Dr. C. Anastasio

Researchers:

UCLA: Michelle Xiaobi Kuang, J. Adlin Scott, David H. Gonzalez-Martinez, Tiffany Charbouillot

CSU Fresno: Kennedy K-T Vu, James Baroi, Catalina Olea, Annabelle Lolinco, Kylie Markarian

UCD: Jessica G. Charrier, Alexander S. McFall, Nicole K. Richards-Henderson

June 2016

Table of Contents

iii. List of Figures

3

5

6

7

8

9

iv. List of Tables

v. List of Abbreviations

1,2-NAPHQ   1,2-Naphthoquinone
1,4-NAPHQ   1,4-Naphthoquinone
1,4-CRYQ   1,4-Chrysenequinone
2,3-DMAQ   2,3-Dimethyl Anthraquinone
5,12-NAPHQ   5,12-Naphthacenequinone

B-7,12Q	Benzo[a]anthracene-7,12-dione
ACNAPQ	Acenaphthenequinone
Asc	Ascorbate
AQ	Anthraquinone
Atm	Atmosphere
BBHULIS	Biomass Burning Humic-Like Substances
CARB	California Air Resources Board
Cit	Citrate
CLMT	Claremont
DCF	Dichlorofluorescein
DCM	Dichloromethane
DTT	Dithiothreitol
Fe(II), Fe(III)	Iron 2+, iron 3+
FRE	Fresno
Fx	Filter Extract
GC–MS	Gas Chromatography – Mass Spectrometry
GSH	Glutathione
H_2O_2	Hydrogen Peroxide
Hi-Vol	High volume sampler (Tisch Inc.)
HO1	Heme oxygenase 1
HYSPLIT	Hybrid Single Particle Lagrangian Integrated Trajectory
ICP, ICP-MS	Inductively coupled plasma-mass spectrometry
NQN	Napthaquinone
OH	Hydroxyl Radical
OPAH	Oxygenated Polycyclic Aromatic Hydrocarbons
PAH	Polycyclic Aromatic Hydrocarbons
PCoA	Principal Component Analysis
PCR	Polymerase Chain Reaction
Pmol	picomoles
PPT	Parts per trillion
PQN	Phenanthraquinone
PTV	Programmed Temperature Vaporizing
PQ	Phenanthraquinone
PUF	Polyurethane Foam
ROS	Reactive Oxygen Species
SIM	Selective Ion Monitoring
SCAQMD	South Coast Air Quality Management District
SLF	Simulated (or Surrogate) Lung Fluid; a buffered solution @ pH 7.4 containing 200 μM each of ascorbate, glutathione, urate and citrate
SLFx	Surrogate Lung Fluid Extract
SoCAB	Southern California Air Basin
PM	Particulate Matter
UA	Uric Acid
VIF	Variance inflation factor

ii. Executive Summary

Determining the 'causative agent' in particles responsible for damaging health is the subject of increasing research activity, but many questions remain. Oxidative stress mediated by reactive oxygen species (ROS) is a leading hypothesis for the mechanism by which particulate pollution contributes to a range of illnesses, including asthma and cardiovascular mortality. ROS are generated in response to inhalation of particulate matter (PM), but the ability of the particles themselves to generate ROS may also be important. This work is aimed at understanding the components in particles responsible for ROS formation by the particles themselves under physiological conditions, the interplay between hydrogen peroxide (H_2O_2), hydroxyl radical ($\bullet OH$) and their relationship with another ROS assay, dithiothreitol consumption (DTT).

There is a growing body of literature that shows ambient particles can generate significant amounts of H_2O_2 and $\bullet OH$ and consume DTT when extracted in laboratory solutions. The most likely promoters for the formation of these reactive oxygen species (ROS) are transition metals, quinones, and possibly other unknown organics. To date, studies have focused on limited segments of the phenomenon, measuring single ROS (H_2O_2, $\bullet OH$, or oxidative potential of ROS formed [DTT assay]) and their relationship with transition metals or quinones, or other aspects of chemical composition. Here we combine measurements of most of these components, in two field campaigns and complementary laboratory studies.

We conducted one field campaign in summer at Claremont, an inland site in the South Coast Air Basin), aimed at capturing photochemical smog; and another in winter in Fresno, which has significant contributions from biomass burning. The field samples were subjected to a wide range of assays: dithiothreitol consumption, hydroxyl radical production, H_2O_2 production/consumption, speciated iron (Fe(II) and Fe(III)), total soluble metals by inductively coupled plasma mass spectrometry, and quinones and polycyclic aromatic hydrocarbons. Samples were collected on PTFE (Teflon®) filters and extracted in simulated lung fluid, a buffered solution containing salts and the antioxidants ascorbate, glutathione, and uric acid; with citric acid to mimic proteins that may chelate transition metals *in vivo*. The field studies were augmented by laboratory studies to investigate the contributions of transition metals and quinones to ROS formation.

All samples were extracted in a cell-free simulated lung fluid (SLF) containing the antioxidants ascorbic and uric acids and glutathione, as well as citric acid, and buffered at pH 7.4 and with an ionic strength to mimic lung lining fluid. Lab findings support past results that physiologically relevant concentrations of antioxidants present in lung lining fluid can have an enormous influence on the ability of redox-active species to generate ROS. In both the H_2O_2 and $\bullet OH$ assays, ascorbate (Asc) is the dominant reductant, acting as the source of electrons that are pushed from Asc onto the redox-active species (e.g., metal or quinone), which then shuttles the electron to dissolved O_2 to make ROS. Thus the presence of Asc in the assay greatly increases the production of $\bullet OH$ and H_2O_2 and is likely a better mimic for the chemical production of ROS *in vivo* than simpler solutions. For Cu (a major source of ROS), we also find that citrate (Cit) enhances ROS production, glutathione (GSH) greatly suppresses $\bullet OH$ and H_2O_2 production, and urate (UA) has no effect. For quinones, we find that the addition of Cit, GSH, and UA suppresses H_2O_2 generation compared to a solution containing only Asc. Given these results,

using a surrogate lung fluid (SLF) with these four antioxidants may be the most physiologically relevant way to estimate ROS production by the cell when exposed to PM.

Samples used for mass, •OH, H_2O_2, soluble speciated Fe, brown carbon and some transition metals were collected with a size cut-point of 4 μm (due to a flow control error), and others at 2.5 μm (quinones, DTT, some transition metals). The PM4 and PM2.5 sample sets are complete for Claremont, however for Fresno the PM4 set is complete but the PM2.5 set contains only 2/3 of the samples. Comparisons with several PM2.5 data sets (our own measurements as well as nearby SCAQMD and CARB stations) indicate the PM4 samples contain approximately a 30% contribution from coarse aerosols. Fresno exhibited much higher average PM4 mass concentrations (33 ± 15 μg/m^3) compared to Claremont (23 ± 5 μg/m^3), even though there were three rain events during the Fresno field campaign. Diurnal variations in average mass concentration were modest at both sites; day to day variations were larger, especially around the rain events in Fresno.

Average values for both •OH and H_2O_2 are relatively low compared to most comparable literature, although the literature is fairly small, and measurements were made under a variety of different conditions, so comparisons are difficult. Part of the lower activity is due to sample aging; however, some previous measurements were made on stored samples. DTT consumption levels, in contrast, are on the higher end of literature values. Normalized to mass, H_2O_2 production was much higher in the Fresno samples, while both •OH and DTT consumption were nearly identical in the Fresno and Claremont samples. A deeper look however suggests very different stories for the two sites.

•OH and DTT were very strongly correlated with mass, with R^2 values between 0.62 and 0.75 for •OH production and 0.79 and 0.88 for DTT consumption, for Fresno and Claremont samples respectively. In contrast, H_2O_2 was only weakly correlated with mass. Despite these very strong correlations, in perhaps two cases was mass significant in a multivariate regression, and in those cases mass provided only a modest enhancement to predictability. Single variable regressions also show strong correlations between some metals, including iron and copper, and biomass burning HULIS. In contrast, ROS was generally uncorrelated with quinones. While co-linearities are present, they are not overwhelming by standard statistical criteria.

One of the objectives of the study was to compare ROS assays with one another. We find that many of the same independent variables appear to drive •OH formation, DTT consumption and H_2O_2 concentration overall, but overall, these ROS are not strongly correlated to one another. The strongest correlations are between •OH radical formation and DTT consumption, with $R^2 = 0.48$ and 0.68 for Fresno and Claremont, respectively. Correlations of both DTT concentrations and •OH formation with H_2O_2 concentration are considerably weaker.

Fresno is well known to have significant contributions from biomass burning in winter; our samples contained high levels of absorbing carbon at night and into the morning, consistent with biomass burning, likely due largely to residential wood burning in the area. We measured optical absorption of material on our filters at 370 and 880 nm to obtain estimates of the quantity of brown and black carbon, respectively on the Fresno filters. While mass absorption

coefficients are available for similar samples collected at sites as impacted by biomass burning, including Fresno, quantification using optical absorption measurements is subject to substantial uncertainties. Additionally, because the filters were collected for chemical analysis, they had somewhat higher mass loadings than ideal for optical measurements and needed to be subjected to a filter loading correction. Resulting best estimates indicate that biomass burning particulate matter contributed 7.7, 4.3 and 8.4 $\mu g/m^3$, for morning, afternoon and overnight samples respectively.

Transition metals sufficiently soluble in SLF to pass through a 0.2 μm filter were measured by both UCD and UCLA by ICP-MS. Many of the ICP-MS elements were below detection limits, but reliable data were obtained for Cu, Fe, La, Mn, Ni, Pb and Se were obtained for both sites, and partial data for Cr and Co for the Claremont samples. Our soluble element concentrations fall within the range reported in the literature. Additional measurements were made of soluble iron by oxidation state (Fe(II) and Fe(tot), and Fe(III) by difference) using the chelator Ferrozine. The Ferrozine assay resulted in much lower concentrations than ICP-MS. In all cases, the Ferrozine assay results were much more strongly correlated to ROS activity than Fe measured by ICP. This supports the notion that solubility, binding, and/or chelation/complexing of transition metals in aerosols play significant roles in the resulting ROS activity.

Measurements of nine 2-4 ring quinones were measured in PM2.5 samples from the Fresno and Claremont sites by Gas Chromatography-Mass Spectrometry (GC-MS). To increase the sensitivity of the technique, the GC-MS was modified from the conventional inlet system to allow introduction of much larger sample volumes using a programmed temperature-vaporizing (PTV) inlet. Average daily quinone mass loadings were typically a few ng m^{-3} or less in Claremont, with 1,2-naphthoquione, 1,4-naphthoquinone, 1,4-chrysenequinone and benz[a]anthracene-7,12-dione as the major contributors. Despite being sparingly soluble in water, most of the quinones are typically extracted into the SLF. Over 50% of the quinones are found in the particle phase, and the more volatile quinones (1,2- and 1,4-naphthoquinone) are more prevalent in the gas phase. Back trajectory analysis using the HYSPLIT model is consistent with a strong source of quinones southwest of the sampling site (Long Beach). When samples are separated by time of collection (morning, afternoon, overnight), afternoon quinone mass loadings are most strongly associated with transport from this location, suggesting a photochemical source of these compounds. In Fresno, phenanthraquinone was the most prevalent compound observed in PM$_{2.5}$ samples. Samples with back trajectories originating in the Bay Area contained higher quinone mass loadings than other samples, and mass loadings in overnight samples were significantly lower than those collected during the morning and afternoon. These measurements are thus also consistent with photochemical production during transport from an industrial location. Correlations between quinones and ROS were weak or non-existent in all cases.

The large differences in chemical composition between the Claremont and Fresno samples produce different relationships. The Claremont samples have relationships that are qualitatively consistent with laboratory results. •OH formation by the Claremont samples is related to manganese and copper, followed by iron, selenium and vanadium; potentially selenium and vanadium are have indirect effects by either changing chelation of the redox active species Mn,

14

Cu and Fe (selenium) or possibly correlating with primary organic carbon which in turn also interacts with the redox active transition metals (vanadium). All five species together predict 87% of the •OH variability, and the first three 84%. Correlations with hydrogen peroxide are much weaker, however the best predictors are copper and manganese. For DTT, an adjusted R^2 of 0.91 is obtained from a multivariate regression on soluble iron measured with the Ferrozine assay, copper and manganese, in decreasing order. The correction for the soluble copper in the solution based on lab results increased the correlation strength markedly.

In contrast to Claremont, the mass of biomass burning HULIS was by far the dominant variable in all multivariate regressions for the Fresno samples. In several cases, it was the only variable with a significant correlation at the $p < 0.05$ level, although dependencies on the transition metals iron and copper (for the DTT assay, but only significant with 95% confidence if other variables are included) and iron (for the •OH assay, highly significant, especially iron (III)), were evident in some cases. Predictability was high, above 84% for both DTT and •OH for BBHULIS alone. As was the case for Claremont, Fresno H_2O_2 had much weaker relationships with independent variables in the dataset.

Aqueous processes involving solubility can be concentration-dependent, and investigations of DTT response to transition metals in laboratory solutions indicates this assay has a strong dependence on the aqueous copper and manganese concentrations. To test for this potential issue in the field samples, we investigated the dependence on mass of mass-normalized •OH, H_2O_2, DTT consumption, as well as soluble copper, iron and other transition metals for the field samples. In general, more mass is expected to produce more signal, thus for this analysis signals were first mass-normalized. Plotting the mass-normalized values against mass in the sample will reveal a mass-dependent trend if present. For mass-normalized •OH, H_2O_2, and transition metals, mass dependences were very slight or non-existent for 2-hour extraction times. After 24 hours of extraction, however, H_2O_2, •OH and almost all mass-normalized transition metals have a mass dependence. Most but not all have negative slopes, consistent with reductions in solubility or activity coefficients as the solutions become more concentrated.

In contrast to •OH and H_2O_2, mass-normalized DTT was strongly dependent on the mass of the sample. To correct for this bias, we developed a method using dissolved metals in SLF in the laboratory that enables producing robust mass-normalized DTT results. The bias results from the non-linear concentration-response curves from Cu and Mn in the DTT assay, and application of the correction method removes this dependence effectively. This previously unappreciated complication, which is important in samples where Cu and/or Mn make a significant contribution to the DTT response, may prevent meaningful comparisons of DTT results obtained at different PM concentrations.

In laboratory solutions, we find that Cu, PQN, 1,4-NQN, and 1,2-NQN can all generate significant amounts of •OH and H_2O_2, while Fe can generate •OH but not H_2O_2 (although H_2O_2 is likely a short-lived intermediate in the Fe-mediated production of •OH). The other 8 transition metals we tested (Mn, Co, V, Ni, Pb, Zn, Cd, and Cr) did not produce appreciable •OH or H_2O_2 in SLF. For DTT, the laboratory results suggest a similar set of actors, but with the addition of Mn. The addition of Fe to solutions containing Cu and/or quinones significantly suppresses H_2O_2

15

generation, and increases •OH generation, but not in the 1:1 ratio that would be expected from the Fenton reaction. We quantified concentration-response curves for H_2O_2 and •OH production from each of the metals and quinones, and in mixtures of these species. These concentration-response curves, combined with typical particulate concentrations of transition metals and quinones, suggest that Cu may dominate H_2O_2 generation from $PM_{2.5}$, while Cu, Fe, and synergistic interactions of these two metals dominate •OH generation. Using a previous set of source-oriented PM samples collected from Fresno, we find that we can predict the generation of •OH from PM extracts but not the production of H_2O_2. We suspect that this latter discrepancy is caused by organic species in the PM extracts, which might bind Fe and make it less able to destroy H_2O_2 compared to our laboratory solutions; similarly, these organics might also reduce the ability of Cu to generate H_2O_2 compared to laboratory solutions. These results for •OH formation, DTT consumption and H_2O_2 concentration are in good qualitative agreement with results from the field measurements.

The results indicate dominant roles for soluble copper, iron and manganese, and also biomass burning aerosol (where present) in the production of reactive oxygen species in simulated lung fluid.

I. Introduction

Recent epidemiological studies have shown a strong relationship between particulate pollution and adverse health outcomes, including increased mortality. Oxidative stress mediated by ROS is a leading hypothesis for the mechanism by which particulate pollution causes a range of illnesses, including asthma and increased cardiovascular mortality (Dellinger et al. 2001; Imlay 2003; Zhou et al. 2003). ROS are generated as a biological response to inhalation of particulate matter (Cho et al. 2005; Li et al. 2003), but the ability of the particles themselves to generate ROS may also be important. In *in vitro* studies, hydrogen peroxide and •OH radicals at levels well below those associated with ambient samples has been shown to damage lung epithelial cells (Brown et al. 2004; Holm et al. 1991; Li et al. 2002; Oosting et al. 1990). Additionally, an *in vivo* study (Morio et al. 2001) showed that two-hour exposures to hydrogen peroxide dissolved in ammonium sulfate particles produced symptoms associated with respiratory distress, while gas-phase peroxides or particles alone elicited on minimal responses. Morio et al. (2001) exposed animals to elevated PM and gas phase H_2O_2 in an effort to create an exposure environment with elevated particle-phase H_2O_2, but were not able to measure particulate peroxide concentrations. We duplicated the particle generation system used for the *in vivo* study in our laboratory (Paulson et al. 2009c) and found that because ambient particles generate H_2O_2, while ammonium sulfate particles do not (they simply follow gas-liquid partitioning, eqn. (2) below), the peroxide concentrations used in that study were well within the normal range for particulate peroxide levels in polluted areas. This indicates that short exposures (2 hours) to peroxide levels generated by ambient particles produces measurable changes in lung physiology related to inflammation and respiratory distress. The ROS mechanism work described here may have the synergistic benefit of helping to unravel the cause of particle-mediated damage to human health.

16

Recently, Bates et al. (2015) were able to shown the correlation between an ROS assay and health endpoints caused by inhalation of PM. Bates et al. (2015) found that DTT was correlated with Heme Oxygenase (HO-1), a biomarker for oxidative stress, and emergency department visits for asthma, wheeze and congestive heart failure (Bates et al. 2015a). However, many studies have quantified ROS formation by ambient particles using different methods including cellular bioassays and chemical assays, and showed important components of PM that are responsible for ROS production and corresponding cellular damage. Bioassays provide a direct cellular response by quantifying PM-induced ROS within cells. Different cells types have been studied. Several studies quantified ROS formation by PM in rat alveolar macrophage cells (Delfino et al. 2013; Heo et al. 2015; Landreman et al. 2008; Schafer et al. 2003) while Schafer et al. used endothelial cells from porcine aorta; all studies used dichlorofluorescein diacetate (DCFH-DA) as a fluorescent probe for ROS detection. Several studies reported various cellular damage induced by PM. Liang et al observed DNA damage in human hepatoma G2 cell, possibly induced by intracellular ROS formation by PM_{10}, detected by DCFH-DA, which increased 8-hydroxydeoxyguanosine formation (Jiang et al. 2010). Delfino et al. (2013) assessed the formation of ROS using both abiotic (DTT) and cellular method (DCFH-DA) and showed that Fractional Exhaled nitric oxide (FE_{NO}), a biomarker for airway inflammation, was correlated with both DTT and macrophage ROS. Li et al. (2003) also showed the that DTT was correlated with the PAH content in ultrafine particles and HO-1 expression (Li et al. 2003).

The 'ROS' family includes H_2O_2 and •OH, superoxide ($O_2^{.-}$) and the HO_2 radical. The complex web of reactions that governs concentrations of ROS is not well understood. A few, likely important reactions, many of which are highly pH sensitive, are as follows (Deguillaume et al. 2005):

$$Fe(II) + O_2 \rightarrow Fe(III) + O_2^{.-} \tag{R I.1}$$

$$Fe(II) + O_2^{.-} + 2H^+ \rightarrow Fe(III) + H_2O_2 \tag{R I.2}$$

$$Fe(II) + H_2O_2 \rightarrow Fe(III) + OH^- + OH^. \tag{R I.3}$$

$$Fe(II) + OH\cdot \rightarrow Fe(III) + OH^- \tag{R I.4}$$

$$O_2^{.-} + H^+ \rightarrow HO_2 \tag{R I.5}$$

$$HO_2 + HO_2 \rightarrow H_2O_2 + O_2 \tag{R I.6}$$

$$2O_2^{.-} + 2H_2O \rightarrow H_2O_2 + 2OH^- + O_2 \tag{R I.7}$$

$$HO_2\bullet + \tag{R I.8}$$
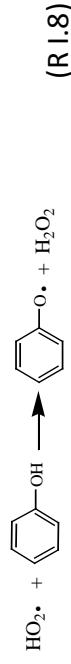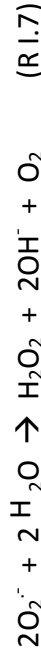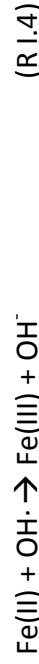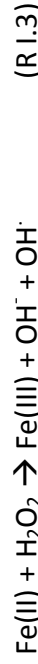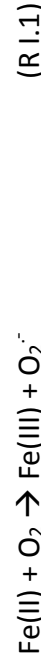
Analogous reactions to (R1-4) also occur for Cu(I) (Deguillaume et al. 2005). Phenolic compounds can enhance H_2O_2 generation from HO_2 (R8), by consuming only one HO_2 molecule per H_2O_2 produced (Faust and Allen 1992).

1.1 Atmospheric Chemistry of ROS: Hydrogen Peroxide.

Gas-phase hydroperoxides are formed in the atmosphere via gas-phase reactions of HO_2 with itself and with RO_2 (e.g., (Lightfoot et al. 1992)), and water reacting with the 'Criegee radical' product of alkene ozonolysis (Hasson et al. 2001a; Hasson et al. 2001b). Measurements of gas phase H_2O_2 concentrations have been made using about twenty different methods. Maximum H_2O_2 concentrations range from ppt levels up to a maximum of 10 ppb, with a strong dependence on NO_X, location, and season (Jackson and Hewitt 1999; Lee et al. 2000). Less common measurements of organic hydroperoxides, such as methyl-, hydroxymethyl-, and 1-hydroxyethyl hydroperoxide and peracetic acid in ambient air, indicate that organic hydroperoxides comprise 10% to 60% of the total gas phase hydroperoxide loading (e.g., (Fels and Junkermann 1993; Heikes et al. 1987; Hellpointner and Gäb 1989; Hewitt and Kok 1991)).

Hydroperoxides, as well as •OH and HO_2, are expected to partition between the gas-phase and liquid water according to Henry's law:

$$A_{(g)} \Leftrightarrow A_{(l)} \qquad \text{(R I.9)}; \qquad H_A \times P_A = [A] \qquad \text{(R I.10)}$$

where H_A is the Henry's law constant (M atm^{-1}), [A] is the liquid-phase concentration of A (M), and P_A is the gas-phase partial pressure of A (atm). H_A for H_2O_2 is 1.0×10^5 M atm^{-1} at 25 °C (Sander 1999). Our measurements at two sites in the Los Angeles (LA) area indicate average gas phase H_2O_2 concentrations of about 1.1 ppb, and an aerosol mass loading (PM10) of about 45 μg/m^3, of which ~45% should be water. Under these conditions, Henry's law predicts an aerosol hydrogen peroxide concentration of 0.04 ng/m^3, or 0.11 mM, in the aerosol liquid water (Arellanes et al. 2006).

To date, about a half-dozen studies have reported ROS measurements in fine and/or coarse mode aerosols. In the earliest study, Hewitt and Kok (Hewitt and Kok 1991), using the same H_2O_2 analysis method as the one employed here, briefly mention measurements of aerosol phase hydroperoxides, with H_2O_2 mass loadings of up to 10 ng m^{-3} at a rural Colorado site. More recent measurements indicate averages ranging from 2 to over 200 ng/m^3 (below). All of these measurements far exceed the values predicted by Henry's law. In a detailed study using simultaneous measurements of gas and aerosol phase H_2O_2 concentrations, our group found that the average factor by which the H_2O_2 associated with particles exceeded the expected value from Henry's law was about 700 (Arellanes et al. 2006). Our measurements were made by extracting the particles in aqueous solution (at pH 3.5) for 2 hours. More recent results indicate that the 2 hr extraction underestimates the total ability of particles to generate H_2O_2 by 5 - 70% depending on the aerosol; some particles stop generating H_2O_2 after an hour or so, while others continue to generate H_2O_2 for days (Arellanes 2008; Wang et al. 2010a). These results suggest that when particles are suspended in the atmosphere, they release H_2O_2 continuously, as gas-liquid equilibrium is rapidly established. The total mass of aerosol particles is too small for this to be a significant source of H_2O_2 to the gas phase.

More recent measurements, primarily in urban areas, have particles size-segregated into fine and coarse or more finely divided modes. Among all measurements there is a high degree of variability, so that it is difficult to be certain if one mode or another generates more H_2O_2. UCLA

measurements of H_2O_2 associated with fine mode particles at 4 sites in the LA area ranged from 5 ± 5 ng/m^3 to 12 ± 9 ng/m^3 (Arellanes et al. 2006; Hasson and Paulson 2003; Paulson et al. 2009b), similar to 10 ± 7 ng/m^3 in Taipei (Hung and Wang 2001). Vankatachari and co-workers found much higher concentrations in Rubidoux, CA (Venkatachari et al. 2005); 85 ng/m^3, but more similar values in Flushing, NY; about 16 ng/m^3 (Venkatachari et al. 2007). See et al. (See et al. 2007) also found high values in Singapore; 90 ± 40 ng/m^3. The Taipei, Rubidoux, Flushing and Singapore measurements (Hung and Wang 2001; See et al. 2007; Venkatachari et al. 2005; Venkatachari et al. 2007) used a dichlorofluorescein assay which is calibrated using H_2O_2, but which likely measures additional, unidentified oxidants.

Our measurements indicate that normalized to particle mass, H_2O_2 associated with fine particles around the LA area had similar averages, clustering around 0.5 ng/μg, somewhat higher than the value reported for Taipei (0.32 ng/μg (Hung and Wang 2001)). For coarse mode particles (PM > 2.5), we have found average concentrations ranging from 14 ± 10 to 33 ± 13 ng/m^3 (Arellanes et al. 2006; Hasson and Paulson 2003; Paulson et al. 2009b). Hung and Wang (Hung and Wang 2001) reported 1.15 ± 0.06 ng/m^3 associated with rather low mass concentrations of 3.2-10 μm particles in Taipei. Venkatachari et al. (Venkatachari et al. 2005; Venkatachari et al. 2007) reported H_2O_2-equivalent ROS concentrations of 40 ng/m^3 and 5 ng/m^3 in Rubidoux and Flushing, respectively. Normalized to particle mass, H_2O_2 associated with coarse mode particles was much more variable than were the fine mode particles, ranging from (0.36 ± 0.20 ng/μg) to (1.05 ± 0.30 ng/μg) in the LA area (Arellanes et al. 2006; Hasson and Paulson 2003; Paulson et al. 2009b) and 0.3 ± 0.1 ng/μg in Taipei (Hung and Wang 2001). For most of both the fine and coarse mode data sets we have collected, particle-associated H_2O_2 is not correlated with particle mass, indicating chemistry plays a dominant role.

Shen and co-workers (Shen et al. 2010) measured H_2O_2 generation by fine- and coarse-mode particles collected at Fresno. In the absence of ascorbate, Fresno particles extracted into PBS (pH 7.4) generated H_2O_2 levels that were similar to those described above for the South Coast PM (in the absence of ascorbate). But the addition of ascorbate enhanced H_2O_2 formation in the Fresno PM extracts by approximately 50 -fold. Parallel extractions including the chelator desferoxamine showed that transition metals were responsible for the bulk of H_2O_2 generation. Measurements of soluble transition metals in the PM extracts, combined with "calibration curves" of H_2O_2 generation as a function of Cu concentration, showed that Cu could explain nearly all of the H_2O_2 generation in the extracts with ascorbate.

1.2 •OH in Ambient Particles.
OH radicals are more reactive than other ROS, able to initiate oxidation of essentially all organics and many inorganic species at appreciable rates. As a result, they are short lived and their steady-state concentrations in condensed phases in the atmosphere are low (e.g., (Anastasio and McGregor 2001; Anastasio and Newberg 2007)). Like H_2O_2, they undoubtedly partition between the gas and condensed phases, but they are also generated by aerosols after inhalation (Charrier and Anastasio 2010; Jung et al. 2006b; Vidrio et al. 2008b; Vidrio et al. 2009). In sunlight they arise from a variety of sources, including nitrate photolysis (Anastasio and Newberg 2007) and metal redox chemistry (Vidrio et al. 2008b), and in some cases have been shown to be generated at rates similar to the estimated rate of uptake from the gas phase (Anastasio and Newberg 2007). Their primary source in the dark may be

breakdown of H_2O_2, catalyzed by transition metals such as iron ((Vidrio et al. 2008b); R3 above). *As far as we are aware, there are no published studies to date that consider the balance between H_2O_2 and •OH; this is a primary focus of the current project.*

1.3 Potential Sources of Reactive Oxygen Species in Ambient Particles. There are several possible promoters for the formation of the H_2O_2 that is generated by aerosol particles, two or possibly three of which have the potential to account for the high levels of continuous generation observed in peroxide assays. As •OH is thought to arise largely from H_2O_2 via (R3) and similar reactions, •OH may share these sources. Light reactions are known to generate H_2O_2 in cloud and fog water (e.g. (Faust et al. 1993)). The compounds responsible for the photochemical formation of H_2O_2 have not been clearly identified, but may include transition metal complexes (Faust et al. 1993; Faust et al. 1997; Zuo and Deng 1997) and a variety of organic material such as humic acids (Anastasio et al. 1994; Faust and Allen 1992). Particle ROS generation data (above) are attributable to dark reactions however, as samples were collected and extracted away from light sources. Because equilibration between the gas- and aerosol-phase takes minutes, while sample collection requires a few hours, aqueous photochemistry cannot be the origin of the observed ROS.

A few possible mechanisms are likely to explain only a fraction of observed H_2O_2 generation activity:

(1) **Salts.** High concentrations of salts (common in aerosols) can enhance Henry's law uptake of H_2O_2 from the gas phase (Chung et al. 2005; Lind and Kok 1986), by up to a factor of 2 or 3.

(2) **Other hydroperoxides.** In clouds and fogs, H_2O_2 concentrations tend to be lowered from their H_A equilibrium values due to the reaction of H_2O_2 with S(IV) compounds, the first step of which is reversible (e.g., (Sauer et al. 1996)). These species could possibly release H_2O_2 in extraction solutions. Further, aqueous hydroxy-hydroperoxides decompose to H_2O_2 and the corresponding aldehyde, another potential source of H_2O_2. Both of these processes, however, increase with increasing pH (Hasson et al. 2001a; Hellpointner and Gäb 1989; Marklund 1971), in the opposite direction of the pH trend we have measured (below and (Arellanes et al. 2006))(Hasson et al. 2001a; Marklund 1971), so while these mechanisms may contribute to the observed H_2O_2, they are not likely to be a dominant source.

Plausible promoters for the formation of substantial quantity of ROS are as follows:

(3) **Redox chemistry of transition metals.** Transition metals are capable of generating H_2O_2 through redox reactions (e.g., R1-R3), either as free ions or as metal-ligand complexes. Soluble transition metals are generally present in ambient aerosols at concentrations above the measured equivalent concentrations of H_2O_2, so that catalytic cycles are not necessary to explain measured ROS formation in the absence of added antioxidants (Arellanes 2008; Paulson et al. 2009b; Wang et al. 2010a). Our measurements in Riverside, CA indicate that soluble Fe, Cu and Zn concentrations are correlated strongly with H_2O_2 generation (Paulson et al. 2009b; Wang et al. 2010a). Additionally, the dependence of H_2O_2 generation on the pH and composition of extraction solution, the initial formation rate of H_2O_2, as well as the change of H_2O_2 with extraction time, are all consistent with a role for metal-mediated H_2O_2 generation.

20

Fine mode results from the Riverside study are less clear, but suggest a contribution from transition metals, as well as an additional source. See et al. (See et al. 2007) found a relationship between ROS generation activity and a somewhat different list of soluble transition metals (Cd, Co, Cu, Fe, Mn, and Ni) in wood smoke, gas cooking and other source aerosols. Jung et al. (Jung et al. 2006b) investigated •OH production by soot and a few ambient PM samples from Davis; they found that transition metals accounted for a significant fraction (though not all) of •OH from the ambient particles, and suggested that material associated with the soot carbon was responsible for a portion of the remainder. Vidrio et al. (Vidrio et al. 2009) did a more thorough study using $PM_{2.5}$ collected in Davis over the course of a year; they found that soluble Fe appeared to be the dominant precursor for •OH generation. *This project expanded the small previous data set that had begun to reveal specific metal activity in ambient aerosols.*

(4) **Redox chemistry of quinones.** In recent years, the presence of quinones in particulate matter has received considerable attention (e.g., (Roginsky et al. 2000)). Some of the key reactions of a typical quinone (1,4-naphthoquinone) are shown in Figure 1. The oxidation of semiquinone radical anions to quinones, and of hydroquinones to semiquinone radical anions,

is accompanied by the reduction of oxygen to the superoxide radical anion followed by reduction to form hydrogen peroxide.
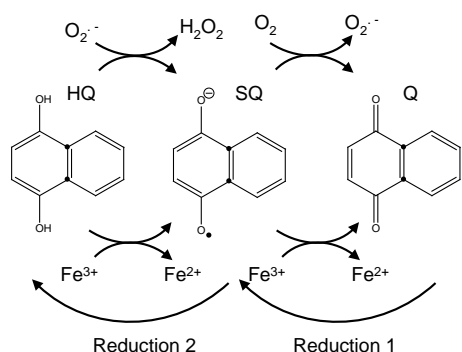
Figure 1. Quinone redox chemistry scheme.

Electron Paramagnetic Resonance measurements of ambient PM2.5 has identified semiquinone-like signatures at concentrations as high as 10^{17} radicals/g (Dellinger et al. 2001). The radicals survive within the collected samples for months, and recent work suggests that they are stabilized by the surface of the PM (Dellinger et al. 2007). When exposed to water and oxygen, stoichiometric conversion of semiquinones to quinones followed by the disproportionation of superoxide to produce hydrogen peroxide (R7) would result in the formation of approximately 10^{-3} ng H_2O_2 per μg of PM. This is about two orders of magnitude lower than the observed hydrogen peroxide associated with ambient PM. Ambient PM2.5 samples have been shown to contain a range of redox-active quinones at levels as high as 10 ng/m^3 (Chung et al. 2006a), although mass loadings are more typically of the order of 10^{-1} ng/m^3 (Allen et al. 1997; Cho et al. 2004b; CRPAQS 2001; Fraser et al. 1998; Hannigan et al. 1998; Koenig et al. 1993; Ligocki 1989; Wilson et al. 1995; Yassaa et al. 2001). The presence of reducing agents in PM capable of Reduction steps 1 and 2 in Fig. 1 would result in redox cycling that would lead to a buildup of hydrogen peroxide. While specific PM components capable of these reactions have not been identified, the complexity of PM suggests that species capable of donating electrons to the quinones/semiquinones may be present. Previous work also suggests that photochemical reduction of quinones at wavelengths between 300 and 480 nm may initiate the conversion of quinones to semiquinones (Reduction Step 1) in particulate matter (Chen and Pignatello 1997; 1999). In addition to the direct reduction of oxygen to hydrogen peroxide by redox cycling, hydro- and semi-quinones can reduce transition metals, such as Fe(III) (Fig. 1), thus the reactions between transition metals and hydroquinones/semiquinones may jointly affect the

21

ROS content. *Speciated quinone concentrations and their relationship to H_2O_2 and •OH is a focus of this study.*

(5) **Other complex organic material.** Hewitt and Kok (Hewitt and Kok 1991) observed H_2O_2 formation from the viscous material formed from the ozonolysis of cyclic alkenes, and suggested it might be from a hydrolysis reaction of this material. This material is now known to include diacyl peroxides (Ziemann 2002), peroxic acids (Venkatachari and Hopke 2008), and oligomeric compounds (Docherty et al. 2005). Consistent with this, we observe H_2O_2 formation from pure secondary organic aerosols generated by oxidizing terpenes or aromatics in a smog chamber (Paulson et al. 2009b). While quinones might form to a degree in the toluene system, rationalizing quinones in the terpene system is more difficult, so other organics may have a role. Laboratory studies have provided ample evidence for organic peroxides, but not necessarily *hydroperoxides* in secondary organic aerosols (SOA) (Tobias et al. 2000; Ziemann 2002). Further, while our system can measure many hydroperoxides (approximately C_5 or smaller) (Hasson et al. 2001a; Hasson et al. 2001b; Hasson and Paulson 2003), we rarely observe evidence of hydro- or hydroxyhydro-peroxides other than H_2O_2 in particles. *Other organics, however, appeared to be contributing. This project helped to elucidate this phenomenon.*

1.4 Atmospheric Sources of Quinones in Ambient Aerosols. Quinones likely have both primary and secondary sources in the atmosphere. At urban sites, automobile/diesel engine exhaust is often the major primary source of oxygenated-polycyclic aromatic hydrocarbons (OPAH, including quinones), although other sources may contribute significantly (Schauer and Cass 2000). Alternatively, OPAH may be formed via the atmospheric oxidation of PAHs. For example, the NO_3-initiated oxidation of phenanthrene (Wang et al. 2007) is likely to be the major secondary source of phenanthraquinone. Consistent with a significant secondary source of OPAH from photo-oxidation processes, a correlation between OPAH levels and NO_x and O_3 concentrations has been reported at sites in the U.S. and North Africa (Wilson et al. 1995; Yassaa et al. 2001). Recent measurements of phenanthrene and phenanthraquinone loadings along air mass trajectories in Los Angeles basin support the notion that the majority of quinones observed result from photochemical oxidation of phenanthrene (Eiguren-Fernandez et al. 2008c). On the other hand, Fraser et al. (1998) measured levels of several OPAHs levels at four sites in Los Angeles, and found that for a number of species, OPAH levels were lower downwind of the primary PAH source (Fraser et al. 1998). Also, OPAH levels did not increase during the afternoon when photochemical oxidation processes occur most rapidly (Fraser et al. 1998). The authors of the latter study further argued that levels of many OPAH compounds were consistent with known emission rates from primary sources (Fraser et al. 1998).

Quinones are components of particulate matter that have been associated with oxidative stress, potentially leading to inflammatory effects and DNA damage (e.g., (Shang et al. 2013; Shang et al. 2014)). Their contributions to reactive oxygen species (ROS) generation compared to other redox active species present in particulate matter are unclear, however, and some questions remain regarding their origins in the atmosphere (direct emission vs. *in situ* photochemical production).

Reported quinone mass loadings are typically well below 1 ng.m^{-3} (e.g., (Cho et al. 2004b; Fraser et al. 1998; Haefliger et al. 2000; Koeber et al. 1999; Wilson et al. 1995; Yassaa et al. 2001)). A California Air Resources Board study (CRPAQS 2001) measured mass loadings for over 100 organic compounds, including four quinones, in Fresno during 2000-1. The quinone levels reported are significantly higher than data from other locations. Mass loadings of acenaphthenequinone, anthraquinone, and benzo[a]anthraquinone are highest during Winter, while very high levels of chrysenequinone are reported for Summer. Work from our lab is qualitatively consistent with this work, with eleven 2-4 ring quinones observed at a site in Fresno during 2004-5 (Chung et al. 2006b). Mass loadings for the majority of these species were highest during the Winter.

Literature data do not clearly show if aerosol-phase quinones are mostly primary or secondary in origin. Quinones are expected to be generated in combustion processes. While the dataset for quinone emission factors is limited, the available data are consistent with this intuitive result. For example, Jakober et al. report emissions of several quinones in the gas and particle phases, with emissions as high as 28 mg L^{-1} of fuel consumed (Jakober et al. 2007). Fraser *et al.* (Fraser et al. 1998) measured oxygenated PAH (OPAH) levels that were lower downwind of the primary PAH source, and noted that OPAH levels did not increase during the afternoon when photochemical oxidation processes occur most rapidly. The authors concluded that levels of many of the OPAH compounds detected were consistent with known emission rates from primary sources.

Two earlier studies (Wilson et al. 1995; Yassaa et al. 2001) report a correlation between OPAH levels and NO$_x$ and O$_3$ concentrations at sites in the US and North Africa. These data are consistent with a significant secondary source of OPAH from photo-oxidation processes. More recently Eiguren-Fernandez et al reported measurements from the LA Basin and concluded that while direct emissions were important close to primary sources, photochemical transformation of PAHs was the major source of quinones at downwind sites (Eiguren-Fernandez et al. 2008a; Eiguren-Fernandez et al. 2008b). A similar conclusion was reached for samples collected and analyzed in the UK (Alam et al. 2013). Measurements of anthraquinone and naphthacenequinone from our lab during summer 2004, where high mass loadings were observed only for back trajectories passing over the Bay Area (Chung et al. 2006b), are consistent with this picture. However, due to the limited number of wintertime measurements no clear conclusions could be made regarding the relative importance of photochemistry versus local sources during this period.

Quinones are components of particulate matter that have been associated with oxidative stress, potentially leading to inflammatory effects and DNA damage (e.g., (Shang et al. 2013; Shang et al. 2014)). Their contributions to reactive oxygen species (ROS) generation compared to other redox active species present in particulate matter are unclear, however, and some questions remain regarding their origins in the atmosphere (direct emission vs in situ photochemical production).

Reported quinone mass loadings are typically well below 1 ng.m^{-3} (e.g., (Cho et al. 2004b; Fraser et al. 1998; Haefliger et al. 2000; Koeber et al. 1999; Wilson et al. 1995; Yassaa et al. 2001)). A

California Air Resources Board study (CRPAQS 2001) measured mass loadings for over 100 organic compounds, including four quinones, in Fresno during 2000-1. The quinone levels reported are significantly higher than data from other locations. Mass loadings of acenaphthenequinone, anthraquinone, and benzo[a]anthraquinone are highest during winter, while very high levels of chrysenequinone are reported for summer. Work from our lab is qualitatively consistent with this work, with eleven 2-4 ring quinones observed at a site in Fresno during 2004-5 (Chung et al. 2006b). Mass loadings for the majority of these species were highest during the Winter.

Literature data do not clearly show if aerosol-phase quinones are mostly primary or secondary in origin. Quinones are expected to be generated in combustion processes. While the dataset for quinone emission factors is limited, the available data are consistent with this intuitive result. For example, emissions of several quinones in the gas and particle phases from diesel and gasoline engines have been reported, with emissions as high as 28 mg L^{-1} of fuel consumed (Jakober et al. 2007). One field study reported oxygenated PAH (OPAH) levels that were lower downwind of the primary PAH source, and noted that OPAH levels did not increase during the afternoon when photochemical oxidation processes occur most rapidly (Fraser et al. 1998). The authors concluded that levels of many of the OPAH compounds detected were consistent with known emission rates from primary sources.

Two earlier studies (Wilson et al. 1995; Yassaa et al. 2001) report a correlation between OPAH levels and NO_x and O_3 concentrations at sites in the US and North Africa. These data are consistent with a significant secondary source of OPAH from photo-oxidation processes. More recently measurements from the LA Basin are consistent with direct emissions dominating close to primary sources, while photochemical transformation of PAHs are the major source of quinones at downwind sites (Eiguren-Fernandez et al. 2008a; Eiguren-Fernandez et al. 2008b). A similar conclusion was reached for samples collected and analyzed in the UK (Alam et al. 2013). Measurements of anthraquinone and naphthacenequinone from our lab during Summer 2004, where high mass loadings were observed only for back trajectories passing over the Bay Area (Chung et al. 2006b), are consistent with this picture. However, due to the limited number of wintertime measurements no clear conclusions could be made regarding the relative importance of photochemistry versus local sources during this period.

In this work we report new time-resolved measurements of quinone mass loadings at two sites in Fresno and Claremont. These data provide new insights on the sources of quinones in Central and Southern California. The measurements also provide data that can be compared with the metal mass loading, dithiothreitol (DTT) and surrogate lung fluid (SLF) measurements carried out by our collaborators on the same samples to evaluate the relative importance of metals and quinones in ROS generation in these assays.

II. Field Campaign Description

II.A. Description of Field Sites and Sample Collection

Samples were collected during the summer (July 26 – Aug. 13) of 2012 for a 19-day period in Claremont, CA. Claremont is located approximately 50 km downwind of downtown Los Angeles. Samplers were set up on the roof of Sprague Hall (34° 6'23.74"N; 117°42'43.73"W, height 134 ft.) on the campus of the Harvey Mudd College. Two major freeways, I-210 and I-10, are 1-2 km from the site.

Winter samples were collected in Fresno, CA over the period Jan. 16 – Feb. 8, 2013. Samplers were located on the roof of the Industrial Technology building (36°48'55.88"N; 119°44'58.57"W, height 141 ft.) on the campus of California State University, Fresno. The building is located 40 m from Barstow Avenue and about 1 mile from Highway 168, both travelled heavily by passenger vehicles.

PM2.5 mass loading in San Joaquin Valley shows a strong seasonal variation, with a maximum in winter and minimum in summer; at least partly attributable to stagnant events that are common in winter. Particularly on winter nights, organic carbon is thought to be of primary in origin, with wood burning being the most important contributor [Chen et al., 2007; Gorin et al., 2006]. In contrast, $PM_{2.5}$ mass loadings in the Los Angeles region are more constant throughout the year, and are predominantly anthropogenic in origin. In summer, particularly at receptor sites such as Claremont, there is a larger component of photochemical secondary organic and other aerosol [Hasheminassab et al., 2014].

Samples were collected at rooftop sites at Harvey Mudd College, Claremont and California State University, Fresno. Both sites were about 30 m above ground level. Sets of ambient samples (PM_4) were collected three times a day, for approximately 6 or 12 hours, from 7 AM – 1 PM, 1 PM - 7 PM, and 7 PM – 7 AM.

UCLA Samples were collected on acid washed, pre-weighed PTFE filters (PALL, 47mm, 2μm pore size) using 5 URG cyclone inlets. The flow rates were controlled at 50 LPM by rotameters (Kings Instruments 7530), corresponding to a size cut point of 4 microns. The cut point was intended to be 2.5 microns, however due to a misunderstanding on the rotameter operation used to control flow rates, a somewhat lower flow rate was used than that needed for a 2.5 μm cut point. Matched field blanks were created using the same handling procedures as samples, but with the pump turned on for only 30 s. A total of 660 filters were collected (300 from Claremont and 360 from Fresno). These filters were analyzed for mass, hydrogen peroxide and hydroxyl radical, trace metals and iron speciation. Mass, hydroxyl radical quantification and iron speciation were performed on site, while the filters for other analyses were stored in the freezer until use. Hydroxyl radical was generally poorly correlated with iron and H_2O_2, and is discussed separately.

CSUF aerosol samples were collected at both sites were collected on 260 x 300 mm, 0.45 μm pore size Teflon-coated glass filters (Tisch Environmental, Lot#120618003) with a Hi-Volume $PM_{2.5}$ sampler (Tisch Environmental TE-6001-2.5-HVS) operating at 1.13 $m^3 min^{-1}$. Teflon filters

were individually cleaned with three 60 mL aliquots of dichloromethane (HPLC Grade; Sigma-Aldrich) and were then baked for 2 hours. The final aliquot of dichloromethane was retained and analyzed as a blank sample for organics of interests. Clean filters were stored at -20°C in aluminum envelopes rinsed with dichloromethane and then baked for 2 hours until used.

Ambient air was drawn through the cleaned filter at a rate of 1.13 $m^3 \cdot min^{-1}$ using a high volume size selective $PM_{2.5}$ inlet sampler containing 40 impactor jets (Tisch Environmental, TE-6070-2.5-HVS). The flow was calibrated at the beginning and end of each sampling period using a modified 36 inch Dwyer slack tube manometer. Collection periods were between 5 and 13 hours with measurements in the morning (7 a.m. – 1 p.m.), afternoon (1 p.m. – 6 p.m.), and night (6 p.m. – 7 a.m.). Sampling times were matched to sample collections for other analyses performed as a part of this study. Mass concentrations were determined by weighing filters before and after sample collection using a Mettler balance under controlled conditions (relative humidity between 40 and 45%) and temperature between 22 and 24 °C). Collected filters were stored in the room for 24 hours prior to weighing and then were frozen at -20°C until subsequent analyses were performed.

A Tisch Environmental Poly-Urethane Foam (PUF) sampler (TE-PUF 1000) was used to collect total suspended airborne particulates on quartz filters as well as trap semi-volatiles at flow rates of 230 $L \cdot min^{-1}$ with the same sampling time periods as the $PM_{2.5}$ sampler. Calibration flow rates were determined by recording the magnehelic gauge readings before and after each sampling period. Quartz filters were baked at 100 °C for 24 hours, pre-weighed using a Mettler balance, and stored at -20°C in dichloromethane rinsed and baked aluminum envelopes. Poly-Urethane foam (PUF) plugs were pre-cleaned by Soxhlet extraction. PUFs were Soxhlet extracted in 200 mL of 10 percent diethyl ether in hexane solvent and refluxed for 18 hours at a rate of at least 3 cycles per hour. The PUF was removed after refluxed and placed in a pre-cleaned PUF glass holder baked at 100°C for 24 hours. PUF plugs were held at room temperature and out of sunlight exposure until use. The extracted solvent was evaporated using a RapidVap Labconco N_2 Blowdown evaporator with three subsequent washes reconstituted in 2 mL of DCM. The aliquot was saved and stored at -20 °C until analyzed as a blank for the cleaned PUF.

II.B. Analyses

II.B.1   Materials

Methanol (HPLC grade), trifluoroethanol (TFE), sodium citrate tribasic dihydrate (Cit), L-ascorbic acid (Asc), uric acid sodium salt (UA), and L-glutathione (GSH) reduced, hydroxylamine hydrochloride, ethylenediaminetetraacetic acid (EDTA), horseradish peroxidase type II, *para*-hydroxyphenyl acetic acid (POHPAA), potassium hydrogen phthalate were purchased from Sigma Aldrich. Ferrozine (4,4'-[3-(2-pyridinyl)-1,2,4-triazine-5,6-diyl]dibenzenesulfonate), sulfuric acid (reagent grade) and sodium thiosulfate (1 M) were purchased from Fluka Analytic. Sodium phosphate dibasic and potassium phosphate monobasic were purchased from Acros Organics. Nitric acid (70% trace metal grade) and ammonium hydroxide (30% ACS reagent grade) were purchased from Fisher, and trifluoroethanol from Sigma Aldrich (T63002 ≥ 99%). All materials were used as received.

Surrogate Lung Fluid (SLF) was prepared by adding 4 antioxidants (Cit, Asc, UA, and GSH) at physiologically relevant concentrations to phosphate buffer at pH 7.2-7.4. Phosphate buffer contained 114 mM of NaCl, 7.8 mM of sodium phosphate dibasic and 2.2 mM of potassium phosphate monobasic. Phosphate buffer was Chelex-treated to remove trace metals prior adding the antioxidants. The antioxidants were freshly prepared in phosphate buffer for each experiment. Due to the low water solubility, UA was dissolved under constant stirring and heating for about 30 minutes and was cooled to room temperature. A final concentration of 100 μM UA, 100 μM GSH, 300 μM Cit and 200 μM Asc was prepared.

Marques and co-workers (Marques et al. 2011) recently summarized the compositions of half a dozen surrogate lung fluids. Two components are present in all of these fluids, as well as in our SLF: NaCl (which accounts for most of the solute mass) and a pH buffer, typically phosphate and/or carbonate. We used a mixed phosphate-carbonate buffer in our past work (Jung et al. 2006a), but found it was unstable because of CO_2 outgassing, so we switched to phosphate-only buffer.

For ROS generation from PM we have found that the most important component is ascorbate, because it is the source of the electrons that redox-active metals and organics use to make ROS (Charrier and Anastasio 2011; Charrier et al. 2014a; Charrier and Anastasio 2015; Vidrio et al. 2008a). Ascorbate is present in real lung lining fluid and in our SLF but not in the formulations summarized in Marques et al. This is most likely because it is unstable and requires frequent remaking of the SLF. Another important component for ROS is glutathione (GSH), which is also present in real lung lining fluid, and our SLF, but not the SLFs in Marques et al. This is also probably because of stability issues. We have found that GSH is the dominant ligand for Cu in our SLF and it greatly reduces Cu reactivity. The other two trace components of our SLF are citrate (which is a protein surrogate present in all of the SLFs in Marques et al.) and urate, which is present in real lung lining fluid, but not in the Marques et al. formulations. We have found that citrate is important for maintaining Fe solubility, but that urate has no apparent effect on ROS formation.

The other trace species that are present in some of the Marques formulations include organic anions, a metal chelator (DTPA), and surface-active species (DPPC and ABDCB). The organic anions are not strong enough chelators to compete with citrate or GSH to bind Fe and Cu, but they can interfere with ROS formation (e.g., pyruvate rapidly destroys H_2O_2), so they are not included in our SLF. DTPA is not present in real lung lining fluid but is a surrogate for chelators such as Cit and GSH, which we use. We have not tried DPPC and ABDCB in our formulation, but we have used albumin, another surfactant, and found it caused excessive foaming so we stopped pursuing it; these species will chelate metals, but it's not clear if they would be able to pry the metals from Cit and GSH.

Overall, lung lining fluid is very complex and even the best mimics cannot capture all of its properties. But we believe that our SLF does the best job of published fluids in capturing the redox activity of PM and PM components. Before our work, cell-free ROS was typically measured in a fluid with no anti-oxidants, while other groups now sometimes add Asc but not

the other three components present in our SLF. As we move forward SLFs will become more sophisticated, but at the moment our formulation is the most sophisticated solution for redox activity measurements.

II.B.3 Trace metal cleaning and Particle extraction

A rigorous cleaning process was followed for all glass and Teflon containers. After each use, each vessel was washed with warm water and soap, and then rinsed deionized (18 MΩ DI) water (3x), ethanol (3x), and finally DI water (3x). The vessels were then soaked in 1 M nitric acid bath overnight, rinsed with DI water and air dried. Nitric acid baths were replaced after being used twice and kept covered to avoid dust deposition. All analytical solutions were prepared with 18 MΩ DI water that had been passed through a Chelex column to remove trace metals. pH was measured with a bench top pH meter (HANNA Instruments, HI 3220), calibrated daily.

Filters were cut in half using a cleaned ceramic blade. Half filters were extracted in 4 mL aqueous pH3.5 solutions (adjusted using 0.1 N sulfuric acid) in Teflon® Petri dishes with gentle agitation. To increase particle solubility, the filters were wetted first with trifluoroethanol.

II.B.4. Soluble speciated iron: Ferrozine assay

The Ferrozine assay (Oakes et al. 2010) was used to determine concentrations of soluble Fe(II) and Fe(total). The assay was performed with a Liquid Waveguide Capillary Cell (LWCC) (World Precision Instruments), equipped with a UV-Vis detector (Avantes). The UV/Vis instrument used to measure the concentration of iron was a 1-meter-long path flow cell (LPC-FS-1000, Avantes) connected to a halogen source light (AvaLight-DH-S-DUV, Avantes) and a spectrometer (AvaSpec-ULS2048L-USB2, Avantes) with fiber optics (200 μm inner diameter). Using a 1 meter LPC allows the quantification of very low concentrations of iron (up to a few nM). Rapid complexation of divalent iron with Ferrozine (3-(2-pyridyl)-5,6-bis(4-phenylsulfonic acid)-1,2,4-triazine) forms a stable magenta complex that can be probed with UV/Vis spectroscopy at λ_{max} = 562 nm. To account for instrument drift and solution turbidity, absorbance at the non-absorbing wavelength of 700 nm (A_{700}) was subtracted from A_{562}. To quantify Fe(total), a strong reducing agent, hydroxylamine hydrochloride was added to convert all Fe(III) to Fe(II). Calibration of Fe(II) was performed daily and the LWCC was rigorously cleaned before each use. Stock solutions of Ferrozine and hydroxylamine hydrochloride are stable for a month when stored at 4°C in the dark. The Fe(II) stock solution (2 mM iron sulfate (Sigma-Aldrich) at pH 3.5) was freshly prepared for each measurement. Fe(II) calibration curves were made by diluting the stock solution to concentrations between 0.012 and 0.75 μM Fe(II). To avoid interference with light, all solutions were prepared in a dark room equipped with a sodium lamp.

II.B.5 Hydrogen Peroxide

100 μL aliquots were analyzed for H_2O_2 every 30 minutes after initial extraction for the first 2 hours, and again at 24 hours using a High Performance Liquid Chromatography (HPLC) (Shimadzu RF-10AXL) (Arellanes et al. 2006). The eluent system, consisting of pH 3.5 solution adjusted with 0.1 N sulfuric acid and 0.1 mM EDTA, was delivered by an isocratic pump (Shimadzu LC-10-Ai) at 0.6 mL/min. A C18 guard column was installed to remove any

impurities. H_2O_2 was eluted at 0.6 mL/min, after which it was mixed with a fluorescent reagent containing horseradish peroxidase and *para*-hydroxyphenyl acetic acid (POHPAA). The peroxidase enzyme catalyzes the reaction between H_2O_2 and POHPAA, forming a fluorescent dimer, which is detected with a fluorescence detector at the excitation/emission wavelengths of 300/420 nm. A 30% ammonium hydroxide solution was mixed with the dimer prior entering the detector to increase fluorescence signal. Calibrations were performed weekly or when the HPLC conditions were changed. Standards ranging from 10^{-8} to 10^{-6} M were prepared from 0.3% stock solution, which was titrated with sodium thiosulfate to determine the stock solution concentration (about 0.1 M). The detection limit for this method is 10 nM.

H_2O_2 generation from 250 nM $CuSO_4$ in SLF was used as a positive control for the H_2O_2 assay to check for species in the solution that could destroy or form H_2O_2 in SLF. The positive control was analyzed in the same manner as the field samples, and was performed daily. We measured either the rate of H_2O_2 formation by quantifying H_2O_2 at 0, 0.5, 1 and 1.5 hours, or at 2 hours when the HPLC was occupied for other measurements preventing a rate measurement. All sample rates were blank-corrected. The average blank rate was 0.42 ± 0.17 µM/hr and the blank corrected positive control rate was 1.42 ± 0.17 µM/hr. The average positive control 2 hour H_2O_2 concentration was 2.41 ± 0.19 µM/hr.

H_2O_2 production in laboratory solutions was studied at UC Davis using a similar HPLC-fluorescence system as described above. At time zero we mix the redox-active species into 5.0 mL of SLF in a 7.0 mL FEP bottle, seal it, and agitate it on a shake table at setting 5 at room temperature. We measure the H_2O_2 concentrations in each reaction solution at 0, 0.5, 1, and 1.5 hours. At each time point we remove a 0.50 mL aliquot, add 10.0 µL of 5.0 mM desferoxamine (DSF) to chelate metals and help stabilize the H_2O_2, then immediately inject onto the HPLC (50 µL sample loop).

We calculate the rate of H_2O_2 production from the concentrations of H_2O_2 measured at 0, 0.5, 1 and 1.5 hours. In many cases the rate of H_2O_2 production decreases with time causing a slight curvature for most data, and significant curvature for solutions with high concentrations of Fe. We calculate the initial rate of H_2O_2 production using the "b" term of a second-order polynomial ($y = at^2 + bt + c$, where a, b and c are fitted constants) (Wang et al. 2010b).

We measured H_2O_2 production in a positive control (250 nM Cu(II)) and blank (SLF containing four antioxidants) on each experiment day. All sample rates are blank-corrected by subtracting that day's blank rate. If data have an error bar it indicates that two or more replicates were measured and the data are reported as the average ± standard deviation of the blank-corrected initial rates. A small subset of data does not have replicates and are reported without an error bar to identify that only one measurement was made. We could estimate the error from the standard error of the slope of the rate regression, but this under-predicts the actual variability of day-to-day replicates. We estimate that the typical relative standard deviation for our rates is 14% based on variability in the blank-corrected positive control, which has an average (± 1σ) initial rate of H_2O_2 formation of 1.99 ± 0.28 µM/hr (n = 18), with a blank rate of 0.21 ± 0.1. Statistical difference between means (where n ≥ 2) were calculated using the student's *t*-test, with $p \leq 0.05$.

II.B.6 Hydroxyl radical quantification.

Of available probes, terephthalate (TA) is the most sensitive. Terephthalate has one fluorescent product, 2-hydroxyterephthalic acid (TAOH). In this study, TAOH was detected at maximum excitation/emission wavelength (l_{ex}/l_{em}) of 320/420 nm using a sensitive fluorometer (Lumina, Thermo Scientific), resulting in a detection limit of about 10^{-10}. An aliquot of 150uL of solution was measured at 0, 20, 40, 60, 90 and 120 minutes to determine the rate for TAOH formation, and again at 24 hours. Due to the limited amount of extraction solution available (4mL), we used a micro cuvette (QS, 10,00mm, Hella Analytics) for this purpose. The cuvettes were cleaned 3 times with water and 3 times with ethanol and dried in between each sample measurement. Calibration with TAOH standard concentration of 50, 100, 200 and 800nM was performed daily. We use a terephthalic acid yield of 35% at pH 7.4 (Matthews 1980).

Hydroxyl radical generation in the laboratory solutions at UC Davis was quantified using benzoate as the •OH probe and by measuring the *p*-hydroxybenzoate product with HPLC/UV-Vis (Charrier et al., 2015). Experiments are performed with room lights off and bottles are further shielded from light with aluminum foil. At 0, 1, 2 and 4 hours we remove a 0.80-mL aliquot and immediately quench it with 16 µL of 5 mM desferoxamine (DSF) and 16 µL of 21 mM sodium bisulfite ($NaHSO_3$) to bind transition metals and destroy H_2O_2, giving a final concentration of 100 µM DSF and 400 µM sodium bisulfite. After allowing this mixture to react for at least 5.0 min, we add 19.2 µL of 0.5 M sulfuric acid to acidify the solution for HPLC analysis. Samples are stable for at least 18 hours at room temperature in the dark. We calculate the average rate of •OH production from zero to four hours using the linear slope over that time period. In some cases, initial •OH production has a slight lag, so data are not always strictly linear from zero to four hours. On each experiment day we also measure •OH production in a blank and a positive control (1.44 µM $FeSO_4$). All rates are blank-corrected by subtracting the blank rate from the reaction rate. The average (± 1σ) blank and blank-corrected positive control rates are 0.096 ± 0.04 (n=14) and 0.97 ± 0.08 (n=10) µM •OH/hr respectively.

II.B.7 Particle mass and trace metal analysis.

Particle masses were determined using a microbalance (1 µg precision, ME 5, Sartorius) in a temperature (22-24°C) and humidity (42-44%) controlled room. Filters were allowed to equilibrate in the weighing room for one hour before weighing. Charge on the PTFE filters was removed using a charge neutralizer (NRG) for about 10 seconds. During the field campaign, the filters were weighed using a microbalance with similar precision, within an hour of sampling.

To determine water soluble transition metals sample filters where extracted in both pH 3.5 and SLF solution. Filtered aliquots taken at 2 and 24 hours where acidified to 2% by weight HNO_3 and stored in 15 ml Falcon conical centrifuge tubes. An Agilent 8800 ICP-MS was used to measure the following transition metals: V, Cr, Mn, Fe, Co, Ni, Cu, Zn, Se, Cd, La, Pb. Calibration curves where made from a 10 ppm 33 multi-element standard (SCP Science). All measurements where performed using instrumental software. Reagent and field blanks were also analyzed for metals to correct for background concentrations

II.B.7 Estimation of Biomass Burning HULIS and Black Carbon Concentration.

Quantification of the contribution of biomass burning Humic-Like Substances (BBH) and black carbon (BC) on PTFE filters was accomplished using optical absorption at 370 nm and 880 nm respectively. Measurements where performed with an OT21 duel wavelength optical transmissometer (Magee Scientific Corporation). A quartz diffuser backing (Pallflex Fiberfilm) was placed under each PTFE filter to provide an even distribution of light to the detector; care was taken to ensure the filter lay flat against the quartz diffuser. Light absorption at 880 nm is proportional to the concentration of BC (Hansen et al. 1984; Japar et al. 1986), expressed with the following equation:

$$[BC] = \frac{bATN}{\sigma(\lambda)} = \frac{ATN \times A}{\sigma(\lambda) \times V} = \frac{100 \, Ln\left(\frac{Io}{I}\right) \times A}{\sigma(\lambda) \times V} \qquad \text{(R II.1)}$$

Where b_{ATN} is the attenuation coefficient, $\sigma(\lambda)_{ATN}$ (m^2/g) is the specific attenuation cross section, A (m^2) is the filter area, V (m^3) is the volume of air sampled, ATN is the attenuation, I and Io are light transmitted through a sample and blank respectively. The concentration of biomass burning Hulis [BBH] is also calculated from equation 1 using values at 370 nm. $\sigma(\lambda)_{ATN}$ (m^2/g), the attenuation cross section at a specific wavelength, represents a substantial source of uncertainty in the determination of BC and BBH via optical methods. Literature values for sigma span a wide range of values, 2-25 m^2/g (Lavanchy et al. 1999; Liousse et al. 1993; Petzold et al. 1997; Sharma et al. 2002); differences can be attributed to the aerosol source and composition, aerosol age, different filter materials, correction formulas and various thermal and thermal optical techniques to determine BC (Andreae and Gelencser 2006; Liousse et al. 1993; Petzold et al. 1997). For this work we selected σ_{ATN} (370) of 9.6 m^2 g^{-1} and σ_{ATN} (880) of 4.2 m^2 g^{-1} used to convert ATN to BC and BBH concentrations. These values were empirically determined by the EPA for PTFE filters from FRM-CSN sites (Frank et al. 2010). The sites include urban emissions sites and biomass burning emission sites, with σ_{ATN} only varying ± 10% among sites. These values also closely resemble the attenuation cross-sections determined for the Fresno supersite (Watson et al., 2010) which closely resembled our sampling site.

Shadowing Correction

Filter-based optical methods are complicated by the well-known problem that increased filter loading results in shadowing and other optical effects, As a result, direct measurements of ATN tend to underestimate the true BC concentration (Arnott et al. 2005; Park et al. 2010; Weingartner et al. 2003). The same problem is expected for brown carbon. The particle loading effect can be avoided by minimally loading the filters (Kirchstetter and Novakov 2007) , however since our filters were also used for chemical assays, we used higher loadings. Several algorithms have been formulated to correct for nonlinearities due to particle loading (Jimenez et al. 2007; Schmid et al. 2006; Virkkula et al. 2007; Weingartner et al. 2003). We considered the formulations suggested by Virkkula et al. (2006) and Jimenez et al. (2007) as their methods did not require the aerosol scattering coefficients, which we do not have. By exposing the aethalometer to a constant concentration of dilute diesel exhaust, Jimenez et al. (2007)

empirically derived an expression for K(ATN), an attenuation-dependent correction factor to correct for the underestimation of BC and aerosol absorption at 370 nm:

$$K(ATN) = a + b * e(-ATN/100) = a + b *T \qquad \text{(R II.2)}$$

$$[BBH]_c = \frac{bATN}{\sigma ATN * K(ATN)} \qquad \text{(R II.3)}$$

Where a and b are linear regression coefficients, T is the filter transmission and $[BBH]_c$ is the corrected BBH concentration. At 880 nm for the correction of BC, a = 0.13 and b = 0.88. For the correction of BBH at 370 nm, a = 0.38 and b = 0.67. An alternative correction algorithm investigated was proposed by Virkkula et al. (2007):

$$[BBH]_c = [BBH]_{uc} * (1 + K *ATN) \qquad \text{(R II.4)}$$

Where $[BBH]_{uc}$ is the BBH concentration obtained from the instrument via eqn. 1, K is the shadowing correction constant and $[BBH]_c$ is the corrected BBA concentration. In applying this correction to our data, here we use K = 0.0059 and 0.0054 at 370 and 880 nm respectively (Virkkula et al. 2007). The value at 370 nm was determined for a rural setting while the value at 880 nm was determined for an urban setting, both during winter in Finland; Virkkula et al. (2007) found negligible differences between the winter K values determined at a metro station, an urban station and a rural station. The application of equation (Eq. 3) to our data slightly generally resulted in negligible changes to the correlation coefficients, increased the slope and lowered the y-intercept (Figure 2). The shadowing effect was less prominent in the afternoon filters; resulting from their lower mass content, which was roughly a third of the night sample mass Table 1). A summary of the BBH and BC data is presented in Table 1 and 2 respectively. Results from the Virkkula et al. (2007, Eq. 4) expression were nearly identical to results from the Jimenez expression (Eq. 3; $R^2 > 0.99$, slope = 0.99 for BBA and 0.78 for BC, not shown). BBHULIS (estimated from the measurement at 370 nm) is correlated to BC (estimated from the measurements at 880 nm) with $R^2 = 0.97$. The slope of the relationship is obviously largely dependent on the choice of σ; for the values used here the slope is 0.91.

Table 1. Fresno corrected and uncorrected concentrations of BC (µg/m³) for morning, afternoon and night samples. Average % increase corresponds to the average increase in BC concentration between uncorrected and corrected samples.

Date	Morning (µg/m³)	Morning Corrected (µg/m³)	After-noon (µg/m³)	Afternoon Corrected (µg/m³)	Night (µg/m³)	Night Corrected (µg/m³)
17-Jan	9.5	12.8				
18-Jan			6.3	7.5	6.3	10.3
20-Jan					7.2	12.6
21-Jan	7.5	9.6	3.4	3.7		
22-Jan	7.2	9.1				
23-Jan	6.5	8.0				
25-Jan	7.4	9.1				
26-Jan					1.2	1.3
27-Jan	1.2	1.2	0.9	0.9	2.9	3.7
28-Jan	1.7	1.7	0.3	0.3	7.1	12.5
29-Jan	4.8	5.6	1.5	1.5	6.3	10.5
30-Jan	4.8	5.5	2.8	3.0	5.6	8.9
31-Jan	4.3	4.8	2.3	2.4	4.2	5.9
1-Feb	5.4	6.2	5.8	6.9	6.2	10.8
2-Feb	7.9	9.5	2.9	3.2	7.0	12.6
3-Feb					4.0	5.6
4-Feb	9.1	11.7	5.7	6.7	4.8	7.2
5-Feb	6.7	8.0	5.3	6.2		
6-Feb			3.5	3.8		
7-Feb	8.5	10.7				
Average	6.2	7.6	3.4	3.8	5.2	8.5
Std. Dev.	2.5	3.4	2.0	2.4	1.9	3.7
Range	1.2 - 9.5	1.2 -12.8	0.3 - 6.3	0.3 - 7.5	1.2 - 7.2	1.3 -12.6
Ave. % Increase		20		10		58

Table 2. Fresno corrected and uncorrected concentrations of BBH (µg/m³) for morning, afternoon and night samples. Average % Increase corresponds to the increase in BBH between uncorrected and corrected samples.

Date	Morning (µg/m³)	Morning Corrected (µg/m³)	Afternoon (µg/m³)	Afternoon Corrected (µg/m³)	Night (µg/m³)	Night Corrected (µg/m³)
17-Jan	8.9	13.1				
18-Jan			5.8	7.3	6.3	11.5
20-Jan					6.5	11.9
21-Jan	6.4	8.7	3.7	4.2		
22-Jan	6.5	8.7				
23-Jan	5.9	7.6				
25-Jan	6.4	8.1				
26-Jan					1.7	2.0
27-Jan	1.8	1.9	1.2	1.2	3.8	5.7
28-Jan	3.5	4.0	1.1	1.1	6.0	10.9
29-Jan	5.4	6.9	2.9	3.2	6.0	11.1
30-Jan	5.2	6.3	3.5	3.9	4.9	8.3
31-Jan	4.9	5.9	2.5	2.7	4.1	6.5
1-Feb	5.3	6.5	5.3	6.6	5.0	8.6
2-Feb	7.7	9.8	3.6	4.0	6.2	11.9
3-Feb					3.7	5.7
4-Feb	8.2	11.2	5.3	6.5	4.1	6.6
5-Feb	6.2	7.6	5.1	6.3		
6-Feb			3.6	4.1		
7-Feb	7.4	9.7				
Average	6.0	7.7	3.6	4.3	4.9	8.4
Std. Dev.	1.8	2.8	1.6	2.1	1.5	3.2
Range	1.8 - 8.9	1.9 - 13.1	1.1 - 5.8	1.1 - 7.3	1.7 - 6.5	2.0 - 11.9
Ave. % Increase		27		14		67

34
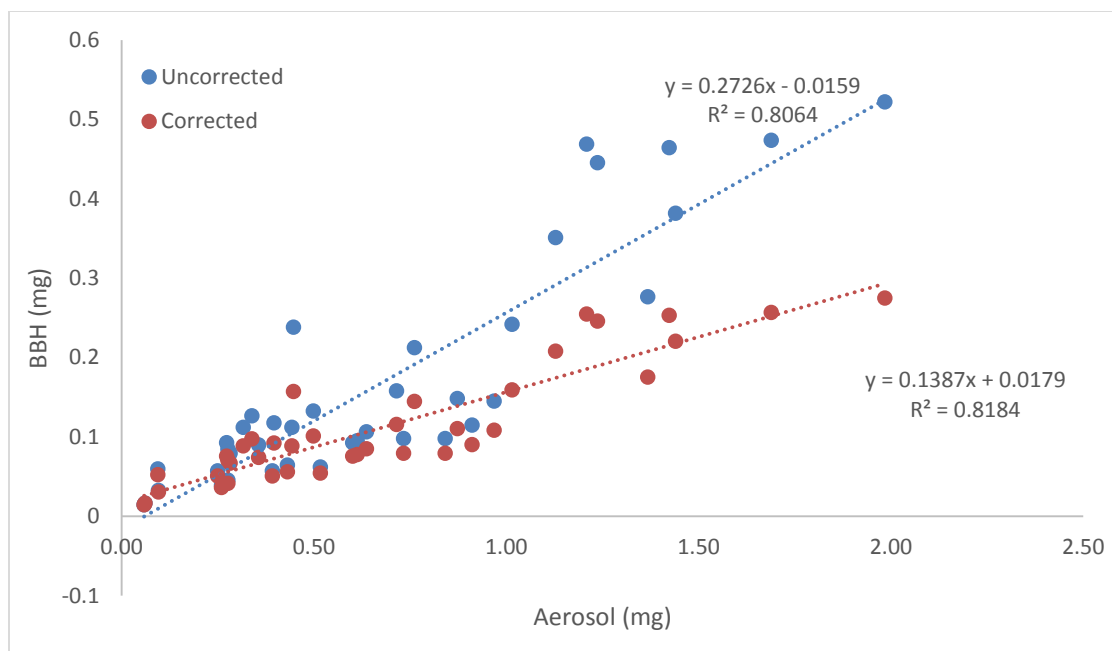
Figure 2. Uncorrected and corrected BBHULIS mass for all Fresno samples combined.

II.B.10 Quantification of Quinones.

A series of extractions were carried out after collection of samples on filter and PUF samples. The filter media underwent two separate extractions; surrogate lung fluid (SLF) and residue filter removal by organic solvation, leading up to analysis. PUF samples were Soxhlet extracted for 18 hours upon collection. All sample extracts were concentrated, and reconstituted in dichloromethane for sample analysis for quinones, polycyclic aromatic hydrocarbons, and additional organic markers by gas chromatography/mass spectroscopy. The extraction procedure is outlined in Figure 3.
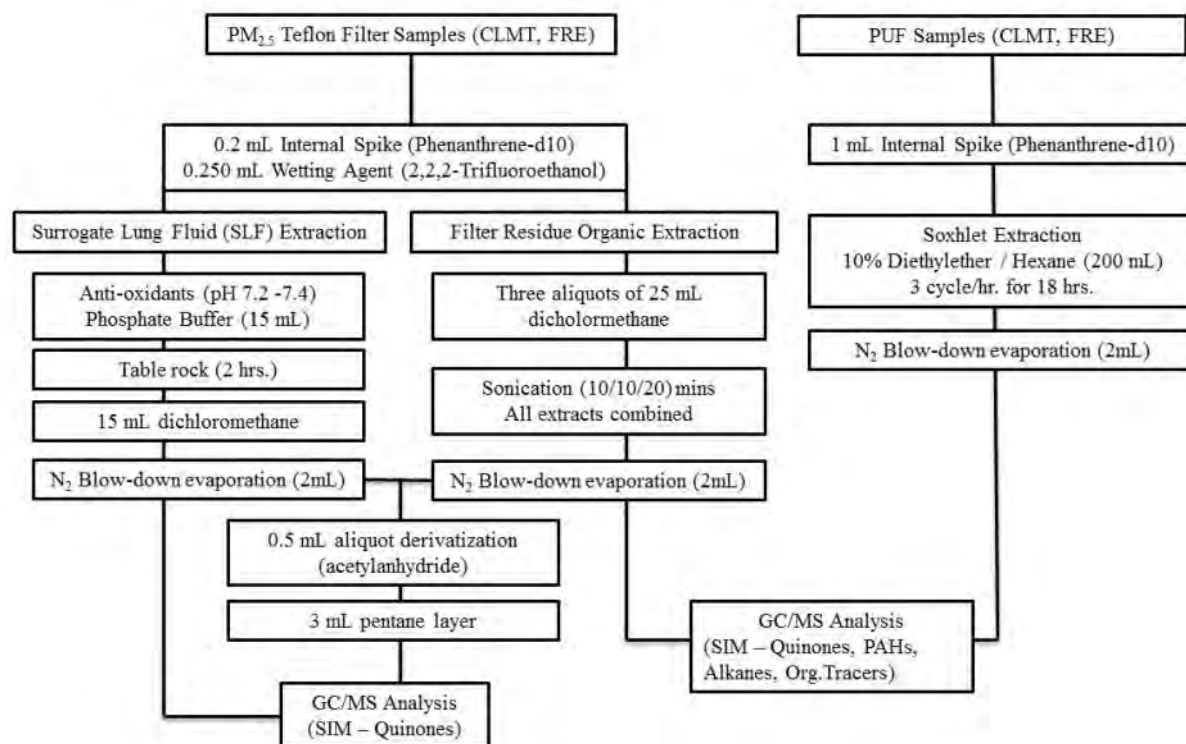
Figure 3. Extraction flow chart for PM2.5 samples.

Initial extractions from filters were performed using a cell-free surrogate lung fluid (SLF). A phosphate buffer solution was prepared in a 1 L volumetric flask by adding 114 mM of sodium chloride (NaCl, Sigma Aldrich, 98%), 7.8 mM of disodium phosphate (Na_2HPO_4, Sigma Aldrich, 98%), and 2.2 mM of potassium dihydrogen phosphate (KH_2PO_4, Sigma Aldrich, 98%) made up with deionized water discharged with 18 MΩ-cm. The solution was kept in the refrigerator (4°C) until used. Freshly made buffer solution was prepared within 1 month or as needed due to the reactivity of the solution degrading.

Stock antioxidants were freshly prepared and added to the buffer solution on the day of each experiment, and stored at 4°C because of their high reactivity and sensitivity to temperature. Uric acid, L-glutathione, and sodium citrate tribasic dehydrate were prepared in a single stock solution. An individual ascorbate stock solution was prepared. The stock solutions were diluted and mixed to make 100μM UA, 100 μM GSH, 300 μM Cit and 200 μM Asc in the phosphate buffer.

Filter Extraction. CSUF Filter samples were cut into 2 by 2 square inches in triplicates, spiked with 200 μL of $1x10^{-5}$ M deuterated phenanthrene which served as an internal standard, and 200 μL of 2,2,2-trifluoroethanol was applied as a wetting agent. The filters were then individually inverted with the exposed surface in contact with the SLF solution prepared in separate petri dishes. Filters were slowly rocked for two hours and then the SLF was removed into a vial for organic extraction with 15 mL of dichloromethane. The DCM layer that resides at the bottom of the vial was further removed into a borosilicate glass tube with an end point

volume of 2 mL. All triplicates of the respective sample were combined into one collection vessel and evaporated to dryness using a Labconco N_2 Blowdown Rapid Evap instrument. All samples were reconstituted with DCM to 2 mL and stored at -20°C for gas chromatography/mass spectroscopy analysis.

Residual Filter Extraction. Residue left on the filter following SLF extraction was extracted by transferring the filter to a clean vial. 3 aliquots of 25 mL of dichloromethane were added to the vial and sonicated for 10 minutes. Vials were removed, inverted, vortexed, and vented to release the pressure in the vial every 5 minutes. This process was repeated two more times for 10 and 20 minutes. All washings were decanted into a LabConco borosilicate glass tube, evaporated to dryness using a Labconco N_2 Blowdown Rapid Evap, and reconstituted with 2 mL of DCM for GC/MS analysis.

Semi-volatile PUF Soxhlet Extraction. PUF sorbent plugs were extracted into 200 mL of 10 percent diethyl ether in hexane solvent using Soxhlet extraction for 18 hours at a rate of at least 3 cycles per hour. Following the allotted time, the solution was allowed to cool, then the apparatus was disassembled and the solvent was decanted into a Labconco borosilicate glass tube. Solvent absorbed to the foam plug was compressed with a pre-cleaned glass rod until no additional liquid was observed. All washings were evaporated to dryness using a Labconco N_2 Blowdown Rapid Evap, and reconstituted with 2 mL of DCM for GC/MS analysis. The PUFs were oven dried at 60 °C and stored out of sunlight exposure at room temperature until analyzed.

Sample Derivatization. A derivatization process was carried out for the analysis of four quinones (1,4-chrysenequinone, phenanthraquinone, 1,2-naphthoquinone, and 1,4-naphthoquinone) to enhance the signals within the GC/MS analysis and previous studies by Cho et al. (Cho et al. 2004a). The procedure converts the carbonyl groups in the quinones to esters, which fragment more readily in the instrument leading to an improvement in detection limits. A fraction of the concentrated sample (0.5 mL) was transferred into a pre-cleaned vial along with 0.2 mL of acetic anhydride and 0.1 g of zinc. Contents were sealed with a PTFE cap, mixed, and incubated at 80°C for three 5 minute intervals. In between each cycle, the contents in the vial were vented, mixed (light swirl), and returned to the dry bath incubator. Subsequent to the 15-minute heating, a second portion of zinc (0.1 g) was added and the same process was carried out. After the final heating, the vials were allowed to cool to room temperature, where then 0.5 mL of distilled deionized water and 3 mL of pentane was added. The contents were mixed and allowed to settle for 10 minutes before taking the top pentane layer for GC/MS analysis.

Chemical Standards and Calibrations

Quinone Calibrations. Quinone standards were spectral grade compounds purchased from Sigma Aldrich and prepared in 99.9% HPLC-grade dichloromethane (Sigma Aldrich) with concentrations ranging from 1×10^{-9} M to 1×10^{-5} M diluted from a stock concentration of 1×10^{-3} M.

PAH Calibrations. Pulverized PAH standards were authentic spectral grade compounds purchased from Sigma Aldrich and prepared in 99.9% high purity dichloromethane (Sigma

Aldrich) with concentrations ranging from 1×10^{-9} M to 1×10^{-4} M diluted from a stock concentration of 1×10^{-3} M.

Instrumentation

GC/MS Analysis Programmable Temperature Vaporization (PTV) Inlet. Organics (quinones and PAHs) were analyzed by Gas Chromatography-Mass Spectrometry (GC-MS). An Agilent 6890 Plus Series GC system was used (serial # US00043853) with a Hewlett Packard 5973 mass selective detector (serial # US01112247) and analyzed using Chemstation software. To increase the sensitivity of the technique, the GC-MS was modified from the conventional inlet system to allow introduction of much larger sample volumes using a programmed temperature vaporizing (PTV) inlet. An improvement in sensitivity is expected to be up to 2-3 orders of magnitude compared to our previous method of 5 µL injections.

Samples were injected into the inlet in solvent vent mode at 40°C cooled with a CO_2 cryogenic trap system with a He carrier gas pressure of 7.62 psi and a total flow rate of 1.0 mL/min. The inlet was then rapidly heated at 300 °C/min to a final inlet temperature of 300 °C. The GC column is an HP-5MS 5% Phenyl Methyl Siloxane capillary column with dimensions of 30 m x 250 µm x 0.25 µm film thickness (Model No: HP 19091S-433). The oven temperature is set to 50°C and held for four minutes then ramped up 5°C/min over a period of 39 minutes to a final temperature of 310°C.

Compounds were run using the selective ion monitoring mode (SIM). Table 3 and Table 4 show the ions used to monitor quinones and PAHs. The limits of detection and quantification were taken to be the concentrations corresponding to signals three and six times greater than the noise at the appropriate retention time.

Table 3. Monitored ions for quinones. The asterisk indicates the ion used for quantitation.
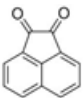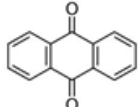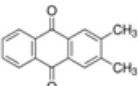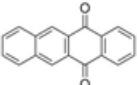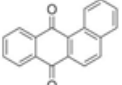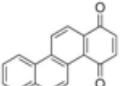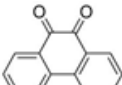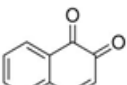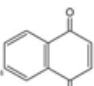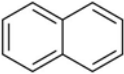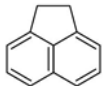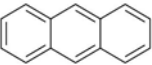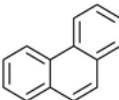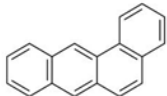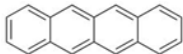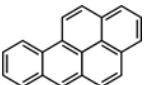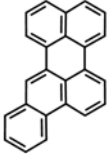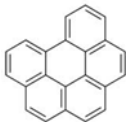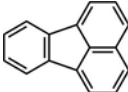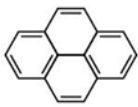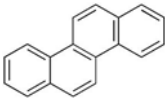
Quinone	Structure	Monitored Ions m/z
Acenapthenequinone		126*, 154, 182
Anthraquinone		208*, 180, 152
2,3-Dimethylanthraquinone		236*, 208, 180
5,12-Naphthacenequinone		258*, 202, 230
Benz[a]anthracene-7,12-dione		258*, 202, 230
1,4-Chrysenequinone		260*, 302, 344
9,10-Phenanthraquinone		210*, 252, 294
1,2-Naphthoquinone		160*, 202, 244
1,4-Naphthoquinone		160*, 202, 244

Table 4. Monitored ions for PAHs.

PAH	Structure	Monitored Ions *m/z*
Naphthalene		128
Acenaphthene		154
Anthracene		178
Phenanthrene		178
Benz[a]anthracene		228
Benz[b]anthracene		228
Benzo[a]pyrene		252
Benzo[b]perylene		252
Benzo[g,h,i] perylene		276
Coronene		276
Fluoranthene		202

| Pyrene | | 202 |
| Chrysene | | 228 |

Peak Identification. Qualitative identification of the quinones present in both the derivatized and un-derivatized samples was achieved by extracting the raw data files with the respective monitored ions for each quinone. The extracted ion chromatograms were inspected for quinone peaks in the same retention time range as seen in previously analyzed quinone standards. Identification of the quinones was further validated by inspecting the mass spectra of the identified peak. The most abundant ion in the mass spectrum of the peak should equal the monitored ion; otherwise, that peak was flagged as suspect. Quantitative analysis was then performed by manually integrating the quinone peaks to obtain an area count.

Method Validation

Signal/Retention Time Response. Gas chromatography/mass spectroscopy analyses were verified by examining a 1×10^{-5} M standard solution of 4,4-difluorobiphenyl (Aldrich) at the beginning and end of each batch. The standard solution is utilized as a reference for major shifts in the retention time or signal indicating that instrument maintenance is required. The threshold for the limit of detection and limit of quantification criteria, signals were required to be three times and six times greater than the noise, respectively. An internal standard was used to correct for the potential variation between analyses. Duplicate samples were analyzed if the internal standard looked suspect and replicates of known concentrations were run to test the variability in the extraction, derivatization, and concentration stages of the protocol.

Extraction and Concentration. The efficiency of the SLF extraction for spiked compounds onto a Teflon filter was determined with the presence with and without the addition of antioxidants to the SLF. Furthermore, the evaporation step was evaluated to determine if this would affect the extraction efficiency.

Instrument Response. The instrument signal response was evaluated by analyzing five replicate samples of a 1×10^{-4} M solution that contained phenanthraquione, anthraquinone, anthracene, phenanthrene, and deuterated phenanthrene. The standard deviation of the average of these five analyses was determined.

In this assay, deuterated phenanthrene was added to the extraction solution as an internal standard to correct for instrument variation. 15mL of dichloromethane (DCM) as added after 2 hours for organic extraction. The extraction solutions were evaporated using a Labconco N_2 blow down Rapid Evap. instrument. The samples were then reconstructed in DCM and analyzed by Gas Chromatography-Mass Spectrometry (GC-MS).

Method Development

The GC-MS used in this work incorporated a PTV inlet, allowing for the introduction of much larger sample volumes compared to previous measurements in our lab. Signal responses for quinone standards were measured as a function of sample injection volume to establish the relationship between these parameters. We found that signal response is essentially linear for injection volumes between 5 and 100 μL, and so detection limits can be significantly improved by introducing larger samples, reducing the need for derivatization.

II.B.10 DTT Consumption Assay

We measured the rate of dithiothreitol (DTT) loss during incubation of a punch (2.28 ± 0.08 cm^2) from each sample filter strip in reaction solution (Chelex-treated 0.10 M phosphate buffer, pH 7.4, and 100 μM DTT,) at 37 °C (Cho et al., 2005; Charrier and Anastasio, 2012; Charrier et al., 2015). We allowed each solution vial to warm for 3 min, then placed the filter punch at the bottom of the vial, added 50 μL of 50% trifluoroethanol (TFE) to the filter to wet it, added 3.0 mL of reaction solution, recorded the start time of reaction, and turned on the shake table for a few seconds to mix the solution. We then monitored the loss of DTT as a function of reaction time using a UV-Vis spectrophotometer (Charrier and Anastasio, 2012). Each sample was measured 2-4 times. Every experiment day we also measured a solution blank in duplicate (i.e., reaction solution with no added filter) and a positive control (0.50 μM CuSO$_4$), both with TFE added. The average (± 1σ) solution blank and positive control values for our experiments were 0.20 ± 0.10 (n = 60) and 0.75 ± 0.09 (n = 30) μM/min, respectively. We also occasionally ran a filter blank, which was a solution blank with a punch of unsampled filter in it; the average value of this blank (after solution blank correction) was 0.07 μM/min. The reported DTT rate for a given sample is the average value of the replicates after subtraction of the solution blank and filter blank.

Rates of DTT loss were normalized in two ways: by PM mass extracted (to give units of pmol DTT min^{-1} μg^{-1}) and by air volume sampled (pmol DTT min^{-1} m^{-3}-air). As we described below, the mass-normalized results depend on the mass concentration of PM used in the assay when Cu and/or Mn are major contributors to the DTT response. This is a consequence of the non-linear concentration-response curves for Cu and Mn (Charrier and Anastasio, 2012). To correct for this bias, we used the "calculation" method to determine the mass-normalized rate of DTT loss at a standard particle concentration in the extract of 10 μg mL^{-1}. This involves measuring the concentrations of Cu, Mn, and other DTT-active species in each sample extract and then using concentration-response curves (e.g., the rate of DTT loss as a function of Cu concentration in the extract) to adjust the measured DTT rate to that expected for a 10 μg mL^{-1} extract. During this work we determined that the equation of the Cu concentration-response curve from previous work (Charrier and Anastasio 2012a) generally under-predicts the DTT response for low Cu concentrations. We re-analyzed the Cu concentration response data to provide better DTT prediction at low Cu concentrations by using a regression to fit Cu concentrations between 0 and 1.5 μM Cu. The updated Cu concentration-response used for this analysis is

$$Y = 0.982X^{0.3279}$$

where *Y* is the DTT response in µM per minute and *X* is the soluble Cu concentration in µM.

II.B.11 Mass/flow rate correction

During the field campaigns, the UCLA group controlled sample flow using rotameters, which are standard ball pressure flow meters. The rotameters appear to have been designed so that the flow calibration is accurate for flows from a pressurized source, leading to atmospheric pressure at the end of the sample stream, not for the sample train we have been using in which the sampling train begins at atmospheric and ends in a vacuum (i.e., flow is driven by a pump). To insure that our sampling trains were assembled correctly during field campaigns, we periodically checked masses on the filters, and found that they were always within 5-8% percent, or better, of one another. However, as we were unaware of the flow reading issue, our flows were not at the desired flow rate. To determine the actual flow rate, we used two independent instruments: a TSI model 4043 digital flow meter, which we had calibrated by the company in September, 2013, and an MKS Baratron (PDR-C-2C). The digital flow meter also reports temperature and pressure. These were arranged in series downstream of the flow meter, and the remainder of the sample train was assembled as usual: Teflon coated cyclone (URG-2000-30ENB), loaded filter holder, followed by the rotameter (2 Kings Instruments 7530, and 2 unlabeled rotameters), consisting of a needle valve and float tube, followed by the Baratron on a T connector, digital flowmeter, and pump (Gast, 2607-V108), as shown in Figure 4.
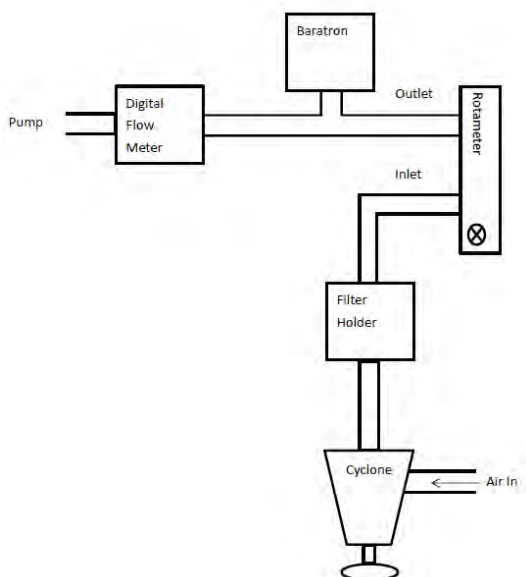
Figure 4. Schematic of setup for flow rate measurement/calibration.

Table 5 shows a collection of data of measurements for our sampling train. The gauge flow rate needs to be corrected using an expression accounting for the change in the buoyancy force due to the actual pressure of the air in the measurement tube. It may also need to be corrected for temperature, however this correction is usually small.

Table 5: Rotameter flow correction data

Noncorrected Rotameter (LPM)	Digital flow meter (LPM)	Pressure Digital (kPa)	Temp (K)	Pressure Baratron (kPa)	Correction factor	Corrected flow rate (LPM)	Size cut point (microns)
92 (king)	54.2±0.4	27.8±0.2	294.6±0.7	32.4±0.4	0.56±0.001	51.8±0.1	4.0±0.007
92 (Cole Palmer, old)	48.9±1.1	25.4±0.1	294.6±1	29.8±0.4	0.54±0.004	49.8±0.4	4.1±0.03

The fundamental expression, arising from the ideal gas law and an analysis of the balance of drag, buoyancy and gravitational forces on the float in the tube, (e.g., float weight = drag – buoyancy. For the situation in which air is used as both the reference gas and the gas of interest then the correction factor (c.f.) is:

$$c.f. = \sqrt{\frac{P_S T_R}{P_R T_S}}$$
                                                                Equation II.B.1

Where $P_{s,R}$ and $T_{s,R}$ are the pressure or temperature for the sample or reference, respectively. A key point is that the correction factor is used for the pressure that the float experiences; downstream of the flow meter. We note that many formulae for flow rate correction are available on manufacturer websites, in different formats and units. Some of these are verifiably incorrect, while some others indicate various assumed definitions of "standard temperature and pressure", and so on. Table 5 also shows the corrected flow rates, calculated from the measured pressures from the two gauges. As the digital flow meter measures gas flow using conductivity, it is insensitive to pressure and temperature within a reasonable range. Further, as it was recently calibrated, we believe it is the most reliable measure of pressure. Table 5 show the correction factors calculated from the pressure (using Baratron for the 3rd calibrations and digital flow meter for the 1st and 2[nd]calibration) and temperature measured from the digital flow meter and the Baratron using the formula above. The corrected flow rate can be calculated as a result as well as its corresponding size cut point. To correct the mass concentrations, we used the corrected flow rate from the pressure measured with the Baratron, as it is directly connected to the outlet of the flow meter and presumably provides the best estimate of the pressure experienced by the top of the float in the rotameter. Additionally, its values lead to a corrected flow rate that is closer values to the flow rate measured by the digital flow meter than the pressure reported by the latter.

Using this corrected flow rate, we can correct our aerosol mass concentration data. The size cut point was obtained from the following expression (where Q is the flow rate):

$$Cut\ Point = 99.6\ Q^{-0.82}$$
                                                                Equation II.B.2

The expression is for the URG cyclone (URG-2000-30ENB), derived from data obtained from manufacturer.

The lower actual flow rate changes the calculation of aerosol mass concentration based on measured filter mass in two ways: first, the flow rate is lower, and second, the aerosol size cut point is larger. The corrected flow rate for the setting used in the field of 92 LPM is 51 LPM, which corresponds to a size cut point of 4 microns.

44

III. Laboratory Results: See Part II of Report.

IV. Field Campaign Results

IV.A. Chemical Composition of Particles

IV.A.1 Mass

Fresno exhibited much higher average mass concentrations (33 ± 15 µg/m^3) compared to Claremont (23 ± 5 µg/m^3), even though there were three rain events during the Fresno field campaign. Diurnal variations in mass concentration were modest at both sites.

VI.A.1.1 Claremont

Generally, our results correlate well with time series measurements from the nearest SCAQMD sites at Upland and Glendora (Figure 5). The measurement locations are separated by several kilometers, and the Claremont measurements were made on the top of a tall building, while the SCAQMD sites are less than 10 m above ground level (AGL), so perfect agreement is not expected. The average mass concentration measured at Claremont was 98% of the Upland measurement, and 27% higher than Glendora.
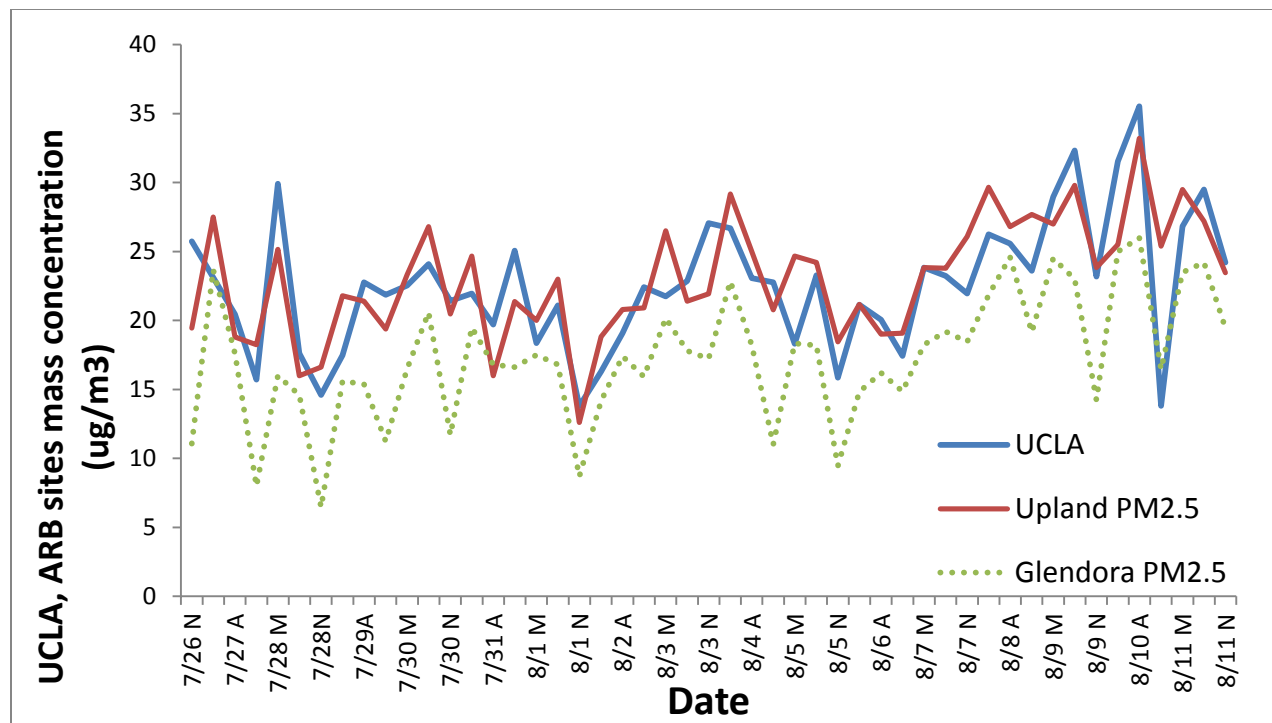
Figure 5. Mass concentration for each sample interval. Data from SCAQMD sites were averaged to match the sampling campaign.

Because our size cut point is slightly larger than 2.5 microns, we also compared our results with the coarse and PM$_{10}$ data obtained from the SCAQMD for the Glendora site (Upland did not have coarse data available). Examination of the time series shows (as expected; typically, not so

much mass resides in the 2.5 – 4 µm range) our PM4 correlates much more strongly with PM2.5 than PM 10. We attempted to improve correlations by calculating a linear combination of the SCAQMD PM2.5 and coarse mass (PM10 – PM2.5), to see if we could improve the fit. Figure 6 shows the correlation of Glendora PM2.5 and UCLA PM4 with 0, 8, 10, 15 or 20% of the Glendora PM10 – PM2.5 subtracted from it. As more of the coarse mass is subtracted in an effort to "correct" the PM4, the correlation does improve very slightly (R^2 = 0.509 vs. 0.502) and the intercept decreases (9.745 vs. 9.945) slightly for 8 and 10% subtracted, above that the correlation progressively degrades.

VI.A.1.1 Fresno

Figure 7 shows time series for co-located CSUF2.5 and UCLA PM4 as well as measurements at two ARB-operated sites: PM2.5 at Clovis-N. Villa, and PM2.5 and PM10 at Garland St. Our PM4 correlates best with Clovis-N. Villa, followed by CSUF (for which only a partial data set is available), then by Garland St. PM2.5, and Garland St. PM10 (Figure 7), with Deming regression R^2 values of 0.94, 0.88, 0.83, and 0.76 respectively. Unfortunately, neither the CSUF nor the Garland datasets are complete, and the period for which all measurements are available is relatively limited (Figure 7).
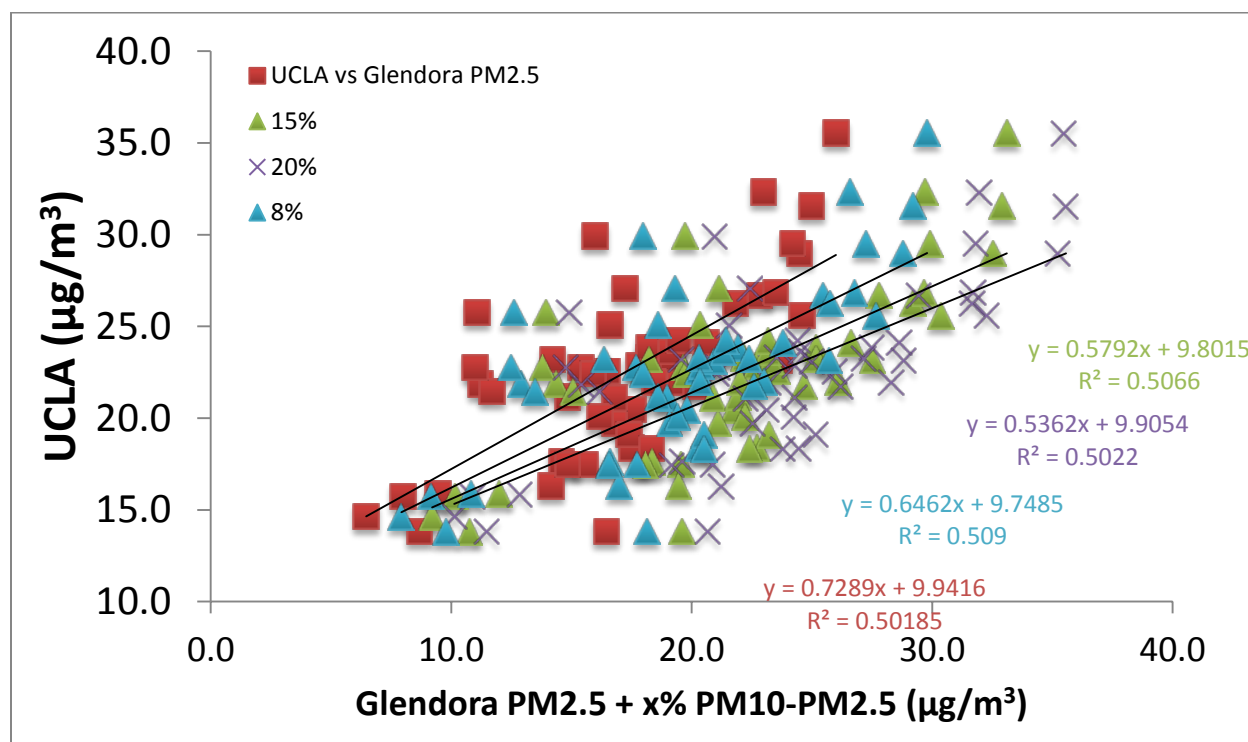
Figure 6. UCLA PM4 vs. Glendora PM2.5 + 0 (red squares), 8 (blue triangles), 15 (green triangles) and 20 (purple crosses) % of the Glendora coarse measurement (PM10 – PM2.5).

46
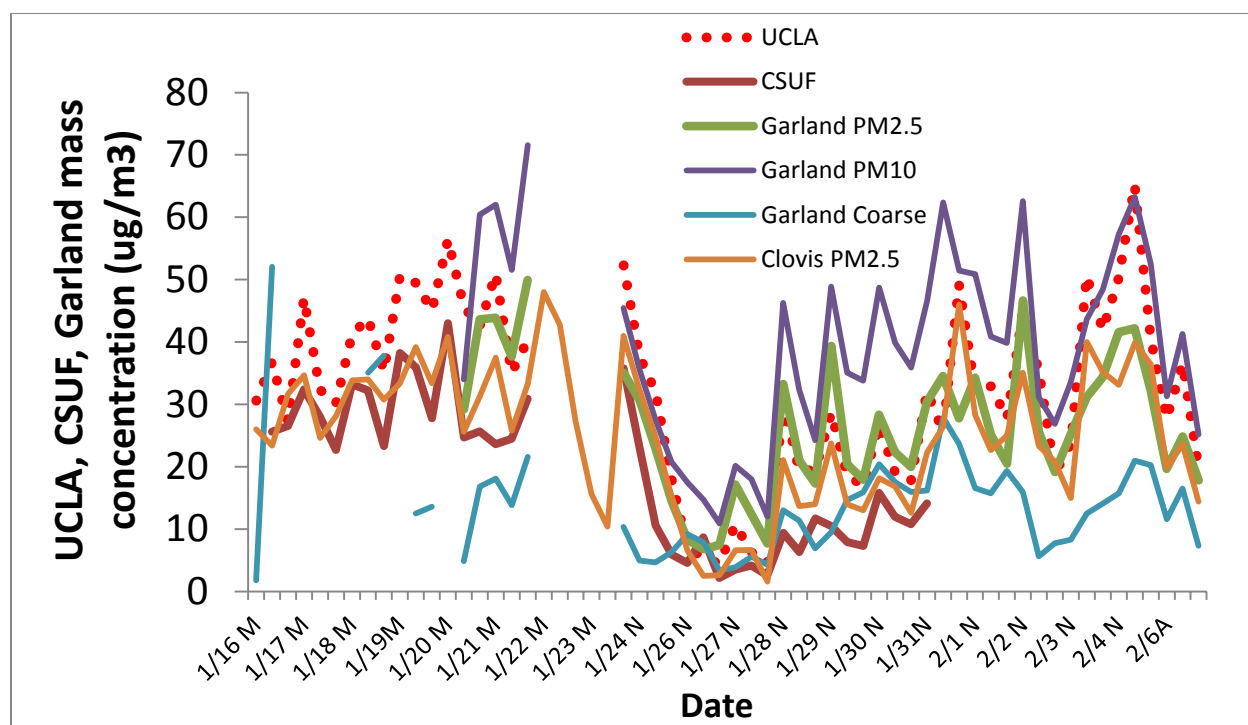
Figure 7. Mass concentration for each sample interval at the nearby Garland and Clovis sites, in addition to measurements of PM2.5 collected by CSUF and PM4 collected by UCLA.

The UCLA measurements vs. all three PM2.5 measurements have nearly the same slope, 1.28 (range 1.25 – 1.31) and intercepts that range from -4.15 to +5.25 μg/m^3. We note that we have used Deming regressions because we are comparing two measurements of the same parameter; neither is dependent on the other and both contain measurement errors. Based on these data, we conclude that about 22% of the measured mass is coarse material. This corresponds to an average of 56% of the Garland St. PM10 – PM2.5 values, although the UCLA values are much better correlated to the measurements at the geographically closer Clovis-Villa and CSUF sites, and coarse mode concentrations can be more variable that PM2.5 measurements. We attempted to improve the correlation with the CSUF measurements by subtracting a fraction of the coarse mode mass (PM10 – PM2.5) from the Garland St. site from the UCLA measurements (not shown), and while subtracting coarse mass brings the UCLA data in somewhat better agreement with the CSUF data in absolute terms the correlation was degraded by doing so.

IV.A.2 HULIS

Absorbing carbon was clearly visible on the filters, and is attributed do residential wood burning (above). Estimates of the HULIS content were made by measuring optical absorption at 370 and 880 nm, for brown carbon and black carbon respectively; the results of the 370 nm estimate are shown in Figure 8. Morning and night samples contained similar contributions from HULIS, while afternoon samples had substantially less. We note that most of the contribution of HULIS appears as an intercept, suggesting that the contribution of HULIS is relatively constant from night to night, while other sources of PM vary. While the contribution of a measurement

artifact in the HULIS estimate (which is notoriously difficult) cannot be ruled out entirely, there is more absorbing material on the night and early morning samples.
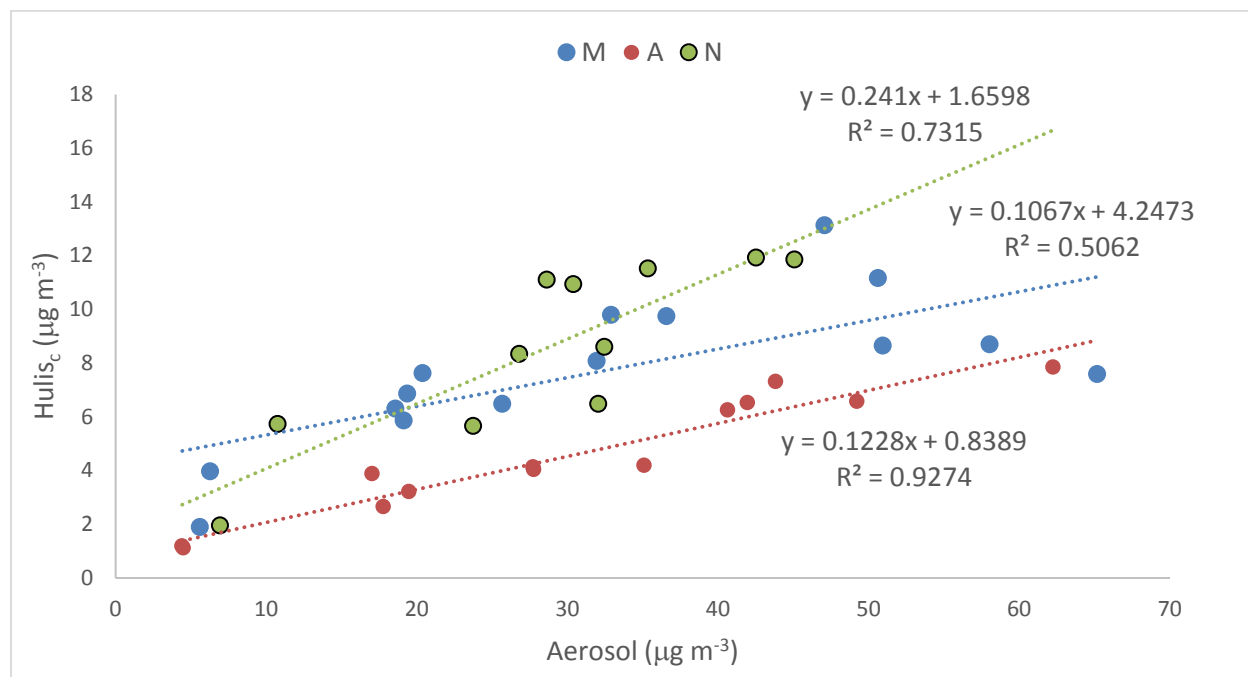
Figure 8. HULIS mass concentration vs. aerosol mass concentration in the Fresno samples; red afternoon, blue morning, and green nighttime samples.

IV.A.3 Soluble metals and speciated iron

Several metals and other elements measured by ICP-MS were below the detection limits. Species that were above the detection limit are summarized in Table 6.

Table 6. Species measured with ICP with signals above detection limits.

UCLA	Claremont (Entire data set)	V	Mn	Fe	Cu	Se	La	Fe(tot) 2hr	Fe(tot) 24hr
	A & N	Cr	Co						
	Fresno (entire data set)		Mn	Fe	Cu	Zn	Pb	Fe(tot) 2hr	Fe(tot) 24hr
Davis	Claremont	V	Ni		Cu		Pb		
	Fresno				Cu		Pb		

Detection limit criteria:

UCLA: Median of sample-(median of blank+2*SD of blank)

UC Davis: metals are above 2*blank.

Table 7 shows average results for soluble speciated iron measurements compared to measurements in the literature. As expected, soluble iron concentrations are higher for extraction solutions at pH 3.5 compared to SLF. The average values are nearly identical for Claremont and Fresno, although the Fresno data are much more variable. Further, the ratio of Fe(II)/Fe(tot) is quite similar between the two measurements; in pH 3.5 solution Fresno appears more reduced, as expected for wintertime particles, but the SLF solution appears to act to adjust the oxidation state of iron.

We note that all of these measurements were made with the Ferrozine method, which measures only Fe(II) directly; Fe(total) is measured after addition of a reductant, and Fe(III) is measured by difference of Fe(total) and Fe(II). The literature values are limited, with a few more measurements available for Fe(II) than Fe(total). Our measurements of Fe(II) and/or Fe(tot) are consistent with those of Oakes et al. (2010, 2012) and Majestic et al. (2007) for urban areas, but significantly lower than the measurements of Upadhyay et al. (2011), for several sites in Arizona, and a measurement at a rural site in Georgia (Oakes et al. 2012).

Table 7. Comparison of soluble speciated iron concentrations in ambient PM$_{2.5}$

Particle type	Season	Extrac-tion	Fe(tot) (ng/m^3)	Fe(II)	Fe(III)	Fe(II)/Fe(tot)	References
Claremont, CA	Summer	pH3.5	13.7±8.8	8.1±8.0	5.6±3.5	0.53±0.22	This study
Fresno, CA	Winter		15.1±8.6	9.6±6.7	5.3±5.1	0.63±0.23	
Claremont, CA	Summer	SLF	8.3±2.9	5.9±2.6	2.4±1.6	0.71±0.18	This study
Fresno, CA	Winter		8.8±10.6	6.2±8.6	2.6±3.5	0.70±0.28	
PM$_{2.5,}$ Fort	Summer		4.3±0.17	2.0±0.08	2.3±0.19[*]	0.47±0.06	
Yargo (Winder GA, rural)	Winter	DI water	5.8±0.23	4.9±0.2	0.9±30[*]	0.84±0.10[*]	(Oakes et al. 2012)
Fire station 8	Summer		13.6±0.18	4.6±0.06	9.0±0.18[*]	0.34±0.03[*]	al. 2012)
(Atlanta, GA,	Winter		49.9±1.64	30.0±1.0	19.9±1.92[*]	0.60±0.05[*]	
Fort	Summer		12.9±0.14	4.0±0.04	8.9±0.15[*]	0.31±0.01[*]	
McPherson	Winter		12.2±0.2	6.9±0.09	5.3±0.18[*]	0.57±0.05[*]	
S. DeKalb	Summer		10.8±0.2	5.8±0.01	5.0±0.024[*]	0.54±0.003	
(Atlanta, GA, urban)	Winter		3.4±0.07	3.0±0.06	0.4±0.09[*]	0.88±0.03[*]	
E. St Louis, IL Los Angeles, Waukesha, WI		Acetate buffer, (pH4.3)	10.8±4.4	7.6±4.1	3.1±2.1[*]	0.71±0.20[*]	(Majestic et al. 2007)
Parking garage[a] ASU, AZ		Acetate buffer,	42.9±5.2	41.6±4.7	1.3±7.0[*]	0.97±0.16[*]	(Upadhyay et al. 2011)
Life Science bldg, ASU, AZ[a]		(pH4.3)	46.7±8.5	46±8.2	0.7±8.2[*]	0.99±0.25[*]	
Post office at US-Mexico border, AZ			31 ± 11	31 ± 11		1±0.5[*]	
CSUF, CA[b]			18±10	17 ± 9	1.2±13.6[*]	0.93±0.73[*]	
Atlanta, GA	Spring			14.8±13.7			(Oakes et al. 2010)
	Summer	PILS[c]		13.4±28.3			al. 2010)
Dearborn, MI				17.7±26.3			

Table 8 shows average metal concentrations measured by UCLA using ICP. Some metals are more soluble in SLF, such as Cu and Se in the Claremont samples and others are more soluble in pH 3.5 extraction solutions, such as iron in all samples.

Table 8. Comparison of several transition metal concentrations in ambient particulate matter

PM Size	Location	Season	Extraction Solution	V	Cr	Mn	Fe (ng/m³)	Ni	Cu	Zn	Se	Pb	Ref
PM₄	Claremont	Summer	pH3.5	0.9±0.4	0.35±0.14	3.5±2.1	167±361		33±18	56±34	0.84±0.71	3.5±1.7	This study
			SLF	1.7±1.3		3.9±1.8	53±29		99±50		4.5±4.9		
PM₄	Fresno	Winter	pH3.5		0.5±0.2	2.9±1.4	121±69		30±16		0.49±0.41	5.5±3.9	
			SLF			0.6±0.6	7.4±12.5		35±31	23±38			
PM₂.₅	Riverside, CA	Summer	pH3.5				118±99		92±83	55±28		12±8	Wang et al. 2010
Ultrafine	Los Angeles-Long Beach Harbor	March - May	Water	1.8-5.4	0.01-0.06	0.1-0.7	1.1-3.5	0.6-1.6	0.8-2.1	1.9-5.4			Hu et al., 2008
Fine				0.8-1.7	0.02-0.04	0.4-1.3	3.1-11.8	0.4-0.5	0.9-3.0	3.9-6.9			
Coarse				0.1-0.7	0.06-0.3	0.3-1.6	0.1-1.8	0.08-0.3	0.6-2.9	2.1-6.5			
PM₂.₅	Singapore (Urban)	December 2005	Water			6.0±0.4	74.5±0.4		361±295	102±6			See et al. 2006
PM₂.₅	Megalopolis Greece (Industrial)			0.25	0.79	1.28	8.51	2.06	0.94	51.7		2.90	Manousakas Et al. 2014
	Patras, Greece (Port)	Yearlong	Ultra-pure water	1.33	1.25	1.25	11.9	4.92	2.67	163		3.16	
PM₂.₅	Steubenville Ohio	yearlong	DI water w/ 2% isopropanol	1.04		7.8	19.6	0.7	3.2	55.6	4.7	8.9	Connel et al. 2005
Ultrafine	Beirut Lebanon	July-August (2011)		6.03±1.69	0.03±0.01	1.5±0.5	5.9±3.2	3.5±0.9	12.4±6.9	25.5±6.7		1.6±1.7	Daher et al. 2014
Fine				8.5±0.6	0.09±0.01	2.9±0.4	17.9±2.6	3.9±0.2	16.2±5.7	36.8±5.5		3.3±1.4	
Coarse				0.07±0.02	0.08±0.04	1.9±0.2	3.2±0.3	0.14±0.02	5.8±2.8	12.6±2.3		1.1±0.98	
PM₂.₅	Thessaloniki, Greece	Winter (2012, 2013)	Milli-Q Water	0.44±0.05	0.07±0.01	1.7±0.2	4.97±0.99	0.3±0.1	0.6±0.1	16.5±2.5		1.6±0.25	Saffari et al. 2013
PM₂.₅	Lahore, Pakistan	Yearlong	Water	0.99±0.36	1.09±0.35	63±11.8	18.9±7.2	3.5±0.2	5.5±1.3	291±189		53±19	Shafer et al. 2010
Coarse				1.05±0.37	1.08±0.28	91.6±11	21.6±6.2	2.9±0.4	8.3±1.6	231±1738		1.02±0	
PM₂.₅	Denver, CO	Yearlong	MQ Water	0.07±0.01	0.05±0.01	1.03±0.1	6.0±0.7		0.47±0.1	1.3±0.2	7.4±1.3	0	Zhang et al. 2008

PM Size	Location	Season	Extraction Solution	V	Cr	Mn	Fe (nmol/mg)	Ni	Cu	Zn		Pb	Ref
PM₄	Claremont	Summer	pH3.5	0.9±0.5	0.36±0.21	2.8±1.5	126±251		24±14	37±20		0.8±0.4	
			SLF	1.6±1.4		3.4±1.9	46±32		80±38				This study
PM₄	Fresno	Winter	pH3.5		0.5±0.6	2±1	65±35		16±13			1±0.6	
			SLF			0.8±	7±		54±	60±			

51

				0.9	8		118	94	
PM$_{2.5}$	Davis, CA	Spring		0.5± 0.4	2.9± 1.8	18± 11	1.6± 1.3	2.9± 1.7	Vidrio et al. 2009
		Summer	SLF	1.4± 0.8	2.7± 2.0	26± 13	0.9± 0.7	4.1± 5.9	
		Fall		0.5± 0.4	4.0± 4.3	37± 10	2.3± 0	1.3± 0.3	
		Winter		0.1± 0.6	3.0±1.5	13± 4	2.5± 1.9	3.9± 2.1	

Correlations among metals are reported in Table 9 and Table 10, for Claremont and Fresno, respectively. Strong correlations between V, Mn, Fe, Cu, Se and La in Claremont measured by the UCLA group are observed, with correlation coefficients > 0.6. Such correlations were observed in the Fresno samples but much less significant.

Table 9. Correlations among metals, Claremont, SLF, non-mass corrected (in nmol). Correlation coefficient is reported and bolded values indicate significant correlations (p <0.05).

		V	Mn	Fe	Cu	Se	Cd	La	Fe(tot) 2hr	Fe(tot) 24l
UCLA Measurement	V	1	**0.70**	**0.75**	**0.65**	**0.76**	-0.38	**0.76**		
	Mn			**0.96**	**0.93**	**0.71**	-0.41	**0.83**		
	Fe				**0.88**	**0.74**	**-0.39**	**0.84**		
	Cu					**0.66**	-0.38	**0.80**		
	Se						-0.30	**0.96**		
	Cd							**-0.39**		
	Fe(tot) 2hr	**0.45**	**0.70**	**0.80**	**0.65**	**0.40**	-0.06	**0.50**		
	Fe(tot) 24hr	-0.15	-0.22	-0.16	-0.30	-0.16	-0.22	-0.24		
Davis Measure	Cu	**0.53**	**0.73**	**0.75**	**0.84**	**0.50**	-0.11	**0.63**	**0.69**	-0.27
	Ni	-0.09	-0.13	-0.06	-0.23	0.10	**-0.70**	0.10	-0.11	0.12
	Pb	**0.49**	**0.75**	**0.75**	**0.63**	**0.63**	-0.16	**0.69**	**0.59**	-0.16
	V	**0.84**	**0.46**	**0.52**	0.34	**0.63**	**0.45**	**0.63**	0.19	-0.22

		Mn	Fe	Cu	Zn	Pb	Fe(tot) 2hr	Fe(tot) 24hr
UCLA Measurement	Mn	1	**0.61**	**0.55**	**0.62**	**0.54**		
	Fe			**0.39**	**0.43**	**0.44**		
	Cu				**0.43**	**0.65**		
	Zn					0.21		
	Fe(tot) 2hr	0.14	-0.083	0.19	-0.085	**0.44**		
	Fe(tot) 24hr	-0.031	0.018	-0.026	-0.16	0.35		
Davis	Cu	**0.56**	**0.34**	**0.78**	**0.45**	**0.66**	0.34	0.29
	Pb	**0.55**	**0.44**	**0.61**	**0.40**	**0.71**	0.25	0.14

IV.A.4 Quinones and other organics

Method Development

The GC-MS used in this work incorporated a PTV inlet, allowing for the introduction of much larger sample volumes compared to previous measurements in our lab. Signal responses for quinone standards were measured as a function of sample injection volume to establish the relationship between these parameters. We found that signal response is essentially linear for injection volumes between 5 and 100 μL, and so detection limits can be significantly improved by introducing larger samples, reducing the need for derivatization.

Claremont
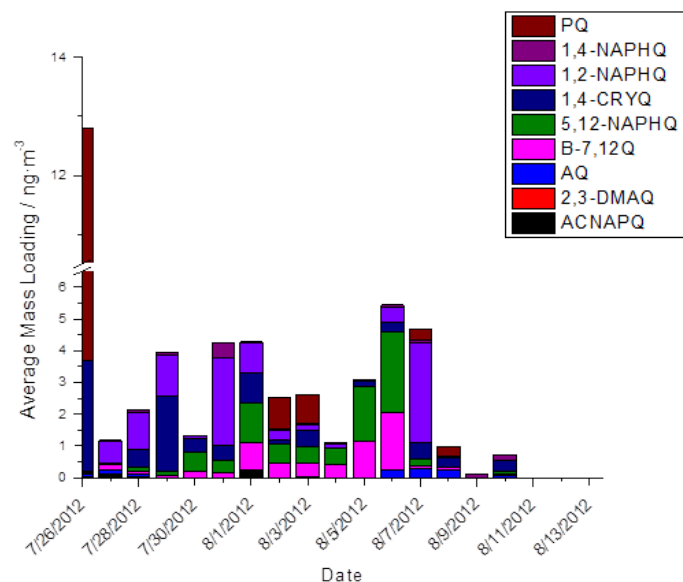
Figure 9. shows quinone measurements from PUF samples. The major quinones in the vapor-phase are 1,2-naphthoquinone (2.9 ± 0.7 ng m^{-3}), 1,4-chrysenequinone (0.6 ± 0.6 ng m^{-3}), benzo[a]anthracene-7,12-dione (0.11 ±0.06 ng m^{-3}), with trace amounts of anthraquinone (0.03 ±0.015 ng m^{-3}) between 7/28/12 – 08/02/12.
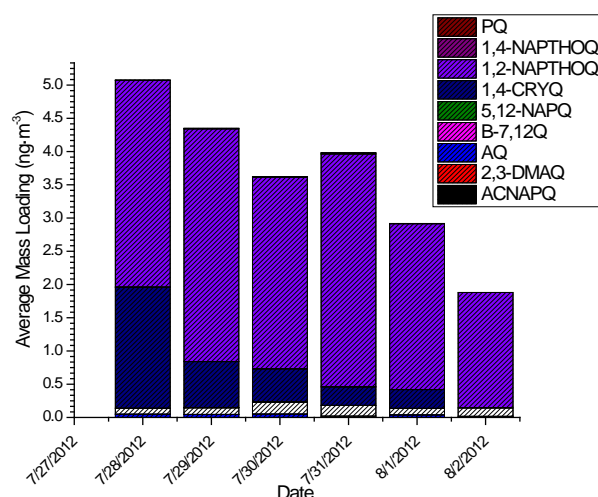
Figure 10. Gas phase quinone mass loadings measured in Claremont, CA during summer 2012

Quinone mass loadings. Total contributions of particle phase quinone mass loadings measured for both soluble organics in surrogate lung fluid and organic soluble solvent extraction were combined and are shown in Figure 9. The total quinone masses were examined for each sampling date from 7/26/12 to 8/13/12. The total bar represents all of the particle-phase quinones observed and the fraction of each individually contributing quinone. The predominant quinones present were 1,2-naphthoquione (0.59 ± 0.93 ng m^{-3}), 1,4-naphthoquinone (0.074 ± 0.10 ng m^{-3}), 1,4-chrysenequinone (0.46 ± 0.90 ng m^{-3}) and benz[a]anthracene-7,12-dione (0.46 ± 0.68 ng m^{-3}). Similar trend was observed for the gas phase quinone mass loadings (Figure 10), with 1,2 –naphthoquinone and 1,4-naphthoquinone being the most abundant quinones in the gas phase.

The distribution of particle and vapor phase quinones collected between 7/28/12 -08/02/12 where a complete data set was analyzed is shown in Figure 11. Quinones with lower molecular weights and higher vapor pressures tend to have greater mass fractions in the gaseous phase than heavier, lower vapor pressure compounds. Hence, 1,2- and 1,4-naphthoquinones are more likely to be found in the vapor phase. The vapor-phase portion accounts for 42% of the total measured quinone. Phenanthraquinone, anthraquinone, and 5,12-naphthoquinone are only seen in the particle-phase. The measurements demonstrate that quinones with higher vapor pressures/lower boiling points (e.g., 1,4-naphthoquinone vs. 1,2-naphthoquinone) are more likely to be found in the vapor phase, which is consistent with the literature. The fraction that contains the particle phase quinones accounts for about 58% of the total gas and particle phase quinones across the data set and is in reasonable agreement with other measurements in the region. For example, previous measurements in the LA basin indicate that vapor phase quinones account for approximately 80% of the total mass collected (Eiguren-Fernandez et al. 2008a).

54
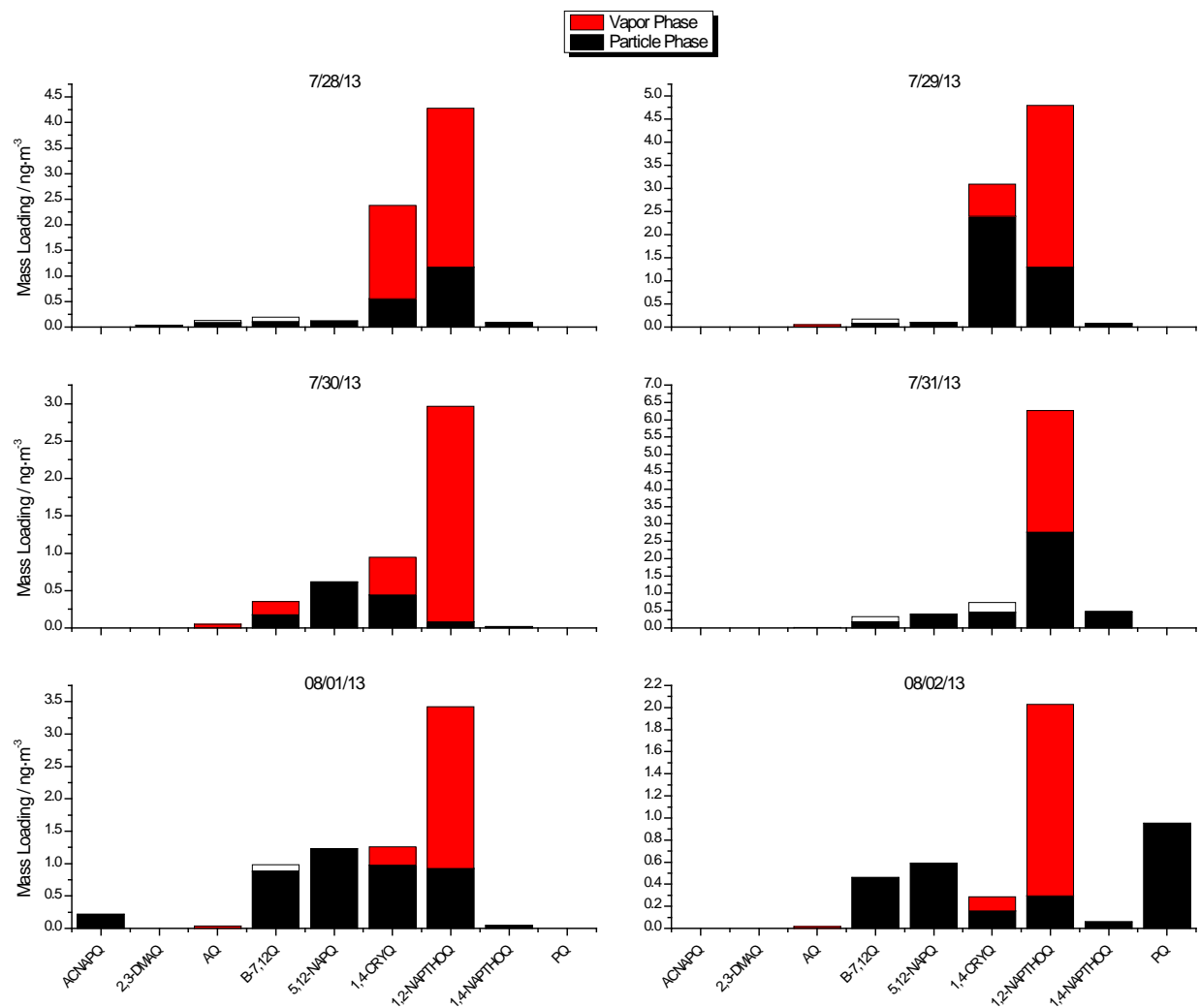
Figure 11. Relative quantities of particle and gas phase quinones in Claremont, CA during Summer 2012.

Vapor-Phase PAH Mass Loadings. Vapor-phase PAHs were analyzed using PUF plug extracts collected between 7/28/12 – 08/02/12. Figure 12 shows the mass distribution of vapor-phase PAHs. The predominant PAHs observed were pyrene (7.1 ±8.4 ng·m^{-3}), naphthalene (1.2 ±1.3 ng·m^{-3}), fluoranthene (5.1 ±5.2 ng·m^{-3}), benz[a]anthracene/chrysene (0.06 ±0.14 ng·m^{-3}) and phenanthrene/anthracene (1.6 ±1.9 ng·m^{-3}) in the vapor-phase.
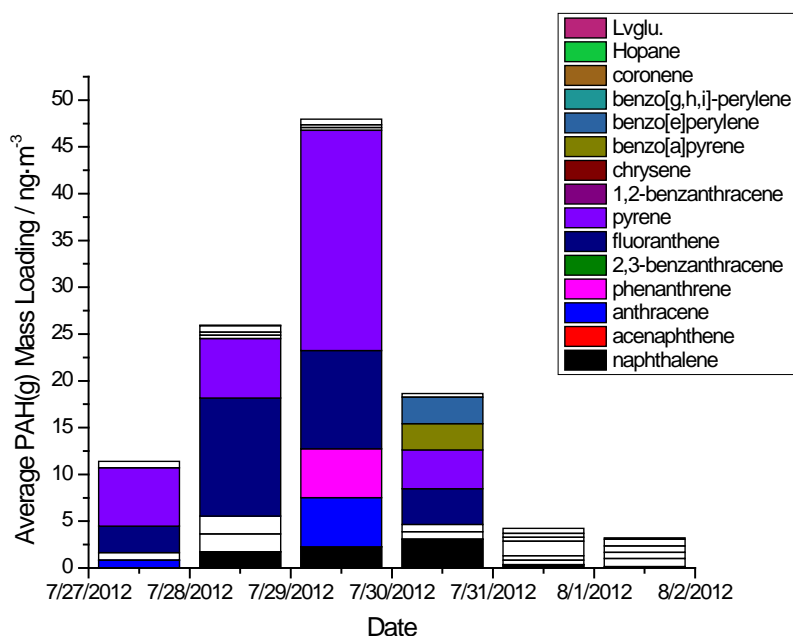
Figure 12. Gas phase concentrations of PAHs collected in Claremont, CA during summer 2012.

Ambient PAH and Quinone Correlation.

The relationship between the average PAH mass loading for each sampling period was and the respective quinone mass loading was evaluated. Any statistically significant correlation was based on the correlation coefficient for each pair. Three of the five sets of comparisons have p-values that are or very close to statistically significant relationships between the parents PAH and the respective quinone. Correlations were found between 1,2-naphthoquinone ($p = 0.021$) and 1,4-naphthoquinone ($p = 0.051$) with its respective parent PAH, naphthalene, as well as for 1,4-chrysenequinone with chrysene ($p = 0.057$). Mass loadings of anthracene-anthraquinone and phenanthrene-phenanthraquinone were not correlated.

Back Trajectory Analysis.

The back trajectories of the measured organics were calculated using the Hybrid Single Particle Lagrangian Integrated Trajectory Model (HYSPLIT) software distributed by NOAA. Within this project, the HYSPLIT model was used to map the back trajectories of the sampled air mass every hour over a 12-hour period for the entire sampling period for Claremont samples, and for 24-hour period for Fresno samples. We examined a 20x20 square grid domain with back trajectories plotted within the region of interest. The concentrations of measured organics were tagged to these back trajectories points. The concentrations of quinones measured within each grid square were then averaged to give the mean mass loading of the compounds for air masses passing through the grid square, resulting in a set of heat maps. In these plots, the colors represent the average concentration for air masses that passed through the corresponding grid square (red = high to blue = low).

56

Spatial Distributions of Measured Quinones and Vapor-Phase PAHs.

The HYSPLIT model was used to calculate back trajectories within the region to generate the heat map shown in Figure 13 for 1,2-naphthoquinone. The map suggests that 1,2-NQ and/or its precursors originated near or off the coast SW of the sampling site. Vapor phase quinones shown in the PUF Figure 13b, show a qualitatively similar pattern. Other quinones show a similar pattern, with air masses passing close to Long Beach containing the highest mass loadings as shown in Figure 14.
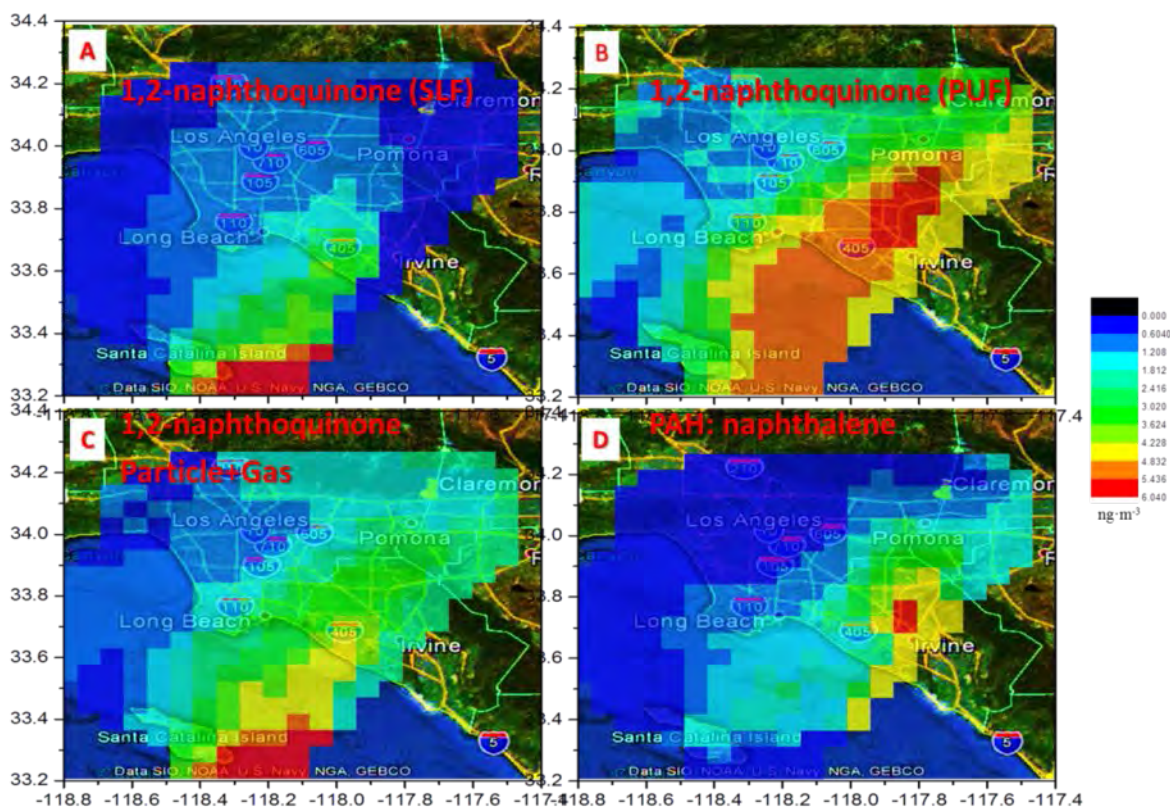
Figure 13. Back trajectory analysis of gas and particle phase 1,2-naphthoquinone, and gas phase naphthalene for samples collected in Claremont, CA during Summer 2012 (see text for details).

57
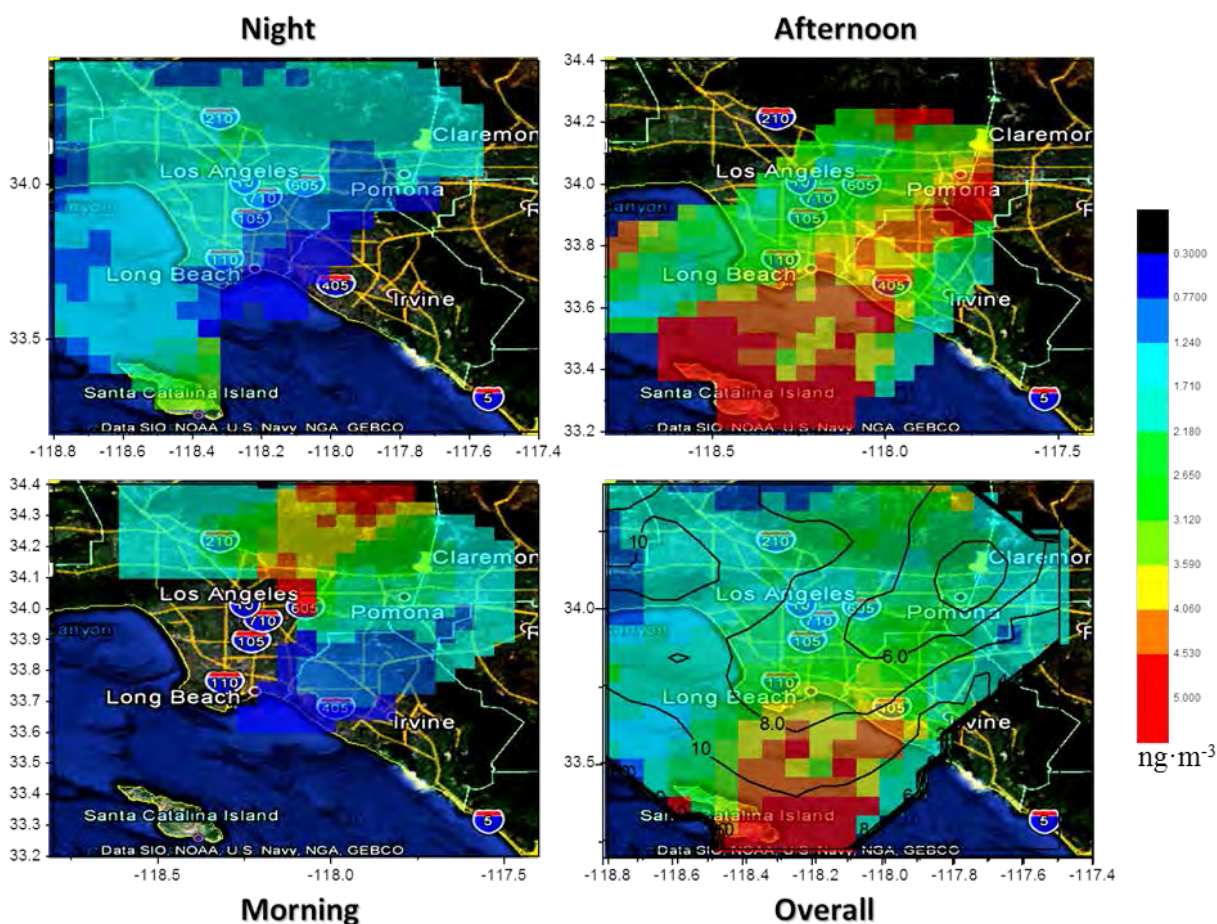
Figure 14. Back trajectory analysis for the sum of quinones measured in Claremont, CA in Summer 2012 (see text for details). Plots are shown for each collection period (Night: 6 pm – 7 am; Morning: 7 am – 1 pm; and Afternoon: 1 pm – 6 pm) as well as for the entire set of samples. Contours in the lower-right panel show the average time for the air mass to reach the collection site in hours.

Temporal Analysis

PAH. Vapor-phase PAH mass loadings were averaged by their collection times, as shown in Figure 15. These levels were compared using a two-tailed student t-test. Afternoon mass loadings were found to be highest, followed by Night samples, with Morning mass loadings lowest. The mean values for all three periods are significantly different from each other at the 95% confidence level.
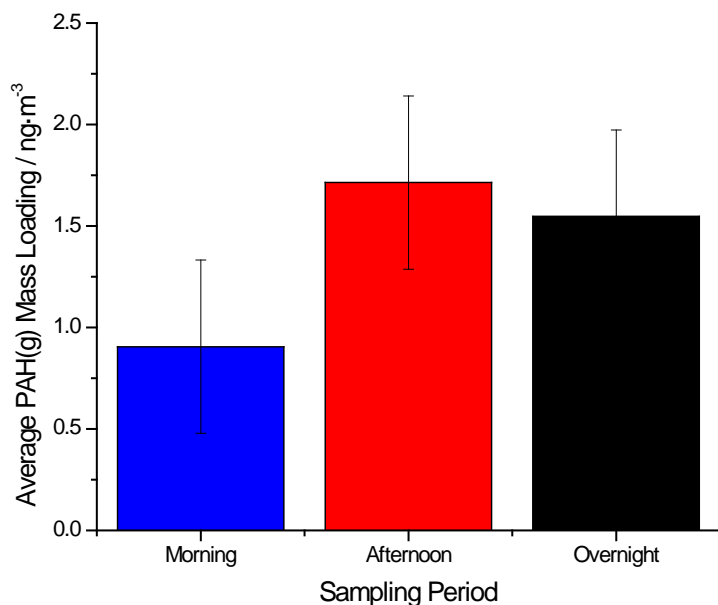
58

Quinones - Spatial Trends. The temporal dependence of quinone mass loadings was evaluated by separating out the back trajectories for samples collected during the three different periods (morning, afternoon, overnight), shown in Figure 14.

Each trajectory shows a large variation in the distribution of measured quinones. The wind direction is seen to be from the W during the night period, afternoon prevailing winds are from the SW, and morning winds between W/SW. As seen in previous back-trajectory models, air masses passing over the region between Pomona and Long Beach to Claremont are correlated with high quinone mass loadings. During the night and morning, low concentrations of measured quinones are observed. In contrast, high mass loadings are observed during the afternoon. This implies that either the emissions of quinones/quinone precursors occur primarily in the morning in this region, or that photo-oxidation of quinone precursors during transport from the coast is the major source of the quinones observed.

The 'overall plot' in Figure 14 shows contour lines that represent the time taken for the air mass to reach the sampling location from that point. Rate coefficients for the gas phase reactions of $\cdot\bullet OH$ with a number of PAHs are known from the literature. Given a typical reaction rate of naphthalene with $\cdot\bullet OH$ of 2.39×10^{-11} molecules$\cdot$cm^{-3} (Phousongphouang and Arey 2002) and a typical atmospheric concentration of $\cdot\bullet OH$ 1×10^{6} molecules$\cdot$cm^{-3}, the lifetimes of PAHs will be of the order of 10 h. This implies PAHs emitted near the coastal region have the potential to be mostly oxidized to form quinones and other oxygenated products that can be measured at the sampling site.

Fresno

Mass Loadings. Three quinones were observed in SLF and DCM filter extracts at mass loadings greater than the limit of detection. Anthraquinone, 1,2- and 1,4-naphthoquinone were measured in a small number of samples. 9,10-Phenanthraquinone (1.5 ± 1.4 ng m^{-3}) was observed in a majority of the samples, as shown in Figure 16.
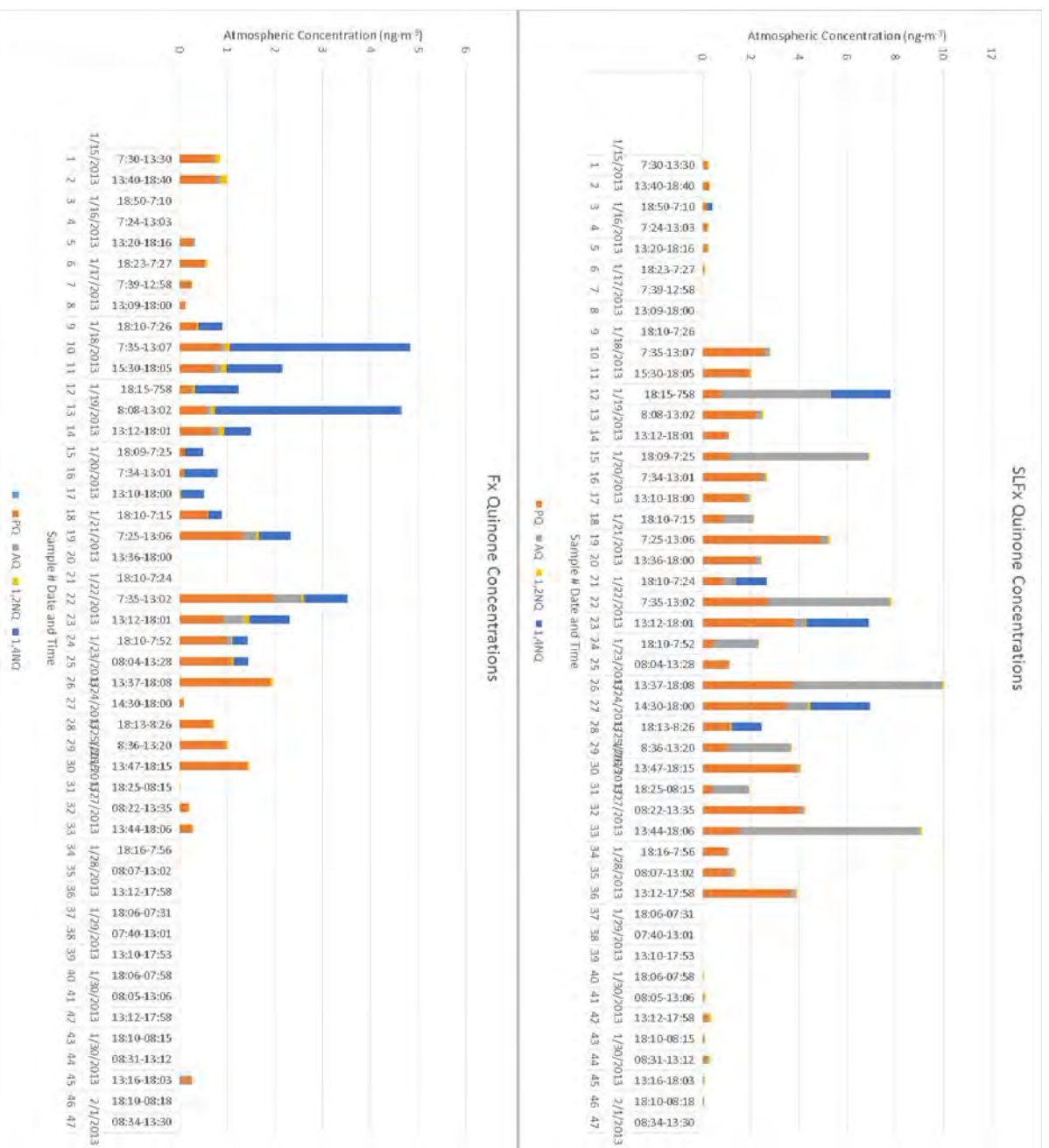
Figure 16. Quinone mass loadings in SLF (top) and DCM (bottom) samples collected in Fresno, CA in Winter 2013.

Temporal Variation. Average morning, afternoon and overnight mass loadings of phenanthraquinone are shown in Figure 17. Mean morning (1.9 ± 1.5 ng m^{-3}) and afternoon (2.1 ± 1.4 ng m^{-3}) mass loadings are indistinguishable, but overnight mass loadings are significantly lower (0.57 ± 0.42 ng m^{-3}). Based on the back trajectory analysis outlined below, these differences do not appear to be a result of differences between the trajectories of samples collected overnight compared to other times of day.
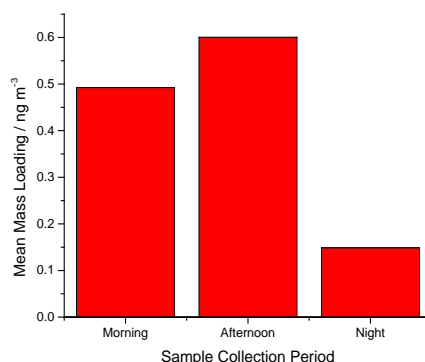
Figure 17. Comparison of particle phase phenanthraquinone mass loadings collected at different times of day in Fresno, CA during Winter 2013.

Spatial Variation. The back trajectory analysis described above for the Claremont samples was repeated for the Fresno data. Since conditions were generally more stagnant during these measurements, back trajectories were run for a longer period (24 hours) than for the Claremont analysis. The heat map generated for phenanthraquinone from this analysis is shown in Figure 18. For the majority of samples, the air mass originated in the Sierra Nevada Mountains to the east, and spent a significant period of time within the San Joaquin Valley before reaching the field site. However, 10% of the trajectories were traced back to the Bay Area. The back trajectory analysis shows that these samples contain a significantly higher mass fraction of phenanthraquinone than the other trajectories, when normalized to the $PM_{2.5}$ mass. The number of samples with air masses originating in the Bay Area is small, and so subdividing these trajectories into morning, afternoon and overnight samples provides limited additional information. We note, however, that overnight samples originating in the Bay Area have lower mass fractions of phenanthraquinone compared to those collected during the morning and afternoon. Collectively, these data imply an anthropogenic source of phenanthraquinone, and suggest that photochemistry plays a significant role in the production of quinones, even during the winter.
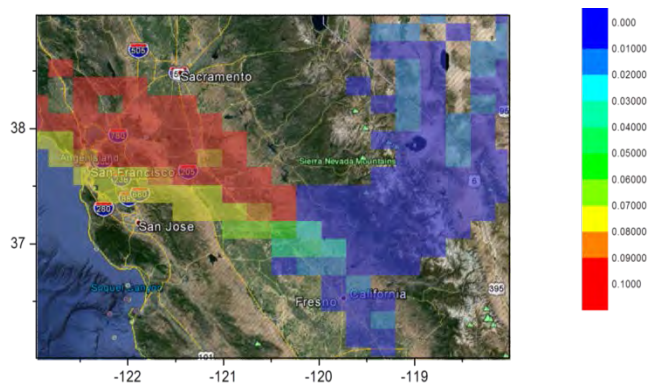
Figure 18. Heat map showing $PM_{2.5}$ mass normalized loadings of phenanthraquinone in samples collected in Fresno, CA during Winter 2013.

61

Leveraged Work and Future Directions

In-vitro ROS measurements. We sought to leverage the rich dataset obtained in this work by developing an *in-vitro* assay to test sections of the filters collected for ROS production. This work was conducted in the lab of Dr. Laurent Dejean (Chemistry Department, California State University, Fresno). Initial work focused on the development of an assay described in the literature (Landreman et al. 2008), which uses dichlorofluorescein (DCF) as a fluorescent probe for ROS production by rat alveolar macrophage cells. This assay is now able to discriminate between ROS production by the cells when exposed to mass-normalized extracts from different samples, as shown in Figure 19. This difference is attributed to variations in the chemical composition of the sample extracts. Once these measurements are complete, the results will be compared to both the metal and organic mass loadings measured as a part of this project, as well as to the results of the SLF and DTT measurements.
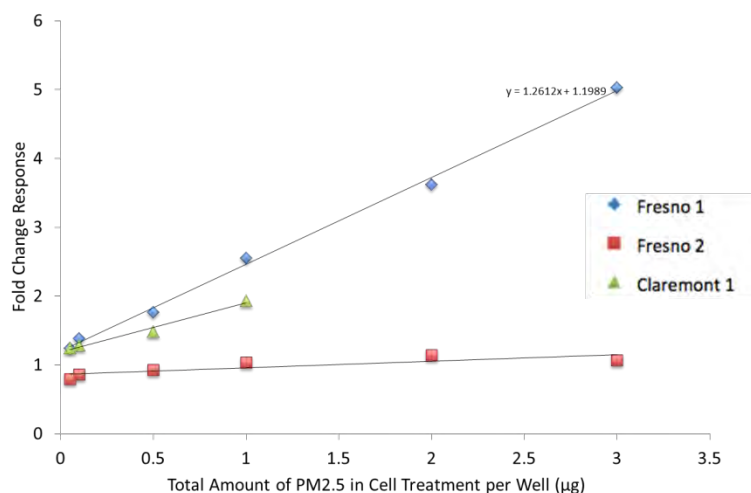
Figure 19. Relative ROS response of rat alveolar macrophage cells exposed to PM extracts (Fresno 1: multi-day sample collected Fall 2013; Fresno 2: overnight sample collected Winter 2013; Claremont 1: Overnight sample collected Summer 2012).

In a second set of measurements, Dr. Dejean's group has used flow cytometry along with DCF and cytox blue (to probe cell viability) to investigate ROS production by populations of alveolar macrophage cells when exposed to sample extracts. Preliminary evidence indicates a measurable increase in the number of cells exhibiting oxidative stress when exposed to the filter samples. This approach should therefore lead to an additional tool to probe the impacts of PM samples on ROS production.

Microbiome Analysis. The lower atmosphere contains significant quantities of microbes that contribute to $PM_{2.5}$ mass. Despite potentially contributing to the adverse health effects of $PM_{2.5}$, little is known about the microbiome of the air in the San Joaquin Valley. A small proof-of-concept study was conducted to explore the potential to probe the microbiome in Fresno air. The goal is to develop a tool that would allow the relationship between the microbial population of the air and health impacts on local populations to be evaluated. This work was conducted in collaboration with Dr. Mamta Rawat (Biology Department, California State University, Fresno) and Dr. Suman Das (J. Craig Venter Institute, Maryland).

The measurements followed an established procedure (Cao et al. 2014). Samples were collected on sterile media (autoclaved Tissuquartz filters) using a Tisch Hi-Vol sampler that was disinfected with ethanol immediately prior to sampling. A total of 13 samples were analyzed. Six air samples were collected for 24 hours at the Fresno site (three collected during summer and three during winter). An additional six filters (three summer and three winter) were placed in the sampler for 24 hours, but the air pump was not turned on. The remaining filter was processed after autoclaving to serve as a negative control. DNA was extracted from these samples at JCVI, and the V4 region of 16S rRNA was amplified in a two-step PCR process with 40 total cycles. Samples were sequenced on the MiSeq with 2 x 300 base pair runs. The resulting sequences are then matched to a library.

The relative genus abundance for the samples and negative controls is shown in Figure 20. Microbial reads are observed in all samples, including both the controls and 'pump off' filter samples. However, the populations of most of the 'filter on' samples appear different from the negative controls and the 'filter off' samples. A principal component analysis of these data, shown in Figure 21, indicates that the filter samples occupy a different space compared to the controls. Collectively the data indicate that we are detecting the microbial population of the air rather than artifacts resulting from contamination. Interestingly, the samples collected during the summer appear to occupy a different space compared to those collected during winter (data not shown). Ongoing work will provide chemical composition data for these samples. Additional funding will be sought to further develop and implement this approach.

Figure 20. Relative genus abundance of microbes collected in Fresno, CA. 'na' are controls; 'off' are samples mounted in the sampler for 24 hours with the pump left off; and 'on' are samples collected in the usual way. Samples ending in 46, 44, 35, 45, 43 and 41 were collected in Summer 2014. Remaining samples were collected in Winter 2015.

63

Figure 21. Principal component analysis of genus levels of filter samples and controls.
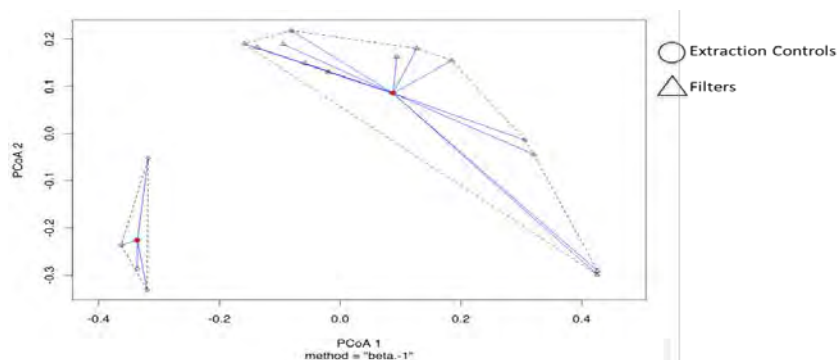
Conclusions

Mass loadings of nine quinones were measured in approximately 100 PM$_{2.5}$ samples collected in southern and central California during summer and winter, respectively. Four quinones (1,2-naphthoquinone, 1,4-naphthoquinone, chrysenequinone, benz[a]anthracene-7,12-dione, and phenanthraquinone) were observed above the limits of detection in multiple samples from Claremont during Summer 2012. In contrast, only phenanthraquinone was routinely observed in Fresno during winter 2013. SLF-extractable quinone concentrations are typically the equivalent of less than 1 ng m^{-3} in PM samples at both sites. These measurements help to provide constraints on the contribution of quinones to ROS generation in the DTT and SLF assays described elsewhere in this report. Temporal variations in mass loadings and back trajectory analyses are consistent with emissions of quinone precursors from industrial locations (Long Beach for the Claremont site and Bay Area for the Fresno site). Despite the different seasons for sample collection at the two sites, the data are consistent with photo-oxidation as an important source of quinones at both locations.

IV.B. Reactive Oxygen Species, Transition Metals, Mass and BBHULIS

IV.B.1 Dithiothreitol (DTT) Redox-Activity of Particulate Matter from Field Campaigns

1 Average Metal and Quinone Concentrations. As discussed earlier, the mass concentrations of metals and quinones at Claremont and Fresno are highly variable in time, especially at the latter site. Figure 22 shows the average values for the metals and quinones at our two sites compared to averages reported from past work in the U.S. In general, our concentrations are similar to previous values, especially compared to the values from larger urban area. Since copper, manganese, and phenanthraquinone (PQ) are expected to be major contributors to the DTT response (Charrier and Anastasio 2012b), we next looked in more detail at their values. Our Mn values are on the low end of previously reported ranges, while our PQ values span the range, with higher values in Fresno (Figure 22). For Cu, the average (± 1 σ) concentrations at Claremont (24.4 ± 12.8 ng m^{-3}) and Fresno (25.1 ± 19.6 ng m^{-3}) are about 30% lower than the average measured previously in Los Angeles during summer (38.2 ng m^{-3}) (Verma et al. 2009a). These values are approximately an order of magnitude higher than those reported for other, much smaller, urban areas, where copper concentrations range from 1 – 2 ng m^{-3} (Figure 22) (Connell et al. 2006; Vidrio et al. 2009). This difference is probably explained by variations in traffic density, as a major source of fine particulate copper appears to be brake wear.
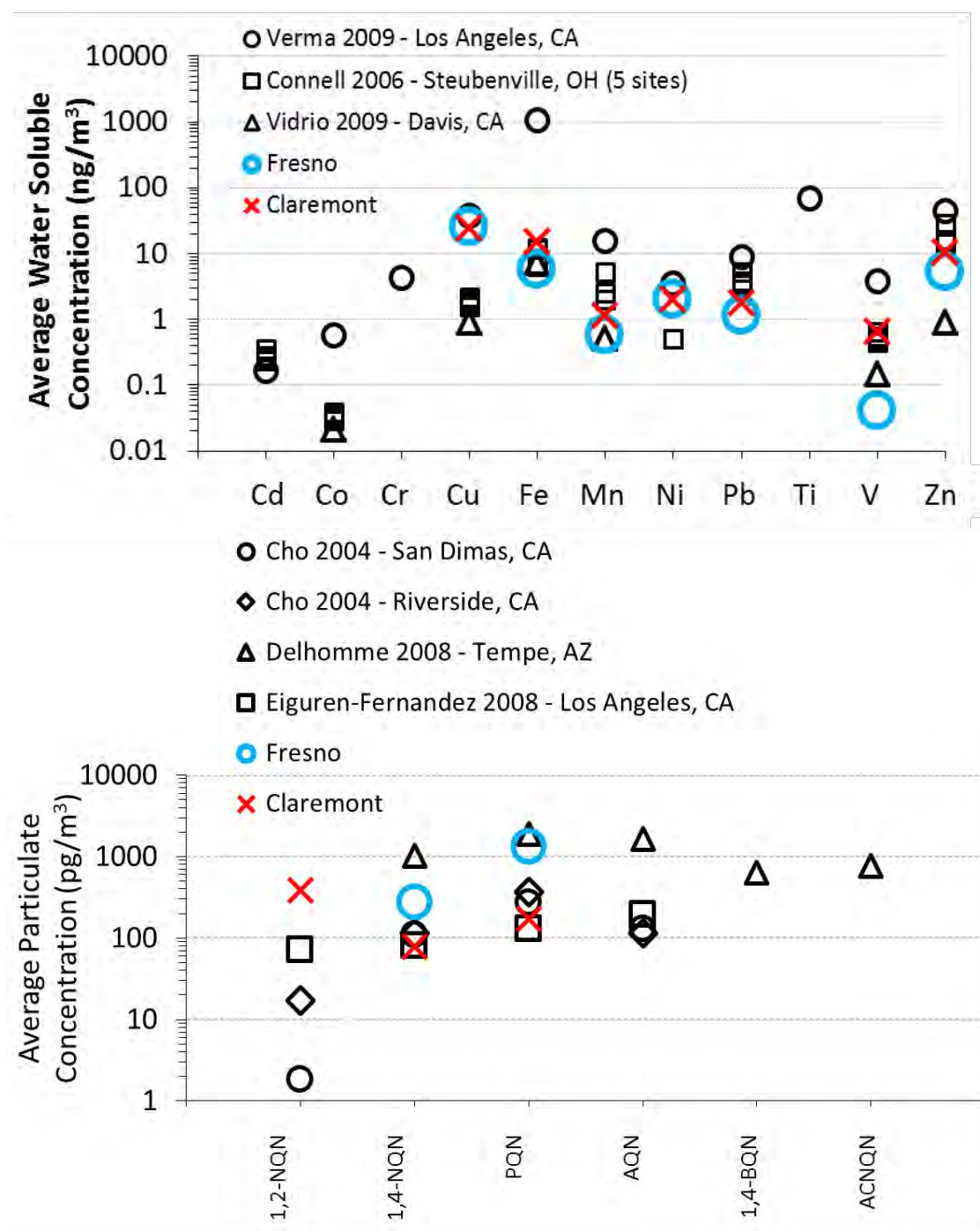
Figure 22 Average soluble metals (panel A) and quinone (panel B) concentrations in our Claremont and Fresno samples compared to water-soluble metals and total quinone concentrations in $PM_{2.5}$ from a number of other studies in urban and suburban areas of the U.S. (Cho et al. 2004b; Connell et al. 2006; Delhomme et al. 2008; Eiguren-Fernandez et al. 2010; Verma et al. 2009a; Vidrio et al. 2009). Each point represents the average value for a given location in each study. 1,2-NQ levels for Fresno samples were always below the detection limit, which ranged from 200 – 870 pg m^{-3}.

However, because our Cu concentrations are quite high, we were interested whether the high-volume sampler might be a source of Cu contamination in our samples. To test whether this could occur, we collected samples at Fresno in summer 2013 under three sampler configurations: (a) Base case, where the exhaust from the sampler was not controlled (which was the condition we used for our Claremont and Fresno sampling), (b) Low case, where the exhaust was routed away from the sampler (through approximately 10 feet of tubing), and (c) High case, where the exhaust was piped directly into the sampler intake. Each case was sampled for one day, with 3 separate periods for morning, afternoon, and overnight, to mimic our field sampling. Figure 23 shows that the copper concentrations in the Base and Low conditions are very low, a few ng m^{-3}, while the High case has very high concentrations, approximately 60 – 100 ng m^{-3}. These results indicate that the Hi-Vol sampler exhaust can be a source of particulate copper, but also suggest that under typical operating conditions sample contamination is minor. However, given the importance of Cu in ROS generation (Charrier and Anastasio 2012b; Charrier et al. 2014a; Charrier and Anastasio 2015), this is an issue that should be examined in more detail.
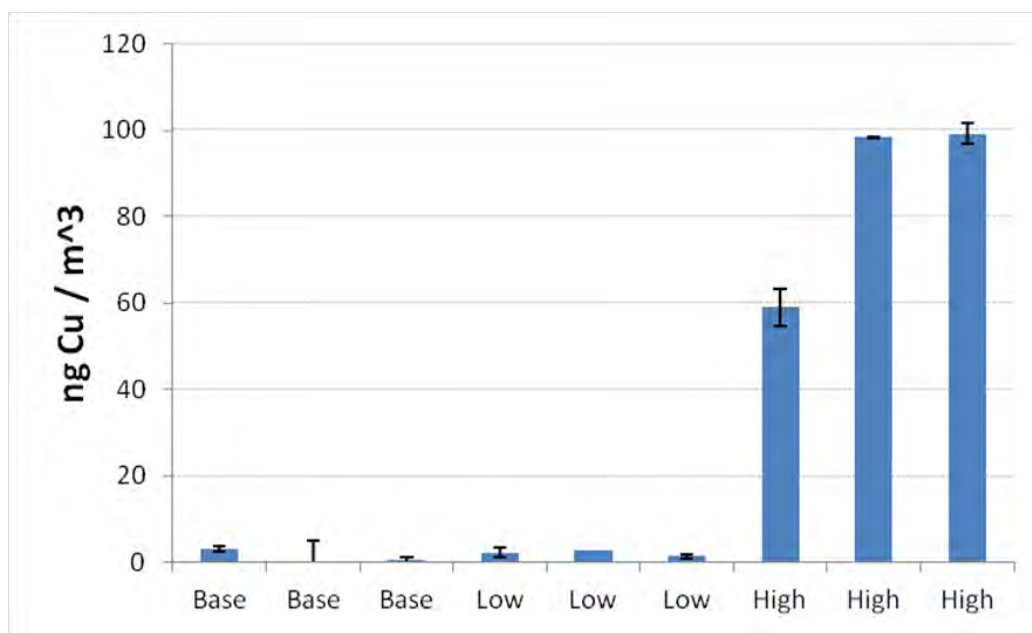
Figure 23. Copper concentrations in samples collected to test whether the sampler is a potential source of contamination. Under each condition (Base, Low, High) we collected a sample during morning, afternoon, and overnight.

Finally, we were curious why the Base case samples in Fresno during the summer 2013 sampling had much lower Cu concentrations than the winter 2013 samples we collected in Fresno. Examining the ARB data from the Fresno 1st Street site (http://www.arb.ca.gov/adam/) shows that Cu has a pronounced seasonal cycle, with minimum values during the summer of a few ng m^{-3} and maximum values in the winter that are highly variable and peak at approximately 30 ng m^{-3} (Figure 24). Overlaid on this plot are the values from our Fresno sampling, which also show high variability but generally good agreement with the 1st Street concentrations. This is additional evidence that our Fresno copper concentrations are not

Figure 24. Mass-normalized rates of DTT loss as a function of the PM mass concentration used in each extract solution. Each symbol represents a different sample.

DTT Rate (pmol/min/µg)

PM mass concentration (µg/mL)

◆ Claremont
■ Fresno

Figure 25. Copper concentrations in ambient samples collected by ARB at the 1st Street site in Fresno (blue diamonds) compared to our Fresno samples (red squares).

Cu Conc (ng/m^3)

— Fresno 1st Street
■ Our Soluble Cu

significantly affected by contamination from the sampler. There is no ARB Cu data for Claremont. so we could not do a comparison for this site.

2 Correcting Mass-Normalized DTT Data. During this project we discovered that a bias in mass-normalized DTT data for samples where Cu and/or Mn contribute significantly to the DTT response, as we discuss in section III.C. Figure 25 shows this problem for our Claremont and Fresno samples: the mass-normalized rates generally decrease with increasing PM mass concentration used in the DTT extract solution. This is a result of the non-linear concentration-

response curve for Cu (and Mn), where the rate of DTT loss approaches a plateau at higher Cu (and Mn) concentrations (Charrier and Anastasio, 2012). To correct the data, we employed the "calculation" method described in section III.C, which normalizes the data to the DTT response expected for the same PM mass concentration for all samples (10 μg mL^{-1}). This correction removes the artifact of mass-dependence of the DTT response and, in doing so, reduces the variability of the DTT response between different samples (Figure 26): (1) the mass-normalized rate is decreased in samples that had an artificially high response because of a low PM mass concentration in the extract, while (2) the rate is increased in samples that had an artificially low response because of a high PM mass concentration. While the PM extract mass in our samples has a large impact on the (uncorrected) mass-normalized rate of DTT loss, it is unclear how important this artifact has been in past studies with DTT.
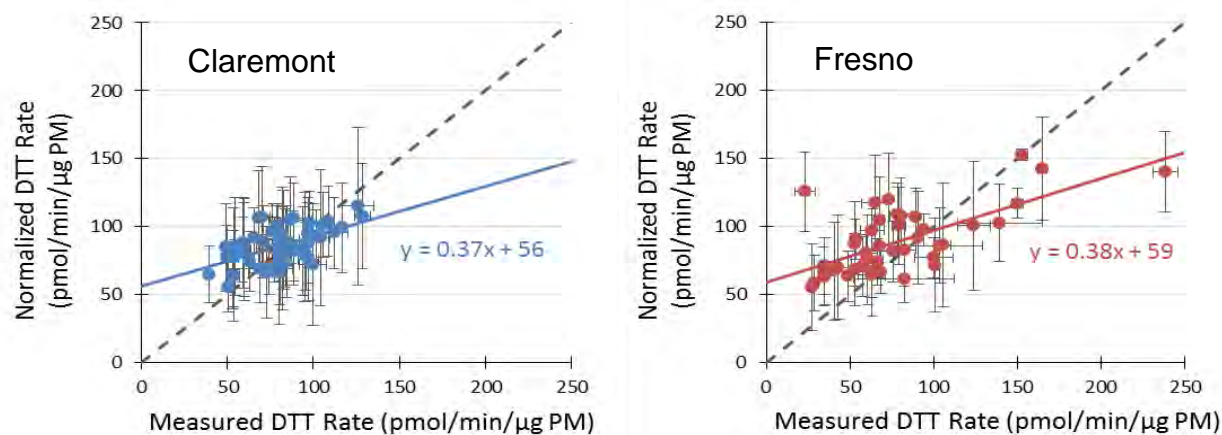
Figure 26. Comparison of the mass-normalized rates of DTT loss in the particle extracts before and after correction to a constant PM mass concentration in the extract. The "measured" rate is the value determined in the DTT extract (divided by the extract PM mass concentration), while the "normalized" rate is corrected to a standard extract PM mass concentration of 10 μg mL^{-1}.

3 Corrected DTT Results. Figure 27 shows the corrected mass-normalized DTT response for every sample collected at our two sites. At Claremont the DTT rates stay within a relatively narrow range, with an average value of 86 pmol-DTT min^{-1} μg^{-1} PM and a relative standard deviation of 16%. The range of values at Claremont (55 – 115 pmol min^{-1} μg^{-1}) is similar to the previously reported (uncorrected) rates, which range from 5 to 170 pmol min^{-1} μg^{-1} for particles collected in Fresno and the South Coast Air Basin (Charrier et al. 2015; De Vizcaya-Ruiz et al. 2006; Ntziachristos et al. 2007; Verma et al. 2009a; Verma et al. 2009b). The PM2.5 mass concentration also is relatively stable (Figure 27), and there is a very weak negative correlation between this variable and the corrected mass-normalized DTT response (*R* = -0.47).
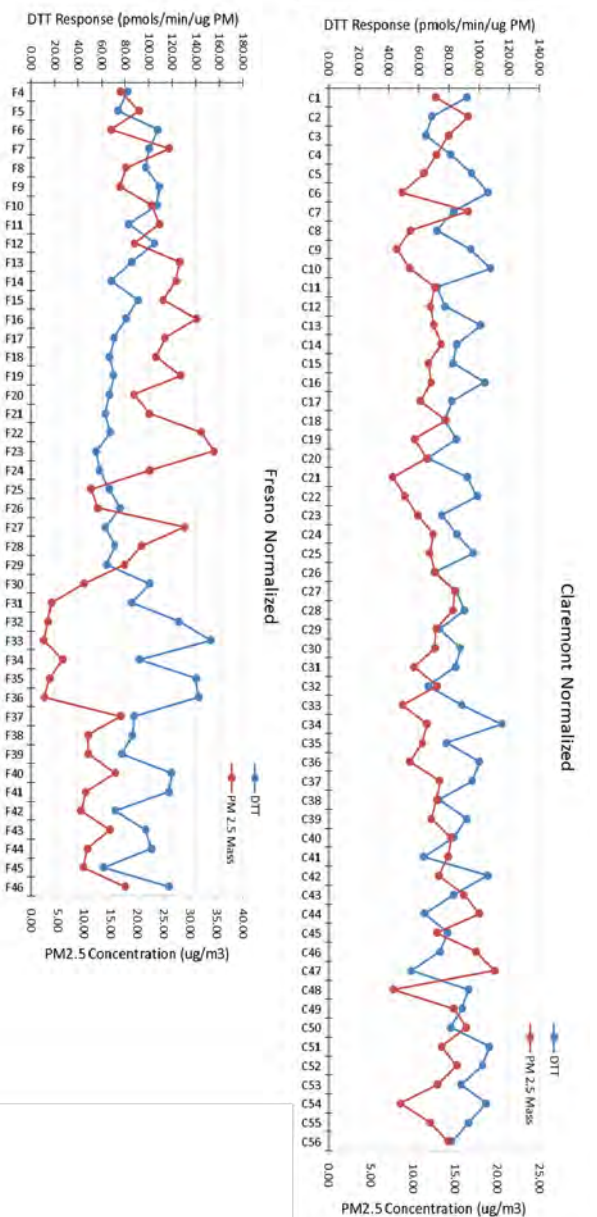
Figure 27. Corrected mass-normalized rates of DTT loss, along with the corresponding PM2.5 mass concentration, at Claremont (top) and Fresno (bottom).

The average corrected, mass-normalized DTT responses for morning and overnight are nearly identical at Claremont, with slightly lower values in the afternoon: average (± 1σ) values are 278 ± 31, 270 ± 35, and 223 ± 29 pmol min^{-1} μg^{-1}, respectively. The same is true for the Fresno morning, afternoon, and overnight samples, with very similar average rates, but standard deviations that are approximately twice as large. (In contrast, if the DTT rates are not corrected for the PM mass concentration bias, the overnight samples have a lower mass-normalized DTT response than morning and afternoon, a result of having the highest PM masses on the filters (because of the longer sampling time) and thus highest PM mass concentrations in the DTT extracts.)

In Fresno, there was more variability in the corrected mass-normalized DTT results, with three somewhat distinct periods (Figure 27): (1) an initial period (samples F4-F15) of intermediate DTT rates (average ± 1σ = 92 ± 14 pmol min^{-1} μg^{-1}), (2) a second period (F16-F29) of lower and nearly constant DTT activity (average = 67 ± 6), and (3) a final, highly variable, period (F30-F46) with low rates similar to those in previous periods punctuated by some of the highest values seen in Fresno (average ± 1σ = 105 ± 26). As in Claremont, there is also an overall weak, negative correlation between DTT rate and PM2.5 mass in Fresno (R = -0.58), which is especially evident at the beginning of period 3 (F13-36), where PM2.5 fell to very low levels (typically below 5 μg m^{-3}) and the DTT rate reached its highest values (Figure 27).

4 Importance of Metals and Quinones in the DTT Responses. In order to quantify the contributions of individual metals and quinones in our measured DTT rates, we combine: (1) the measured concentrations of each metal and quinone in each PM extract with (2) the "concentration-response" curves that express the rate of DTT loss as a function of metal or quinone concentration (Charrier and Anastasio, 2012 and section III.C). The product of (1) and (2) is the calculated DTT response expected from each DTT-active metal and quinone; based on our past work, it appears that mixtures of metals and/or quinones behave additively in the DTT assay (Charrier and Anastasio 2012b). Figure 28 shows these calculated contributions

69

compared to the measured DTT rate for each sample. As is clear from the sea of purple in this figure, copper dominates the DTT response in almost every sample at both sites. This is consistent with our past estimate that Cu plays a dominant role in the DTT response for typical fine particles in the U.S. (Charrier and Anastasio 2012b) as well as with our recent measurements of Cu dominance for source-oriented particles in Fresno (Charrier et al. 2015).

In the Claremont samples, Cu is responsible for an average ($\pm$ 1σ) of (78 $\pm$ 9) % of the DTT response (Figure 28), with morning and overnight having a slightly larger contribution from Cu (80%) compared to afternoon (73%). Unknown species make the next largest average contribution, (11 $\pm$ 10) % on average, while Mn is next, accounting for an average of (8 $\pm$ 3) % (Figure 29). The three measured DTT-active quinones are of minor importance in the average DTT response at Claremont, with a total quinone contribution of (2 $\pm$ 4) % averaged across all of the samples, although there are a few samples where the quinones contribute 11 – 18% of the DTT response (Figure 27). In Fresno, copper is also the dominant DTT-active species, accounting for an average of (70 $\pm$ 15) % of the DTT rate, followed by unknown species (16 $\pm$ 14) %, PQN (9 $\pm$ 15) %, and Mn (5 $\pm$ 3) % (Figure 28). However, unlike the case in Claremont – where Cu is the dominant species in every sample – in Fresno there are a few samples (F32, F33, and F36) where PQN is more important than copper. This occurs during the period of low PM2.5 mass, likely because of rain or a front passing through the city, when copper concentrations were at their lowest concentrations. While PQN is dominant in these samples, in 95 of the 99 samples that we studied at Claremont and Fresno, copper dominates the DTT response.
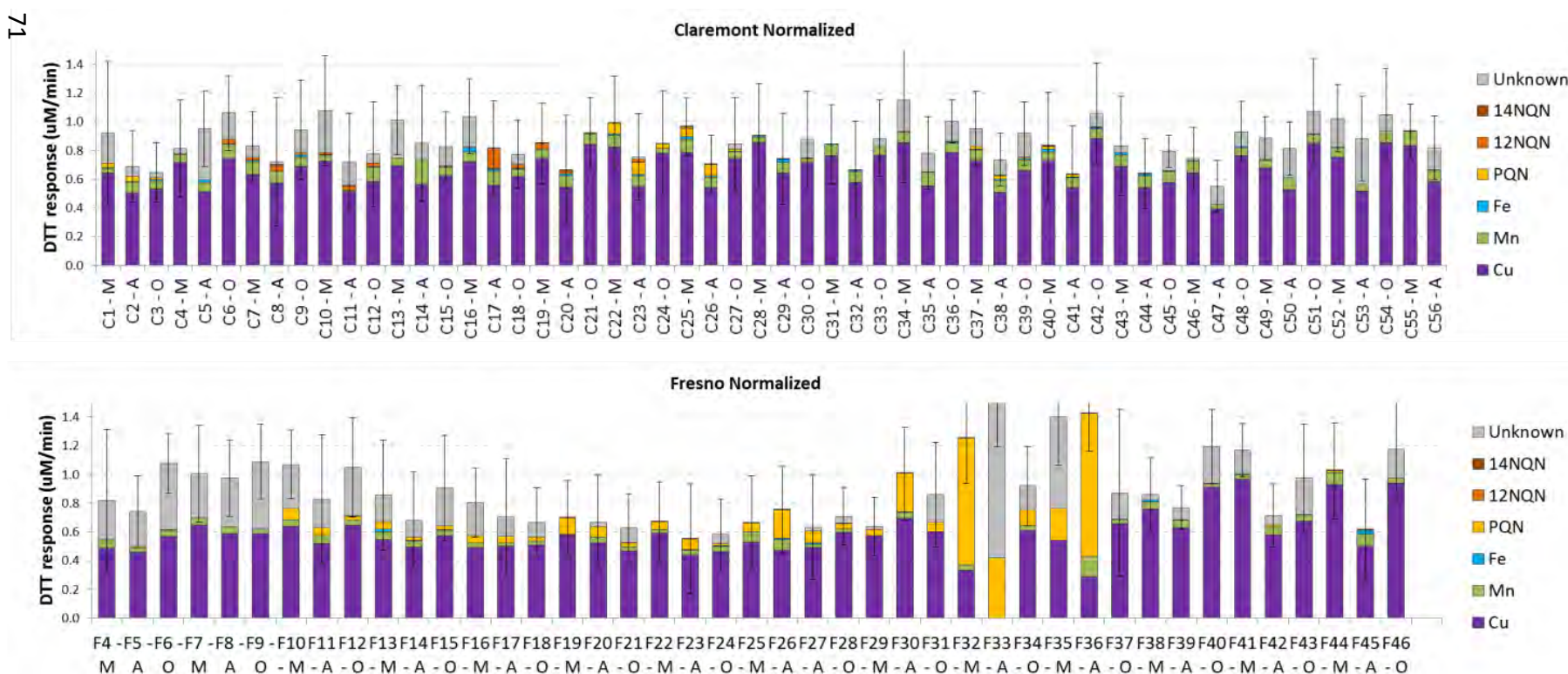
Figure 28. Quantification of the importance of metals and quinones in the measured, corrected DTT response in each sample. Rates are expressed as the values in the DTT extract, normalized to a PM concentration of 10 µg mL–1. The total height of each bar represents the measured rate of DTT loss in that sample, while the colored components of the bar represent the contributions from different DTT-active species (e.g., purple = copper and yellow = PQN). The gray component at the top of some bars is the contribution from unknown species, i.e., the portion of the measured DTT rate that is greater than the sum of the rates from the measured metals and quinones. The sample number is listed on the x-axis, along with an indicator for whether the sample was collected during morning (M), afternoon (A), or overnight (O).
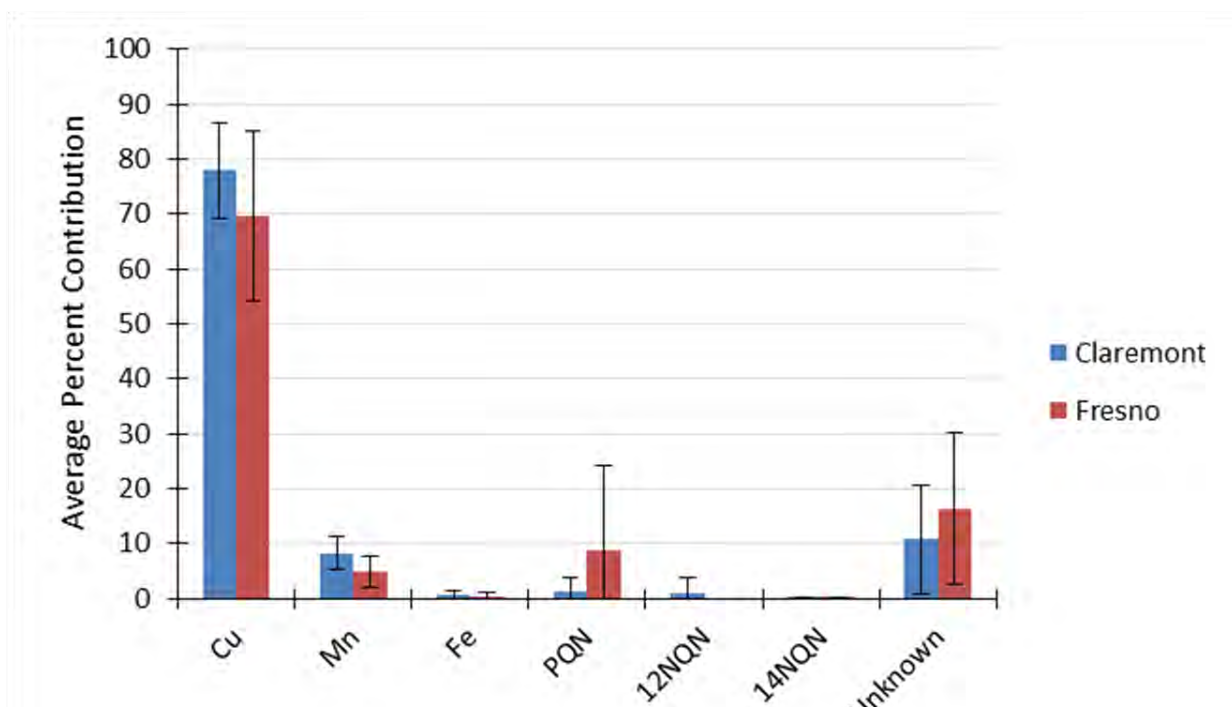
Figure 29. Contributions of individual DTT-active species (and unknown species) towards the rate of DTT loss in the PM extracts, corrected to a PM mass concentration of 10 μg mL^{-1}. The value for each species is the average (± 1 σ) for all samples at a given site.

References

Charrier, J. G., and Anastasio, C.: On dithiothreitol (DTT) as a measure of oxidative potential for ambient particles: Evidence for the importance of soluble transition metals, Atmos. Chem. Phys., 12, 9321-9333, 2012.

Charrier, J. G., and Anastasio, C.: Rates of hydroxyl radical production from transition metals and quinones in a surrogate lung fluid, Environ. Sci. Technol., 4, 9317-9325, 2015.

Charrier, J. G., Mcfall, A. S., Richards-Henderson, N. K., and Anastasio, C.: Hydrogen peroxide formation in a surrogate lung fluid by transition metals and quinones present in particulate matter Environ. Sci. Technol., 48, 7010-7017, 2014.

Charrier, J. G., Richards-Henderson, N. K., Bein, K. J., Mcfall, A. S., Wexler, A. S., and Anastasio, C.: Oxidant production from source-oriented particulate matter - Part 1: Oxidative potential using the dithiothreitol (DTT) assay, Atmos. Chem. Phys., Accepted, 2015.

Cho, A. K., DiStephano, E., You, Y., Rodriguez, C. E., Schmitz, D. A., Kumagai, Y., Miguel, A. H., Eiguren-Fernandez, A., Kobayashi, T., Avol, E., and Froines, J. R.: Determination of Four Quinones in Diesel Exhaust Particles, SRM 1649a, and Atmospheric PM2.5, Aerosol Sci. Technol., 38, 68-81, 2004.

72

Connell, D. P., Winter, S. E., Conrad, V. B., Kim, M., and Crist, K. C.: The Steubenville Comprehensive Air Monitoring Program (SCAMP): Concentrations and solubilities of $PM_{2.5}$ trace elements and their implications for source apportionment and health research, J Air Waste Manage Assoc, 56, 1750-1766, 2006.

De Vizcaya-Ruiz, A., Gutierrez-Castillo, M. E., Uribe-Ramirez, M., Cebrian, M. E., Mugica-Alvarez, V., Sepulveda, J., Rosas, I., Salinas, E., Garcia-Cuellar, C., Martinez, F., Alfaro-Moreno, E., Torres-Flores, V., Osornio-Vargas, A., Sioutas, C., Fine, P. M., Singh, M., Geller, M. D., Kuhn, T., Miguel, A. H., Eiguren-Fernandez, A., Schiestl, R. H., Reliene, R., and Froines, J.: Characterization and in vitro biological effects of concentrated particulate matter from Mexico City, Atmos. Environ., 40, S583-S592, 2006.

Delhomme, O., Millet, M., and Herckes, P.: Determination of oxygenated polycyclic aromatic hydrocarbons in atmospheric aerosol samples by liquid chromatography-tandem mass spectrometry, Talanta, 74, 703-710, 2008.

Eiguren-Fernandez, A., Shinyashiki, M., Schmitz, D. A., DiStefano, E., Hinds, W., Kumagai, Y., Cho, A. K., and Froines, J. R.: Redox and electrophilic properties of vapor- and particle-phase components of ambient aerosols, Environ. Res., 110, 207-212, 2010.

Ntziachristos, L., Froines, J. R., Cho, A. K., and Sioutas, C.: Relationship between redox activity and chemical speciation of size-fractionated particulate matter, Particle and fibre toxicology, 4, 2007.

Verma, V., Ning, Z., Cho, A. K., Schauer, J. J., Shafer, M. M., and Sioutas, C.: Redox activity of urban quasi-ultrafine particles from primary and secondary sources, Atmos. Environ., 43, 6360-6368, 2009a.

Verma, V., Polidori, A., Schauer, J. J., Shafer, M. M., Cassee, F. R., and Sioutas, C.: Physicochemical and toxicological profiles of particulate matter in Los Angeles during the October 2007 Southern California wildfires, Environ. Sci. Technol., 43, 954-960, 2009b.

Vidrio, E., Phuah, C. H., Dillner, A. M., and Anastasio, C.: Generation of hydroxyl radicals from ambient fine particles in a surrogate lung fluid solution, Environ. Sci. Technol., 43, 922-927, 2009.

IV.B.2 Mass dependence of transition metals and ROS

Section III.C (in Part II of this report) presents data indicating that in laboratory bulk solutions the DDT response to copper in SLF is quite non-linear, appearing instead to be roughly biphasic. In complex aerosols and their extraction solutions, there is the additional possibility that the concentration of soluble species depends on the mass of aerosol in the extraction solution—i.e., that there are some saturation effects. Further, as copper and several other transition metals are reasonably correlated with mass, we might expect to see the effects of a non-linear response to copper when we look at the effect of aerosol mass (either on the filter or in the extraction solution, as generally these are directly proportional to one another). That is, all

73

analyses were performed using a fixed filter section, either punch (~1 square inch depending on the assay) or a half filter.

As ambient mass concentrations vary and because nighttime samples were collected for 12 hours while daytime samples were collected for 6 hours, the mass of aerosol on the (half 47 mm) filters covered a fairly wide range, from 0.13 to 0.51 mg for Claremont and from 0.029 to 1.12 mg for Fresno. Generally, these masses were extracted in 10 mL. The expectation is that if the quantity of mass (or individual components) on the filter produces a non-linear response, this may be due to the concentration effects in the solution; keeping in mind it may also be due to variability in other unmeasured components in the particles.
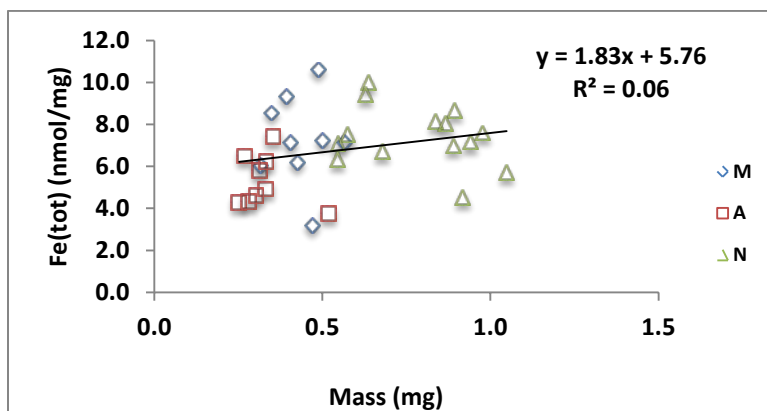
Figure 30. Claremont mass-normalized total soluble iron vs. mass on the filter after 2 hrs of extraction. The line is included to guide the eye; there is no significant correlation. Blue diamonds: morning samples (7 AM – 1 PM), red squares: afternoon samples (1 PM – 7 PM), green triangles, nighttime samples (7 PM – 7 AM).
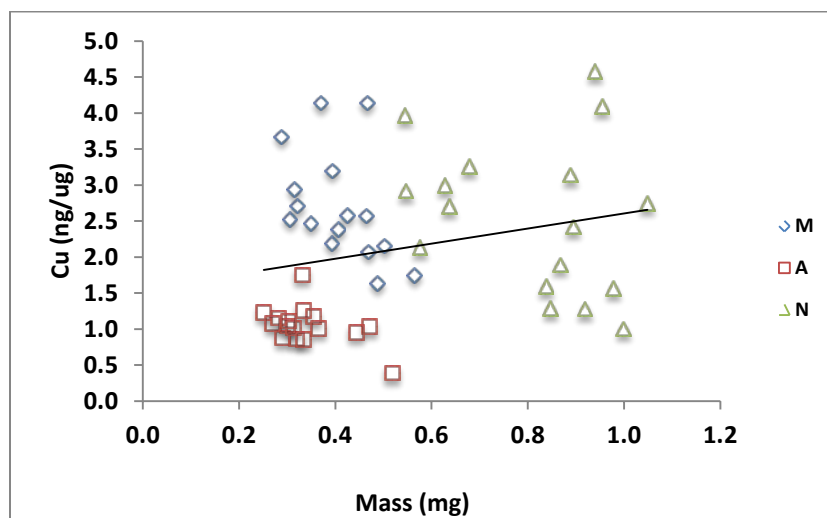
Figure 31. Claremont mass-normalized Cu vs. mass on the filter after 2 hrs of extraction. The line is included to guide the eye; there is no significant correlation. Blue diamonds: morning samples, red squares: afternoon samples, green triangles, nighttime samples.

74

For the Claremont 2 hour extractions, most metrics were not mass dependent. This includes desferoxamine soluble iron (Figure 30), ICP copper and vanadium (Figure 31, V not shown), •OH (Figure 32), H_2O_2 (Figure 33). Two figures (Figures 34 and 35) are shown for DTT; Figure 35 shows the data uncorrected for copper concentration, and Figure 34 shows the data using the procedure described above that accounts for the copper/PM mass in the solution. DTT shows a significant negative slope when the concentration of PM in the solution is not accounted for (Figure 35), and the negative slopes were different for each sub-group of data, morning, noon and night. The algorithm described in section III.C removes the concentration-dependent bias well. Nickel and lead had slight but statistically significant correlations ($p < 0.05$, R^2 from 0.06 – 0.11) but with very low slopes (Figures 36 and 37). Further, since all of the high mass samples are nighttime samples, actual differences in chemical composition of the particles may explain the (slight) differences.
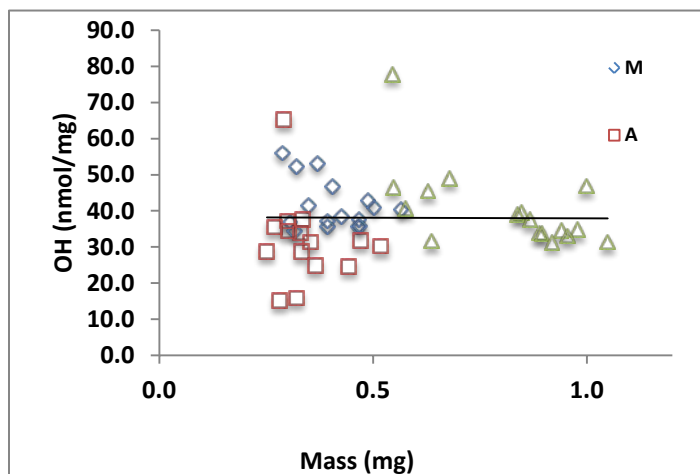
Figure 32. Claremont mass-normalized hydroxyl radical vs. mass on the filter after 2 hrs of extraction. The line is included to guide the eye; there is no significant correlation. Blue diamonds: morning samples, red squares: afternoon samples, green triangles, nighttime samples.
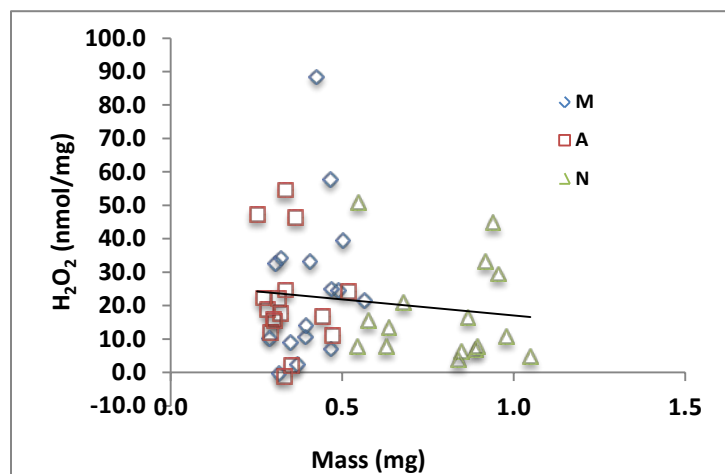
Figure 33. Claremont mass-normalized H_2O_2 vs. mass on the filter after 2 hrs of extraction. The line is included to guide the eye; there is no significant correlation. Blue diamonds: morning samples, red squares: afternoon samples, green triangles, nighttime samples.
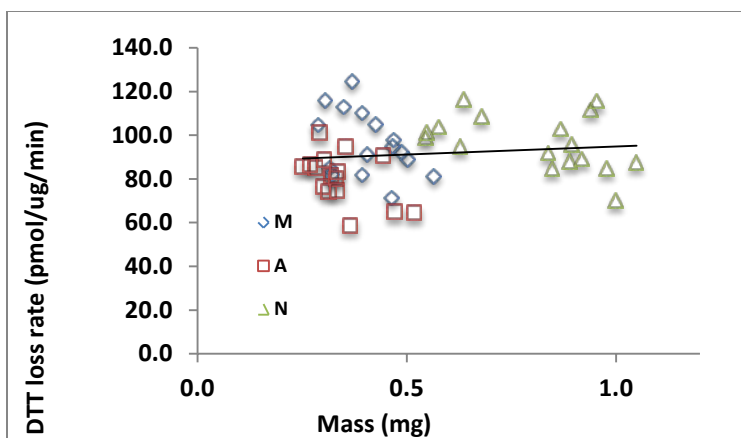
Figure 34. Claremont mass-normalized DTT consumption rate vs. mass on the filter after 2 hrs of extraction. The line is included to guide the eye; there is no significant correlation. Blue diamonds: morning samples, red squares: afternoon samples, green triangles, nighttime samples.
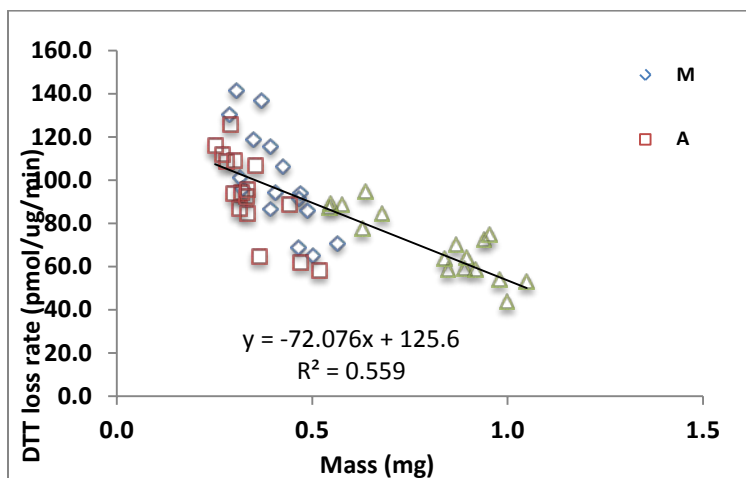
Figure 35. Claremont mass-normalized DTT consumption rate vs. mass on the filter after 2 hrs of extraction, not normalized to copper concentration. The line negative slope is highly significant. Slopes for morning and afternoon data alone are larger than nighttime data. Blue diamonds: morning samples, red squares: afternoon samples, green triangles, nighttime samples.

76
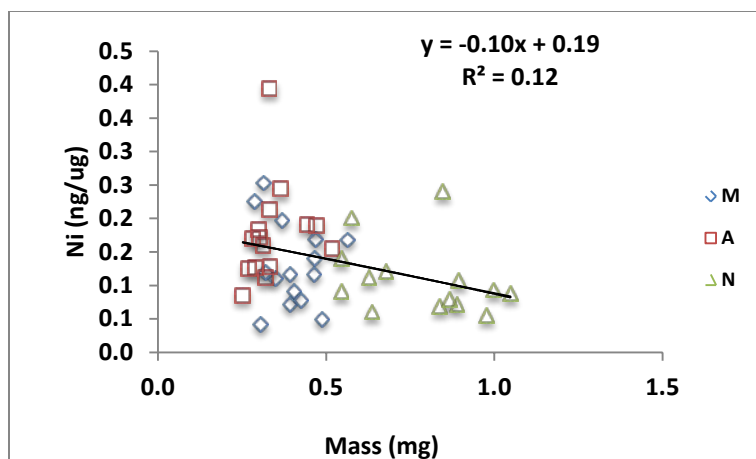
Figure 36. Claremont mass-normalized nickel vs. mass on the filter after 2 hrs of extraction. The correlation is significant at the p < 0.05 level. Blue diamonds: morning samples, red squares: afternoon samples, green triangles, nighttime samples.
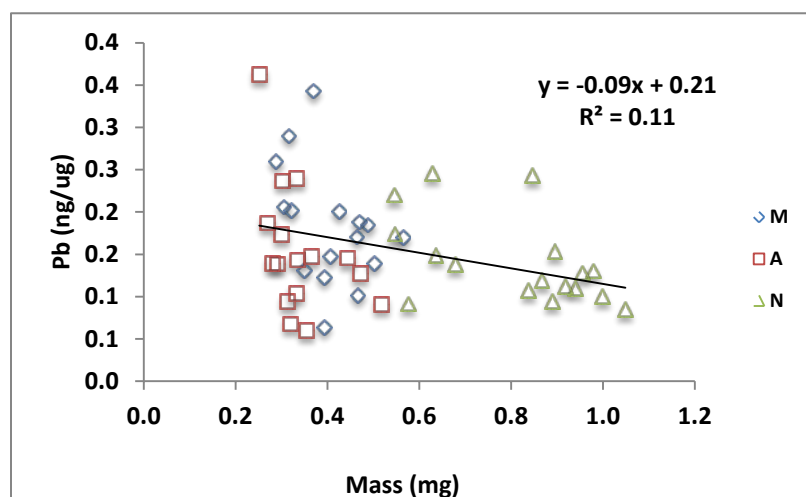
Figure 37. Claremont mass-normalized lead vs. mass on the filter after 2 hrs of extraction. The correlation is significant at the p < 0.05 level. Blue diamonds: morning samples, red squares: afternoon samples, green triangles, nighttime samples.

However, after 24 hours, a period during which much more material undergoes dissolution, there are some pronounced dependences on the mass in solution, including Fe(Total) (not shown). Fe(II) also has a strong correlation, but because of the significant potential confounding contribution of time of day to the speciation of iron, this relationship is not shown. A linear relationship is included, however the data are somewhat non-linear, with much higher values for the lower concentration samples, and similar values for almost all of the higher concentration samples. Certainly there are other possible explanations other than concentration-dependent solubility for this effect, related to differences in the sources and speciation of the iron available for dissolution, and photochemically-induced differences in the organic component. Figure 38 shows a moderate negative correlation between mass in solution and hydroxyl radical formation. Figure 39 shows the relationship between H_2O_2 and mass in solution. The relationship for H_2O_2 is more nuanced; at low mass concentrations, which correspond to high levels of soluble iron, H_2O_2 concentration is strongly negative; i.e.,

formation was lower than that observed in the blank. As the mass increases, corresponding to lower soluble iron, H_2O_2 concentration becomes positive. As discussed in sections III. A and B, H_2O_2 is also related other species, notably copper, however it is most strongly correlated with soluble iron. A relationship for DTT is not shown for 24 hours because DTT was measured only at 2 hours.
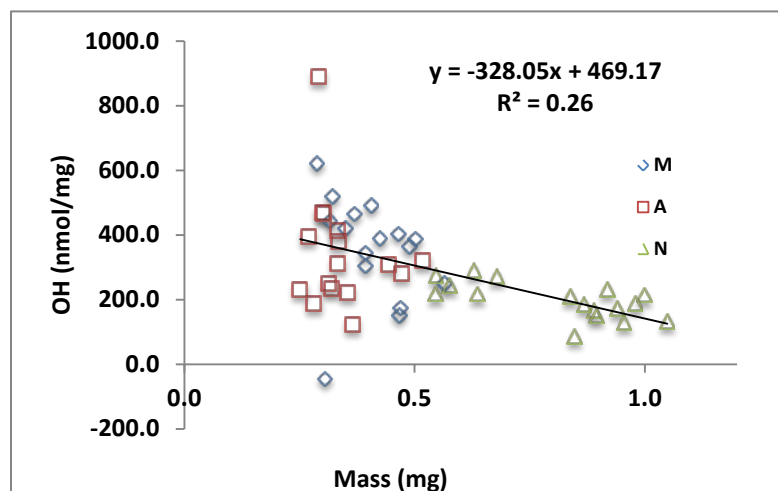
Figure 38. Claremont mass-normalized hydroxyl radical vs. mass on the filter after 24 hrs of extraction. Blue diamonds: morning samples, red squares: afternoon samples, green triangles, nighttime samples.
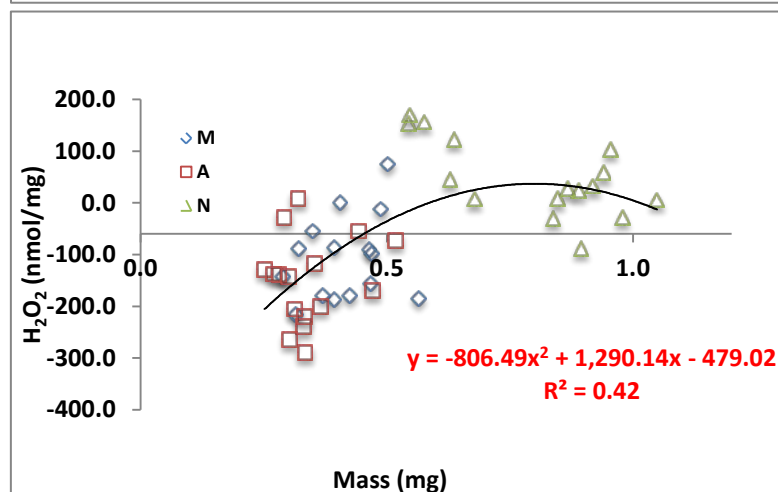
Figure 39 Claremont mass-normalized H_2O_2 vs. mass on the filter after 24 hrs of extraction.

Fresno

The Fresno data show similar trends to the Claremont data although for the two-hour data there are some slight mass-dependent trends. Fe(II), Fe(III) and Fe(total) all have very similar trends to one another; Fe(total) is shown (Figure 40). H_2O_2 does not show and overall trend, however there do appear to be negative (if noisy) trends within the night and morning data (Figure 41). The trend is largely driven by the lowest mass concentration points. •OH (Figure 42) exhibits a slight negative trend with mass driven by a handful of points with very low mass and relatively high •OH activity, collected after rain events. Two of these points had very high iron (not shown; the Fe was off the scale of the axis of Figure 40). There is no trend above a mass loading of about 0.4 mg. With the application of the Cu concentration correction algorithm in

section III.C, DTT shows no correlation with mass (Figure 43), however without this correction, there is a strong negative trend (Figure 44).
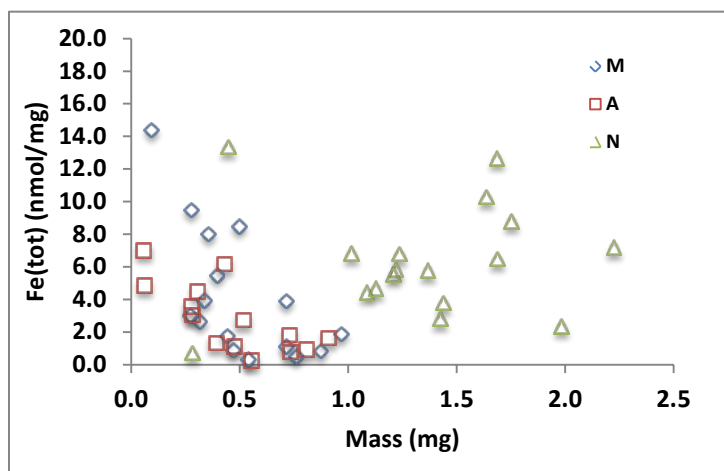
Figure 40. Fresno total iron normalized to mass vs. mass, after 2 hours of extraction. Two points at ~70 and 110 nmol/mg are above the scale of the ordinate axis. Blue diamonds: morning samples (7 AM – 1 PM), red squares: afternoon samples (1 PM – 7 PM), green triangles, nighttime samples (7 PM – 7 AM).
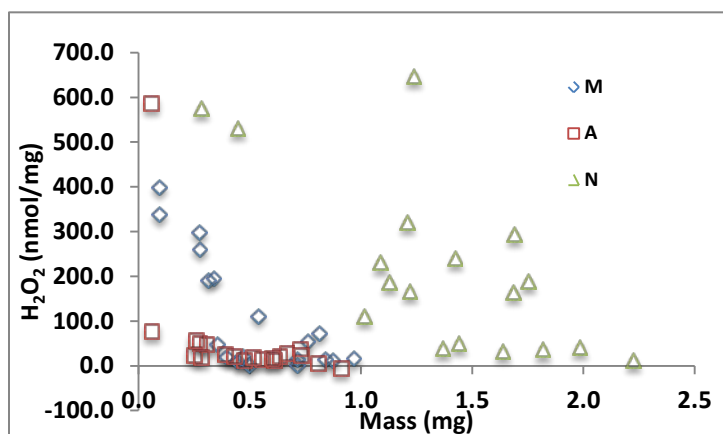
Figure 41. Fresno H_2O_2 normalized to mass vs. mass, after 2 hours of extraction. Blue diamonds: morning samples, red squares: afternoon samples, green triangles, nighttime samples.
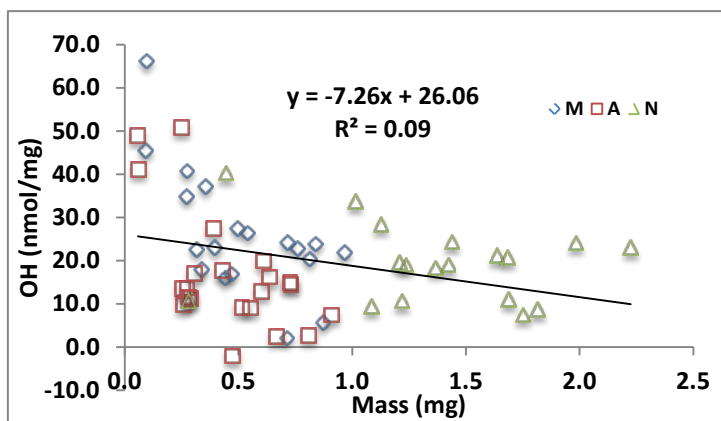
Figure 42. Fresno •OH normalized to mass vs. mass, after 2 hours of extraction. The correlation is significant (p = 0.03). Blue diamonds: morning samples, red squares: afternoon samples, green triangles, nighttime samples.
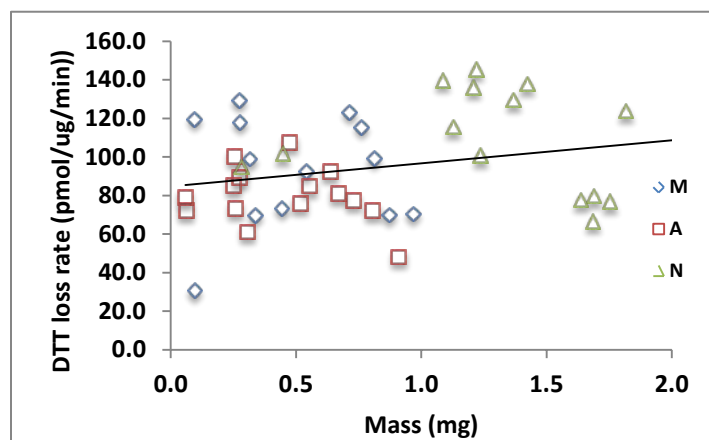
Figure 43. Fresno DTT normalized to mass vs. mass, after 2 hours of extraction, after accounting for copper/PM concentration in solution (Section III.C). There is no significant correlation. Blue diamonds: morning samples, red squares: afternoon samples, green triangles, nighttime samples.

Figure 44. Fresno DTT normalized to mass vs. mass, after 2 hours of extraction, without accounting for copper/PM concentration in solution (Section III.C) The correlation is highly significant. Blue diamonds: morning samples, red squares: afternoon samples, green triangles, nighttime samples.
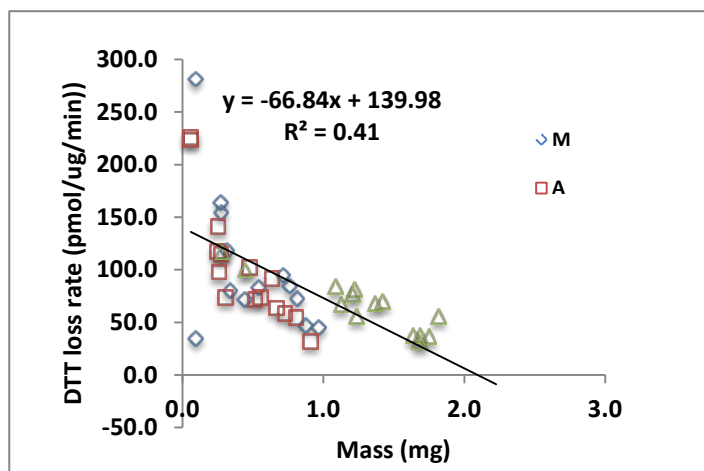
In summary, for the two hour samples, artifacts from the arbitrary choice of extraction volume are very minimal to non-existent, except in the case of DTT. Note that copper solubility is not dependent on the dissolved PM concentration. For complex field samples, normalizing for the mass, copper, iron and/or concentrations of other components in the solution, is a complex process involving several judgments that could introduce bias. Further, complex field samples potentially include a variety of synergistic or antagonistic interactions between two or more transition metals. A few of these have been investigated as part of this project (see discussions of metal-metal interactions in Sections III.A. and B.). Other interactions include organics, which can change solubility and activity of several of the metals most likely to be important here. As a result, we feel that attempting to "normalize" to mass in the solution would introduce additional errors, and these might include investigator bias. As a result, we have do not attempt to normalize for mass in solution for the 2 hour samples.

The effects of the concentration of the solution are much more pronounced for the 24-hour extraction solutions. For these solutions, the effects of concentration are taken into account.

IV.B.2.1 Average Value Comparison with Literature

Table 11 summarizes our H_2O_2 values compared to literature values. The H_2O_2 literature is fairly small, and measurements were made under a variety of different conditions, so comparisons are very difficult. Generally, our values are at the low end of other literature values for comparable extraction solutions. The reasons for this are unclear, and may include differences in aerosol chemical composition as well as sample storage. While in most cases chemical composition is difficult to compare, the samples reported here were stored in a freezer for about 22 months. Sample aging has been shown to result in a substantial drop in H_2O_2 production compared to fresh samples (Fuller et al. 2014; Paulson et al. 2009a).

Consistent with expectations, H_2O_2 production is higher in SLF. As transition metal solubility is much lower at the high pHs of SLF (Deguillaume et al. 2005), and H_2O_2 production in pure water has been shown to be highest at moderately acidic pHs of 3.5 – 5.5 (Wang et al. 2012), higher activity in SLF is not due to the higher availability of soluble transition metals, but rather the influence of antioxidants (Charrier et al. 2014b), Section III.A.. Activity is much higher in Fresno than Claremont samples (Table 11). This is likely the result of BBHULIS, which is strongly correlated with H_2O_2 formation as well as •OH and DTT.

Table 11. Comparison of H_2O_2 literature values

Particle Type	Season	Extraction solution	ng/m³	ng/µg	Reference
PM$_4$, Claremont, CA	S	pH3.5	2.7±1.4	0.12±0.06	This study
PM$_4$, Claremont, CA		SLF	16.8±14.7	0.74±0.61	
PM$_4$, Fresno, CA	W	pH3.5	2.9±2.0	0.10±0.08	
PM$_4$, Fresno, CA		SLF	91.9±119.1	4.2±5.6	
PM$_{2.5}$, Fresno		Phosphate buffer		0.68	Shen et al., 2011
PM$_{2.5}$, Fresno	S 06	Phosphate buffer w/50µM Asc	1428±204	68±27	
PM$_{2.5}$, Fresno	S 08		1564±204	34±3	
PM$_{2.5}$, Fresno	W 07		1666±68	136±17	
PM$_{2.5}$, Fresno	W 09		408±68	17±2	
PM$_{2.5}$, Westside	S 07		136±68	3.4	
PM$_{2.5}$, Freeway		pH3.5 w/ 0.1mM EDTA		0.42±0.3	Arellanes et al., 2006
PM$_{2.5}$, UCLA				0.58±0.03	
PM$_{2.5}$, Riverside campus	S			0.95±0.69	Wang et al., 2012
CRCAES, Riverside	S			0.49±0.55	
PM$_{2.5}$, UCLA				0.11±0.07	
α-pinene SOA				0.93±0.36	
β-pinene SOA				2.12±1.48	
PM$_{2.5}$, Singapore	W	Phosphate buffer, DCFH	194*		See et al., 2007
PM$_{2.5}$, traffic	W	Phosphate buffer, DCFH	513*		

Fine PM, sidewalk, Taipei	S	Phosphate buffer, DCFH	11±8[*]		Hung and Wang, 2001
PM$_{2.5}$, Rubidoux. CA	S	Phosphate buffer, DCFH	193.4[*]		Venkatachari et al., 2005
PM$_{2.5}$, Flushing, NY	W	Phosphate buffer, DCFH	29[*]		Venkatachari et al., 2007

[*] Values were converted from nmol/m^3 reported in original studies to ng/m^3.

Measured values for hydroxyl radical are much lower than values reported in the literature for extraction with ascorbate (Table 12), which is a similar but not identical extraction solution to the SLF used here. Our measured values in both SLF and pH3.5 are much higher, or in the case of Jung et al. (2006), similar to literature values. The SLF and pH3.5 •OH values are more similar than they are for H$_2$O$_2$ (Table 11). We note that metal solubility is expected to be much lower at the higher pH of SLF, but the differences are metal-dependent.

Table 12. Comparison of •OH literature values

Particle Type	Season	Extraction	ng/m^3	ng/μg	Reference
PM$_4$, Claremont	S	pH3.5	3.8±1.6	0.17±0.06	This study
PM$_4$, Claremont	S	SLF	14.3±3.8	0.65±0.20	
PM$_4$, Fresno	Winter	pH3.5	6.8±1.5	0.49±0.41	
PM$_4$ Fresno	Winter	SLF	9.7±5.8	0.70±0.45	
PM$_{2.5}$, Fresno In phosphate buffer, ascorbate (Asc) @ 50 μM if included.	S 06	w/Asc	51 ± 10.2[*]	2.04 ± 0.68[*]	Shen et al., 2011
		No Asc	1.7±1.4	0.06	
	S 08	w/Asc	68 ± 10.2[*]	1.36 ±0.34[*]	
		No Asc	2.4±1.4	0.05	
	W 07	w/Asc	95.2 ± 6.8[*]	7.48± 0.68[*]	
		No Asc	0.82±1.0	0.05	
	W 09	w/Asc	51 ± 10.2[*]	1.53 ± 0.34[*]	
		No Asc	3.7±1.0	0.1	
PM$_{2.5}$, Westside In phosphate buffer, ascorbate @ 50 μM if included.	S 07	w/Asc	61.2 ± 6.8[*]	2.72 ±0.68[*]	
		No Asc	1.4±1.7	0.05	
	W 08	w/Asc	23.8 ± 6.8[*]	1.36 ±0.68[*]	
		No Asc	0.7±0.7	0.03	
PM$_{2.5}$, Davis	Spring	Phosphate buffer w/200C	39.1±25.5[*]	9.52± 1.36[*]	Vidrio et al., 2009
	W			2.89±0.85[*]	
PM$_{2.5}$, Davis				0.36±0.27[*]	Jung et al., 2006
Carbon Black		Phosphate buffer		0.015±0.005[*]	
Flaming Soot				0.002±0.0005[*]	

- [*] indicates values were calculated.
- No standard deviation was reported for mass by (Shen et al. 2011).
- EPR methods were not compared here.

Despite very different chemical composition, DTT consumption rates were nearly identical for the two field campaign sites, and had a small dynamic range. Consistent with this, DTT consumption rates had significantly different dependencies on chemical composition (not shown). DTT values were rather high compared to earlier literature values (Table 13), for unknown reasons.

Table 13. Comparison of DTT consumption rate literature values

Particle Type	Size	Location/	Season	Extraction Solution	DTT consumption rate (nmol/µg/min)	Reference
Ambient	$PM_{2.5}$	Claremont	Summer	Phosphate Buffer	0.092± 0.014	This study
		Fresno	Winter		0.094± 0.03	
Ambient	Coarse	Boyle Heights	Oct to Jan	Milli-Q Water	~0-0.03	[*]Cho et al. 2005
		Claremont			~0-0.02	
		USC			~0-0.02	
	Fine/ Ultrafine	Boyle Heights			0.02-0.04	
		Claremont			0.02-0.04	
		USC			0.01-0.04	
	Ultrafine	Boyle Heights			0.08-0.14	
		Claremont			0.05-0.26	
		USC			0-0.08	
Diesel, Transient	Fine	Thessaloniki, Greece		Milli-Q Water	0.039±0.05	Geller et al. 2006
Diesel stead. state					0.034	
Diesel Particle Filter Transient					0.11±0.02	
Gasoline transient					0.025±0.03	
[a]Baseline	[b]Cruise	California air resources Board's Heavy-duty Diesel emission testing laboratory		Milli-Q Water	0.01	[*]Biswas et al. 2009
[a]CRT					0.06	
[a]V/Z-SCRT					0.01-0.03	
[a]DPX					0.02	
[a]Horizon					0.19	
[a]Baseline	[b]UDDS				0.02	
[a]CRT					0.07	
[a]V/Z-SCRT					0.01	
[a]DPX					0.01	
[a]Horizon					0.16	
[a]Baseline	[b]Idle				0.02	
[a]DPX					0.08	
[a]Horizon					0.06	

Ambient	PM$_{0.15}$ PM$_{2.5}$ PM$_{coarse}$	Downey, CA	Summer	Milli-Q Water	0.061-0.083 0.021-0.036	Ntziachristos et al. 2007
		Riverside, CA	Summer		0.052-0.053 0.026-0.028	
		Caldecott Tunnel B1	Summer		0.111 0.068 0.019	
		Caldecott Tunnel B2	Summer		0.172 0.075 0.032	
		CA-110	Winter		0.042 0.025 0.017	
Ambient	PM$_{0.25}$ PM$_{2.5}$ PM$_{coarse}$	[c]Site 1	March-May	Milli-Q Water	0.035 0.024 0.018	Hu et al 2008
		[c]Site 2			0.032 0.018 0.012	
		[c]Site 3			0.047 0.023 0.017	
		[c]Site 4			0.055 0.014 0.012	
		[c]Site 5			0.033 0.020 0.008	
		[c]Site 6			0.031 0.017 0.012	

[*] Values estimated from graph

[a] diluted diesel exhaust PM with different after-treatment technology implemented: Baseline: no treatments. CRT: continuous regenerating technology, a diesel oxidation catalyst + an uncatalyzed trap. V/Z-SCRT: vanadium/zeolite based selective catalytic reduction technology. DPX: diesel particulate trap with catalytic washcoats. Horizon: a school bus equipped with an electric particle filter.

[b.] driving conditions: Cruise: steady state cruise at 8-kph; UDDS: transient EPA unban dynamometer driving schedule.

[c] Sampling sites in the communities of Los Angeles-Long Beach harbor. Site 1: intersection between a major street and a residential road. Site 2: 3 km north of ocean coast and intersection between 2 major streets. Site 3: semi-industrial area, 1 km north of Highway 1. Site 4: 1 km east of I-710 and 1 km north of I-405. Site 5: background site of Long Beach. Site 6. USC main campus.

IV.B.2.2 Single Variable Correlations

Most of the independent variables (mass, metals, quinones) have at least some co-linearity, although soluble metals are trace components of aerosols, individually contributing no more

than 3% of total mass and usually far less, thus they may be fairly independent of mass. Only in a few cases does the co-linearity reach the level at which it would be expected to be highly problematic (variance inflation factor, VIF > 5). However, many VIF values for our data are moderate, falling in the 1 – 5 range, and multivariate regressions exhibit signs of co-linearity (adding another partly co-linear species to a multivariate regression can substantially change the regression statistics). Therefore, single-variable linear regressions should be interpreted cautiously.

IV.B.2.3 Correlations of ROS with aerosol mass

Generally, correlations with mass are strong, however because many other species are also strongly correlated with mass, there is some co-linearity of component species making a strong contribution to the apparent correlation with mass. Clearly there is no mechanism by which "aerosol mass" should produce ROS; ROS is produced by specific chemical reactions mediated by species in the particles. However, ROS formation clearly does not result from single species, or even from simple addition of production rates for several individual species, but most likely from interplay between many species, including transition metals and their ligands. The correlations with mass however, provide an average view of all of the underlying species taken together.

Hydroxyl radical formation is strongly correlated with mass, at both the Claremont and Fresno sites (Figure 45 and Figure 46). The slope is about twice as high for the Claremont samples compared to Fresno. In both cases, the afternoon samples are significantly less active than the morning samples. The possible reasons for this phenomenon are discussed below.
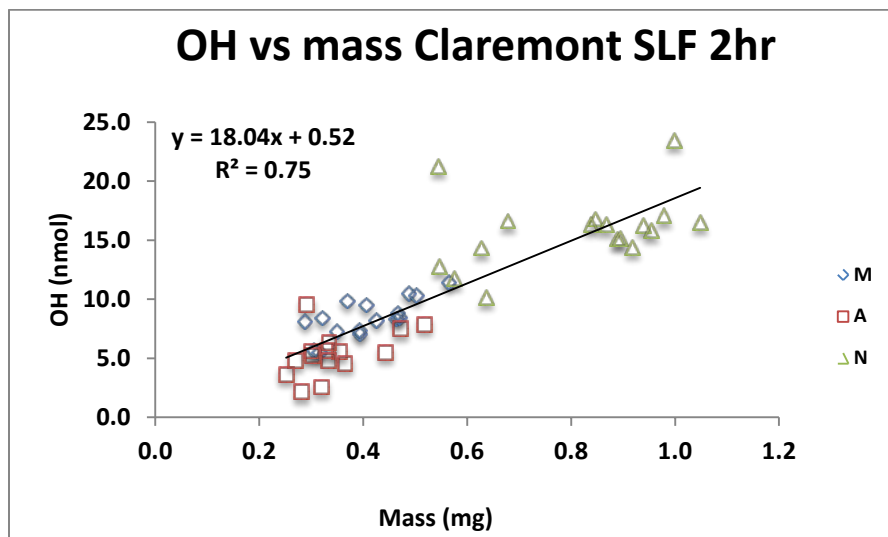
Figure 45. Correlation between aerosol mass (in the sample) and •OH formed after 2 hours extraction in SLF for Claremont samples collected in morning (blue diamonds), afternoon (red squares), and night (green triangles) samples. Note that night samples were collected for approximately twice as long (7 PM – 7 AM) as morning (7 AM – 1 PM) and afternoon samples (1 PM – 7 PM).

OH vs mass Fresno SLF 2hr

$y = 8.56x + 0.30$
$R^2 = 0.62$
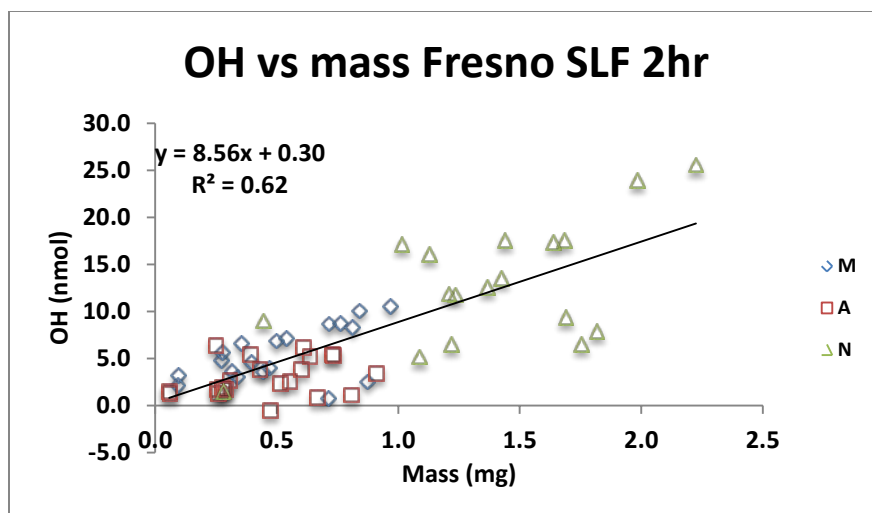
Figure 46. Correlation between aerosol mass (in the sample) and •OH formed after 2 hours extraction in SLF for Fresno samples collected in morning (blue diamonds), afternoon (red squares), and night (green triangles) samples. Note that night samples were collected for approximately twice as long (7 PM – 7 AM) as morning (7 AM – 1 PM) and afternoon samples (1 PM – 7 PM).

Without accounting for the concentration of copper in solution, DTT is strongly correlated with mass ($r^2 = 0.62$ and 0.61 for Claremont and Fresno respectively, not shown). However, once the concentration of Cu is accounted for, the correlation is very strong (Figure 47 and Figure 48), with $r^2 = 0.88$ and 0.79 for Claremont and Fresno respectively.

DTT loss rate vs mass Claremont w/ Cu

$y = 2.18x - 0.02$
$R^2 = 0.88$
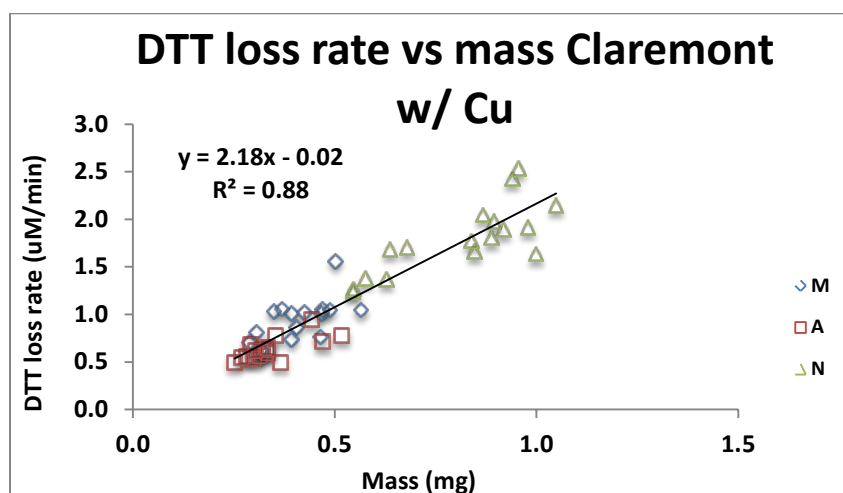
Figure 47. Correlation between aerosol mass (in the sample) and DTT formed after 2 hours extraction in SLF for Claremont samples collected in morning (blue diamonds), afternoon (red squares), and night (green triangles) samples.

DTT loss rate (w/ Cu) vs mass Fresno SLF 2hr

$y = 2.34x - 0.08$
$R^2 = 0.79$

Figure 48. Correlation between aerosol mass (in the sample) and DTT formed after 2 hours extraction in SLF for Fresno samples collected in morning (blue diamonds), afternoon (red squares), and night (green triangles) samples. Note that night samples were collected for approximately twice as long (7 PM – 7 AM) as morning (7 AM – 1 PM) and afternoon samples (1 PM – 7 PM).

Of the three ROS assays performed here, H_2O_2 was the most weakly correlated with mass (Figure 49 and Figure 50). In contrast to •OH and to a lesser extent DTT, activity was indistinguishable as a function of time of day. For the Fresno however, the afternoon samples exhibited zero or near zero activity in all cases, while morning and afternoon samples, while scattered, fell on the same line. The plots also show that the H_2O_2 concentration is several times higher in the Fresno samples compared to Claremont.

H_2O_2 vs mass Claremont SLF 2hr

$y = 6.78x + 1.84$
$R^2 = 0.11$
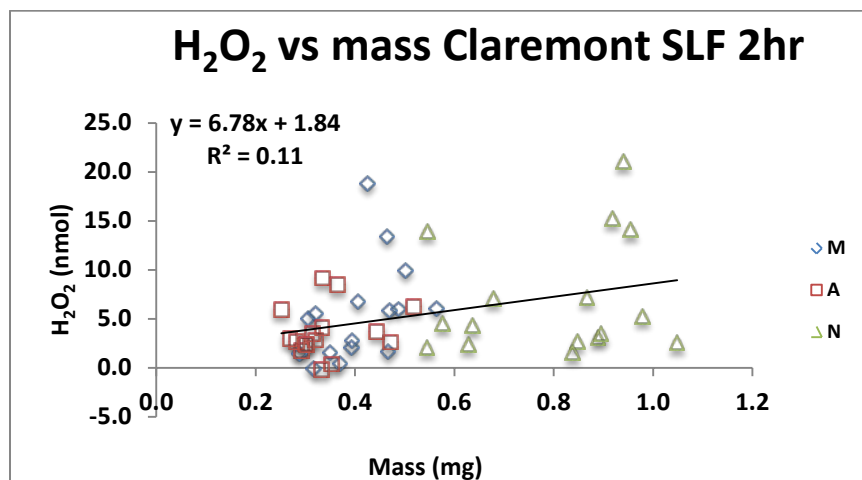
Figure 49. Correlation between aerosol mass (in the sample) and H_2O_2 formed after 2 hours extraction in SLF for Claremont samples collected in morning (blue diamonds), afternoon (red squares), and night (green triangles) samples. Note that night samples were collected for approximately twice as long (7 PM – 7 AM) as morning (7 AM – 1 PM) and afternoon samples (1 PM – 7 PM).

H$_2$O$_2$ vs mass Fresno SLF 2hr

$y = 61.65x - 4.05$
$R^2 = 0.20$

Figure 50. Correlation between aerosol mass (in the sample) and H$_2$O$_2$ formed after 2 hours extraction in SLF for Fresno samples collected during morning (blue diamonds), afternoon (red squares), and night (green triangles). Note that night samples were collected for approximately twice as long (7 PM – 7 AM) as morning (7 AM – 1 PM) and afternoon samples (1 PM – 7 PM).

IV.B.2.4 Correlations between metals and aerosol mass

In some but not all cases, iron, copper and some other metals are strongly correlated to mass. Interestingly, despite a general correlation, the Claremont afternoon samples generally contained very low levels of soluble transition metals, including Fe(total) measured with Ferrozine (Figure 51) or ICP (Figure 52), copper (Figure 53) and manganese measured by ICP (Figure 54), selenium and lanthanum (UCLA ICP, not shown).
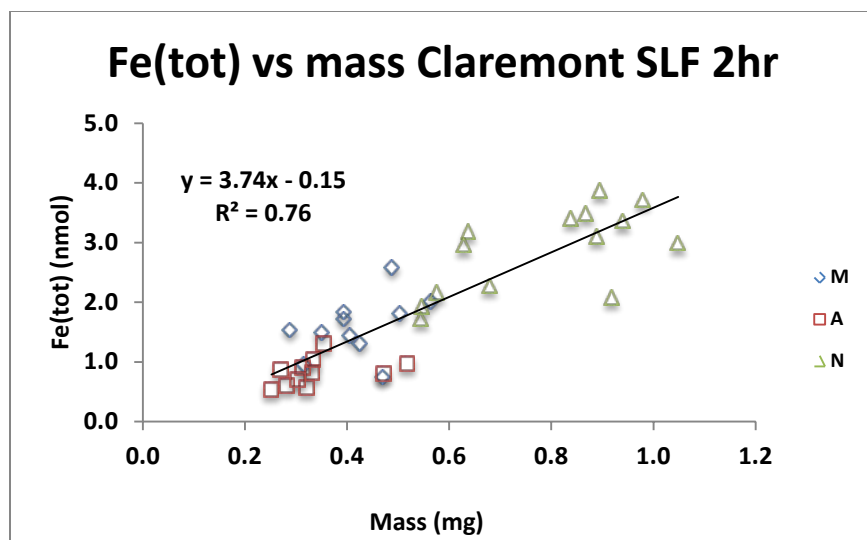
Figure 51. Correlation between aerosol mass (in the sample) and total soluble iron measured with the Ferrozine method after 2 hours extraction in SLF for Claremont samples collected during morning (blue diamonds), afternoon (red squares), and night (green triangles). Note that night samples were collected for approximately twice as long (7 PM – 7 AM) as morning (7 AM – 1 PM) and afternoon samples (1 PM – 7 PM).

Figure 52. Correlation between aerosol mass (in the sample) and total soluble iron measured with the with ICP by the UCLA group after 2 hours extraction in SLF for Claremont samples collected during morning (blue diamonds), afternoon (red squares), and night (green triangles). Night samples were collected for approximately twice as long (7 PM – 7 AM) as morning (7 AM – 1 PM) and afternoon samples (1 PM – 7 PM).
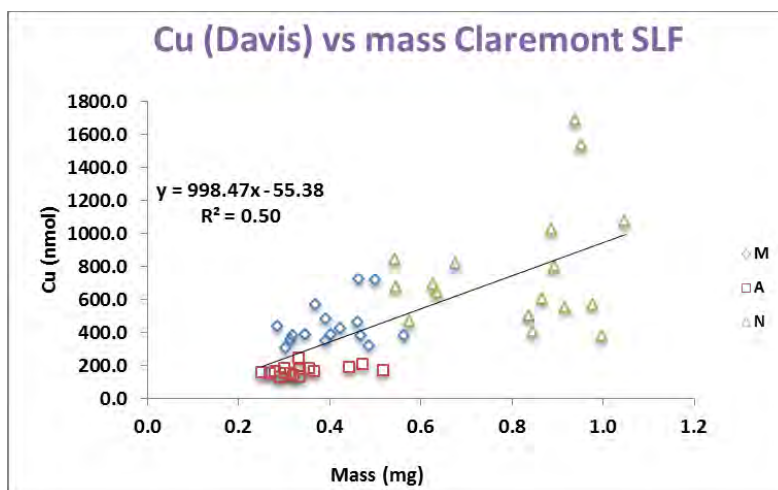
Figure 53. Correlation between aerosol mass (in the sample) and total soluble iron measured with the with ICP by the Davis group after 2 hours extraction in SLF for Claremont samples collected during morning (blue diamonds), afternoon (red squares), and night (green triangles). Night samples were collected for approximately twice as long (7 PM – 7 AM) as morning (7 AM – 1 PM) and afternoon samples (1 PM – 7 PM).

Figure 54. Correlation between aerosol mass (in the sample) and soluble manganese measured with the with ICP by the UCLA group formed after 2 hours extraction in SLF for Claremont samples collected during morning (blue diamonds), afternoon (red squares), and night (green triangles). Night samples were collected for approximately twice as long (7 PM – 7 AM) as morning (7 AM – 1 PM) and afternoon samples (1 PM – 7 PM).

Fresno samples similarly had very low concentrations of several transition metals in the afternoons. In several cases, concentrations in the nighttime samples were much higher than either morning or afternoon, including Mn and Cu (Figure 55, 56 and 57).

90
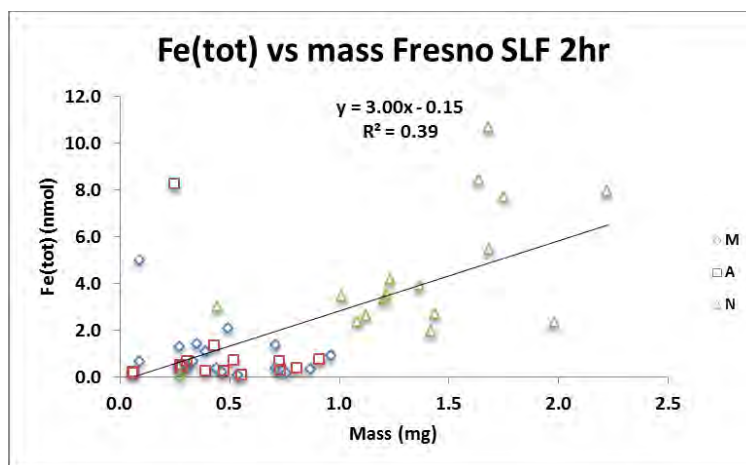
Figure 55. Correlation between soluble iron measured with the Ferrozine assay and aerosol mass (in the sample) after 2 hours extraction in SLF for Fresno samples collected during morning (blue diamonds), afternoon (red squares), and night (green triangles). Night samples were collected for approximately twice as long (7 PM – 7 AM) as morning (7 AM – 1 PM) and afternoon samples (1 PM – 7 PM).

Figure 56. Correlation between soluble copper measured with ICP-MS by UCLA and aerosol mass (in the sample) after 2 hours extraction in SLF for Fresno samples collected during morning (blue diamonds), afternoon (red squares), and night (green triangles). Night samples were collected for approximately twice as long (7 PM – 7 AM) as morning (7 AM – 1 PM) and afternoon samples (1 PM – 7 PM).

Figure 57. Correlation between soluble copper measured by UCD with ICP and aerosol mass after 2 hours extraction in SLF for Fresno samples collected during morning (blue diam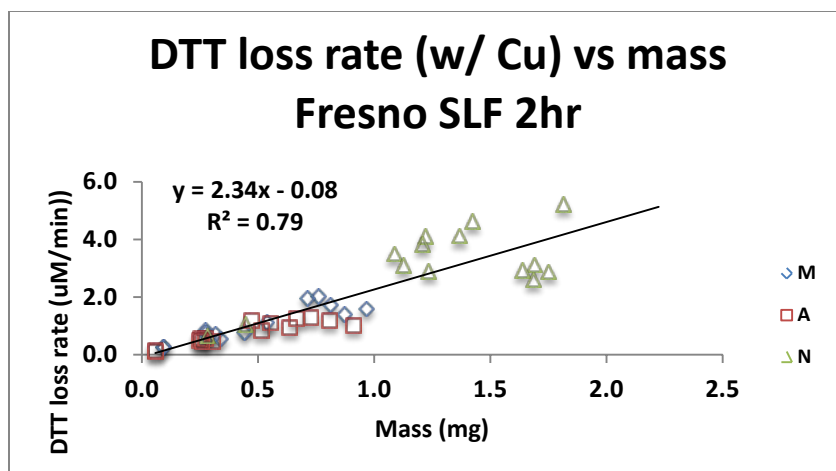onds), afternoon (red squares), and night (green triangles). Night samples were collected for approximately twice as long (7 PM – 7 AM) as morning (7 AM – 1PM) and afternoon samples (1 PM – 7 PM).

IV.B.2.5 BBHULIS vs. mass and metals

Biomass burning HULIS vs mass is shown in Figure 58. Afternoon and night samples fall on essentially the same line (not shown), while the afternoon samples have a smaller contribution from HULIS. As is well known and discussed above, the conversion of optical absorption in general, and optical absorption of particles collected on a filter to mass in particular carries significant uncertainties. As a result, the absolute numbers carry significant uncertainties of order ± 50%.
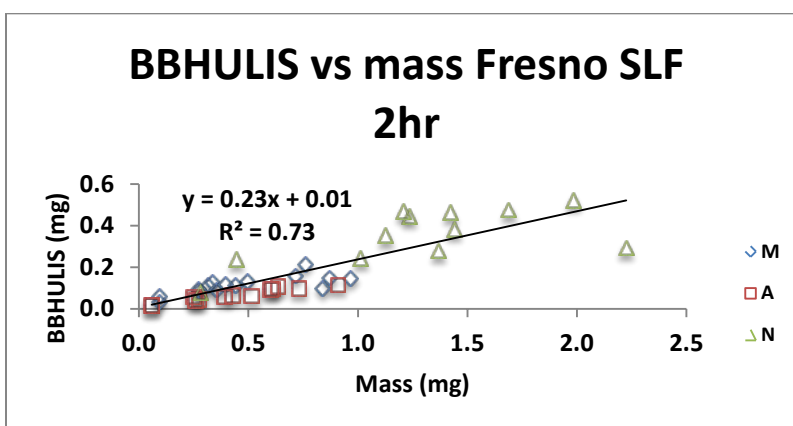
Figure 58. Correlation between estimated biomass burning HULIS and aerosol mass (in the sample) Fresno samples collected during morning (blue diamonds), afternoon (red squares), and night (green triangles). Night samples were collected for approximately twice as long (7 PM - 7AM) as morning (7 AM – 1 PM) and afternoon samples (1 PM – 7 PM).

BBHULIS correlates with Cu, Pb, Fe (Figure 59, Figure 60 and Figure 61), Mn (not shown) in decreasing order, and not at all with Zn (not shown).
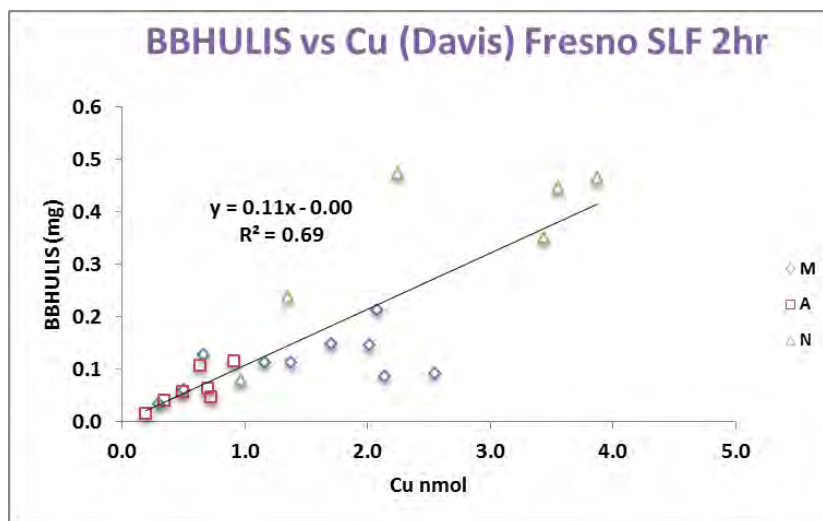
Figure 59. Correlation between BBHULIS mass and copper measured by UCD with ICP in SLF for Fresno samples collected during morning (blue diamonds), afternoon (red squares), and night (green triangles). Night samples were collected for approximately twice as long (7 PM – 7 AM) as morning (7 AM – 1 PM) and afternoon samples (1 PM – 7 PM).
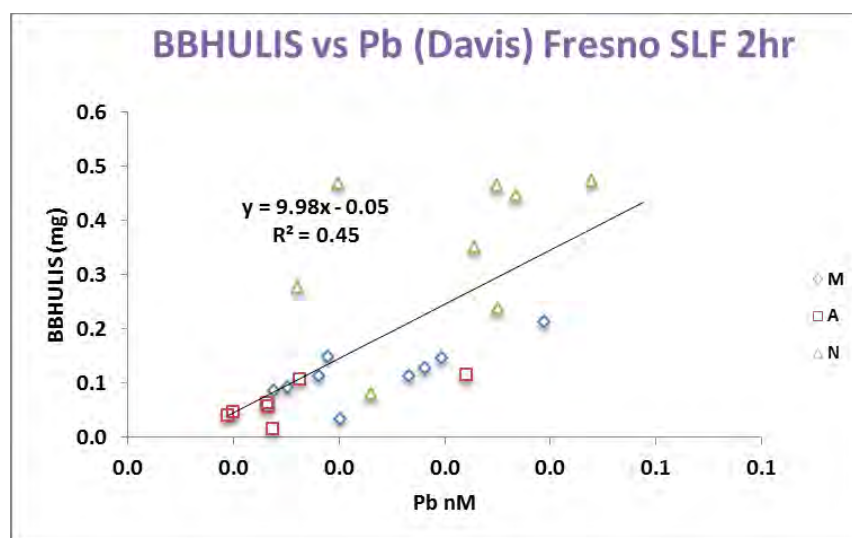
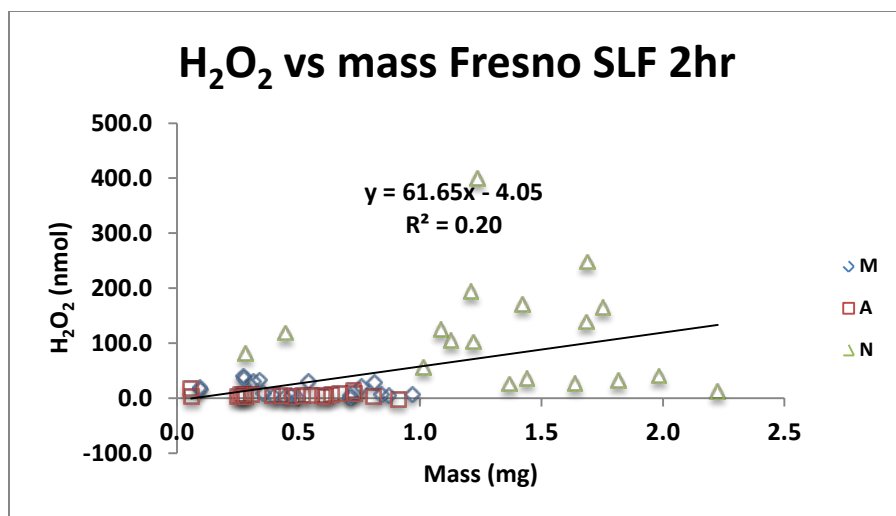**Figure 60. Correlation between BBHULIS mass and lead measured by UCD with ICP in SLF for Fresno samples collected during morning (blue diamonds), afternoon (red squares), and night (green triangles). Night samples were collected for approximately twice as long (7 PM – 7 AM) as morning (7 AM – 1 PM) and afternoon samples (1 PM – 7 PM).**

Figure 61. Correlation between BBHULIS mass and total iron measured with the Ferrozine assay in SLF for Fresno samples collected during morning (blue diamonds), afternoon (red squares), and night (green triangles). Night samples were collected for approximately twice as long (7 PM – 7 AM) as morning (7 AM – 1PM) and afternoon samples (1 PM – 7 PM).

BBHULIS is in turn strongly correlated with hydroxyl radical (Figure 62 r^2 = 0.61) and very strongly with DTT consumption (Figure 63), r = 0.84, but less so with H_2O_2 (Figure 64, r^2 = 0.49).
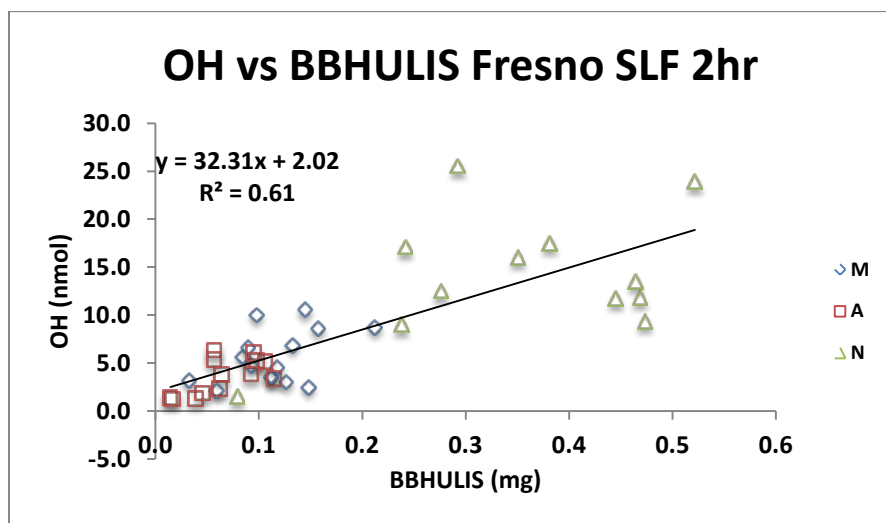
Figure 62. Correlation between •OH formation mass after 2 hours extraction in SLF and biomass burning HULIS for Fresno samples collected during morning (blue diamonds), afternoon (red squares), and night (green triangles). Night samples were collected for approximately twice as long (7 PM - 7AM) as morning (7 AM – 1 PM) and afternoon samples (1 PM – 7 PM).
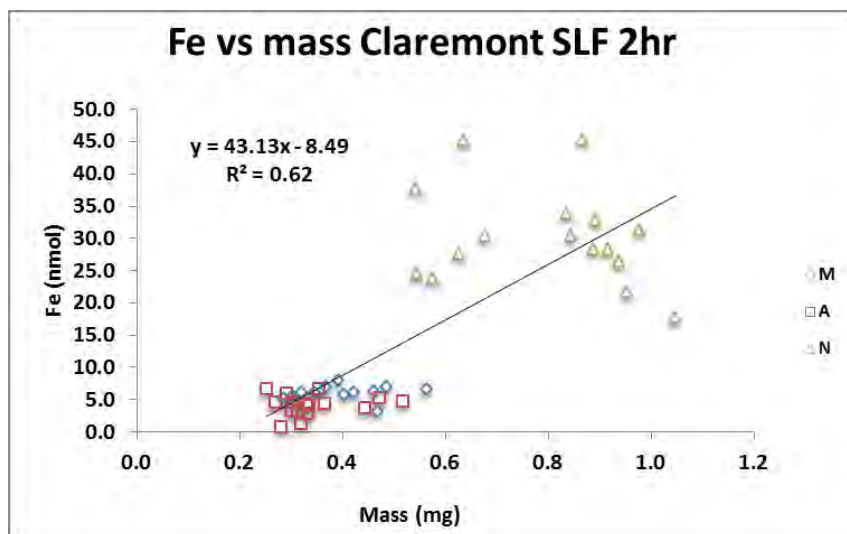
Figure 63. Correlation between DTT consumption rate after 2 hours extraction in SLF and biomass burning HULIS for Fresno samples collected during morning (blue diamonds), afternoon (red squares), and night (green triangles). Night samples were collected for approximately twice as long (7 PM – 7 AM) as morning (7 AM – 1 PM) and afternoon samples (1 PM – 7 PM).
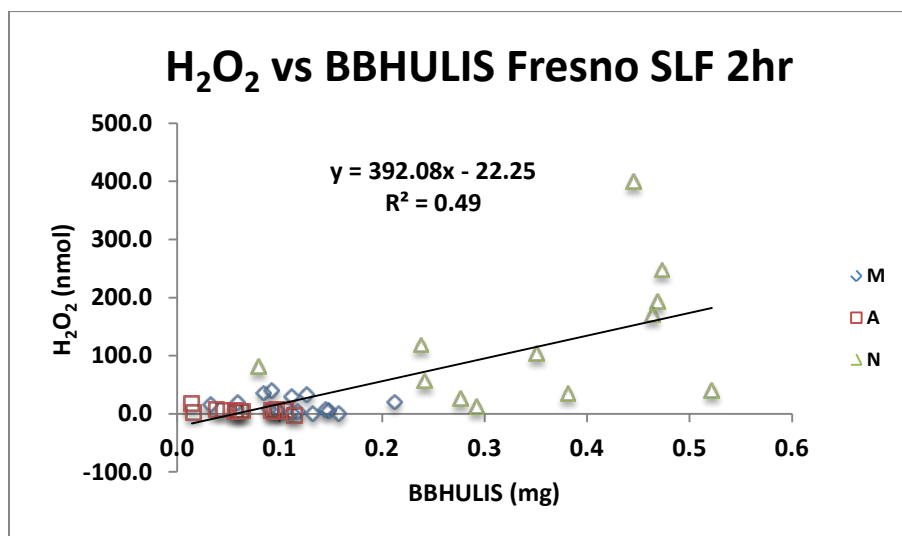
Figure 64. Correlation between H_2O_2 concentration after 2 hours extraction in SLF and biomass burning HULIS samples collected during morning (blue diamonds), afternoon (red squares), and night (green triangles). Night samples were collected for approximately twice as long (7 PM – 7 AM) as morning (7 AM – 1 PM) and afternoon samples (1 PM – 7 PM).

Additionally, there are several strong correlations between •OH formation and DTT consumption and transition metals, a few of which are shown below (Figure 65 and Figure 66).
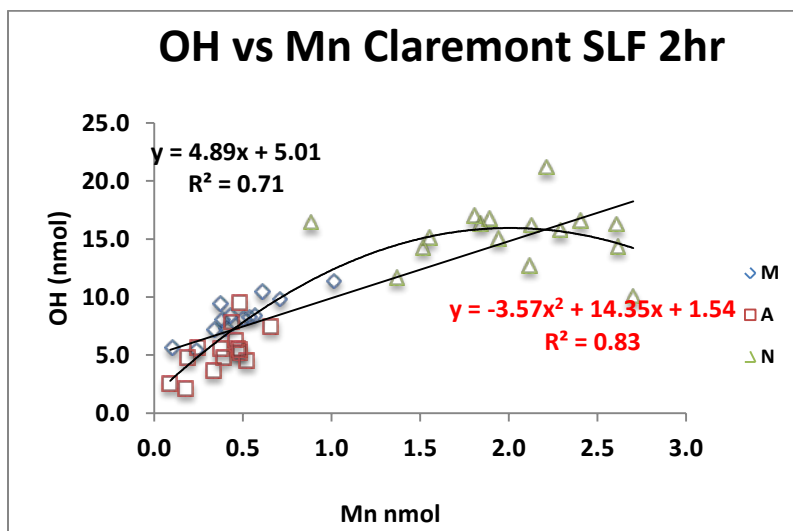
Figure 65. Correlation between •OH formation and Mn measured by ICP by the UCLA group after 2 hours extraction in SLF for Claremont samples collected during morning (blue diamonds), afternoon (red squares), and night (green triangles). Night samples were collected for approximately twice as long (7 PM – 7 AM) as morning (7 AM – 1 PM) and afternoon samples (1 PM – 7 PM).
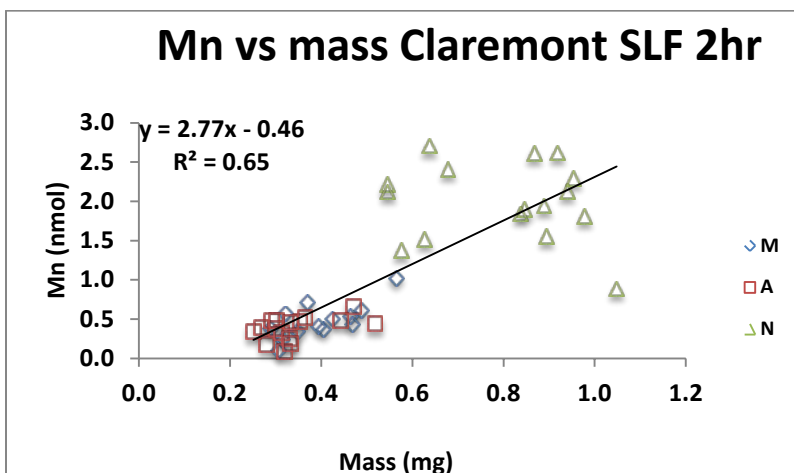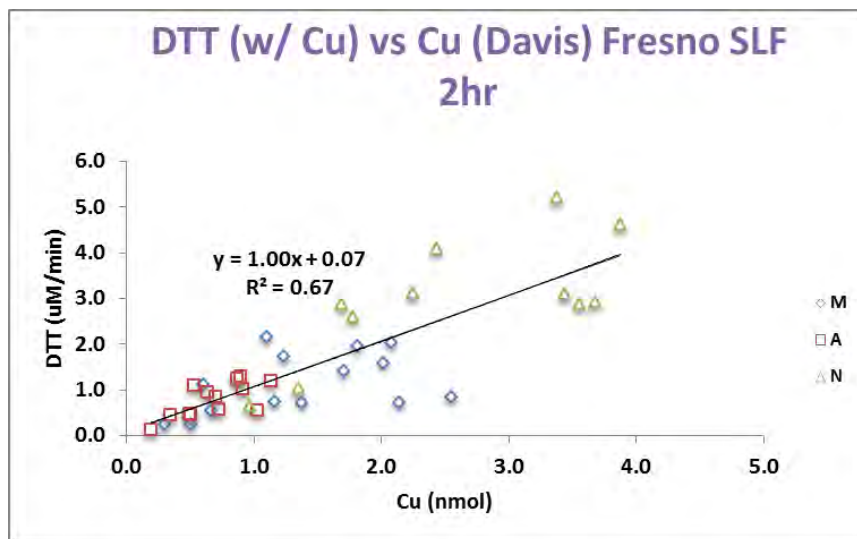

Figure 66. Correlation between DTT consumption rate and copper measured by UCD with ICP after 2 hours extraction in SLF for Claremont samples collected during morning (blue diamonds), afternoon (red squares), and night (green triangles). Night samples were collected for approximately twice as long (7 PM – 7 AM) as morning (7 AM – 1 PM) and afternoon samples (1 PM – 7 PM).

Quinones were uncorrelated with ROS in all cases (Figures 67-70), with the possible exception of phenanthraquinone and hydrogen peroxide in the Claremont samples (Figure 67).
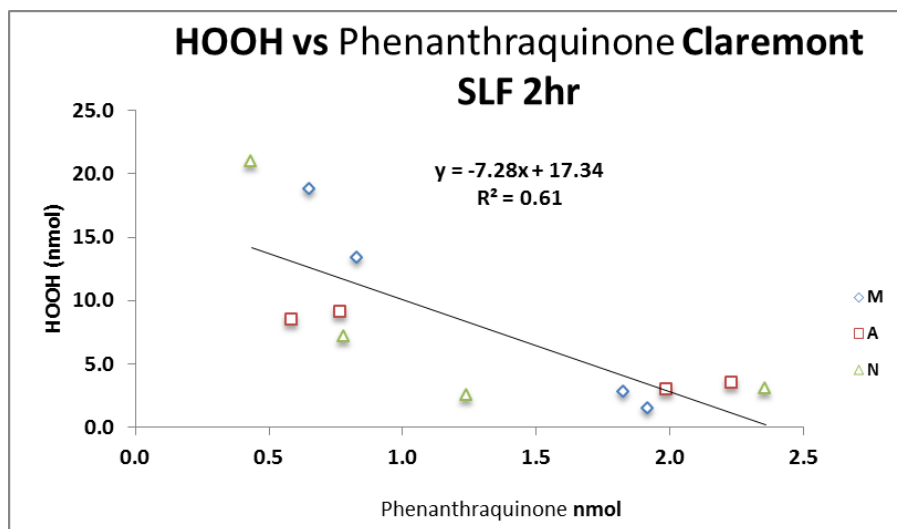
Figure 67. Correlation between HOOH and phenanthraquinone in the Claremont samples.
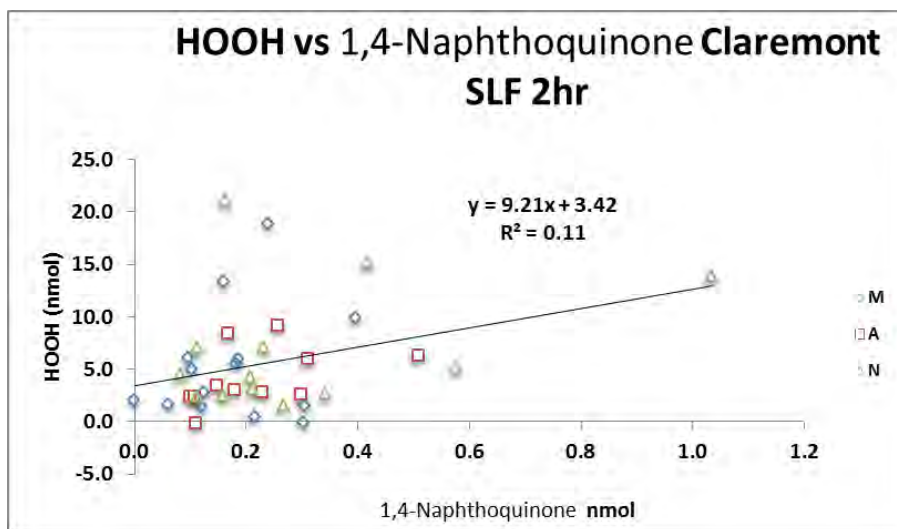
Figure 68. Correlation between HOOH and 1,4-naphthaquinone in the Claremont samples.
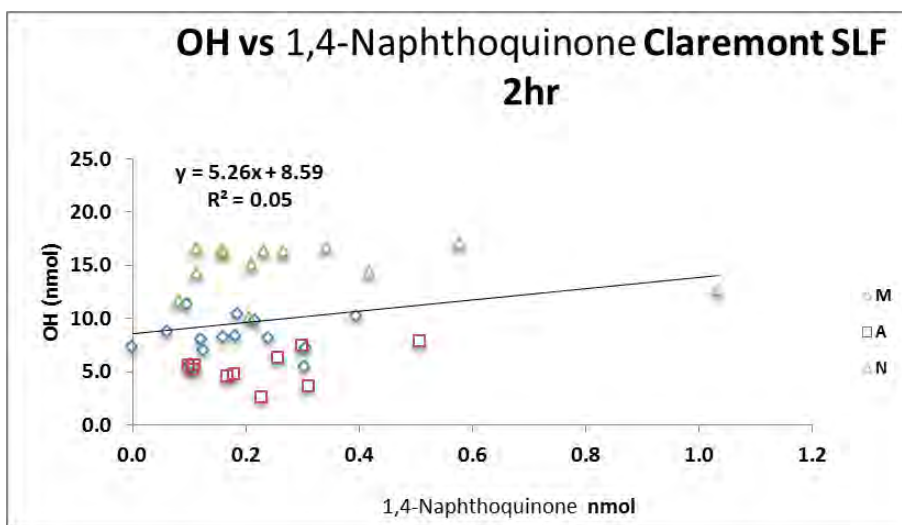
Figure 69. Correlation between •OH formation and 1,4-naphthaquinone in the Claremont samples
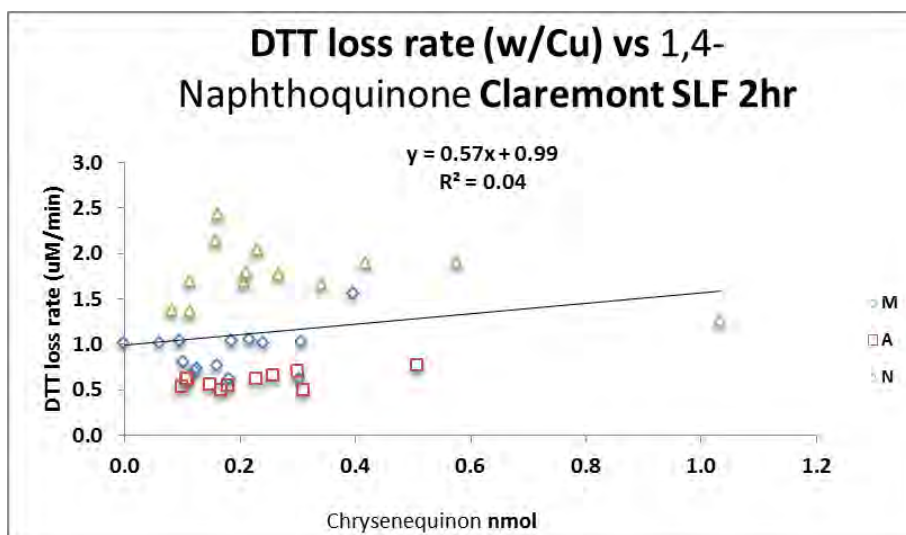
Figure 70. Correlation between DTT consumption and 1,4-naphthaquinone in the Claremont samples

IV.B.3.1 Relationships between ROS Species

•OH formation is fairly strongly correlated with DTT formation in both the Claremont and Fresno samples. In both cases the correlation after the correction for copper in the sample is stronger than without this correction; Claremont R^2 = 0.68, Figure 71 vs. R^2 = 0.56, not shown, respectively; Fresno R^2 = 0.42, Figure 72 vs. R^2 = 0.34, not shown, respectively. The correlations of both •OH and DTT with H_2O_2 concentration are much weaker (Figures 73 and 74).
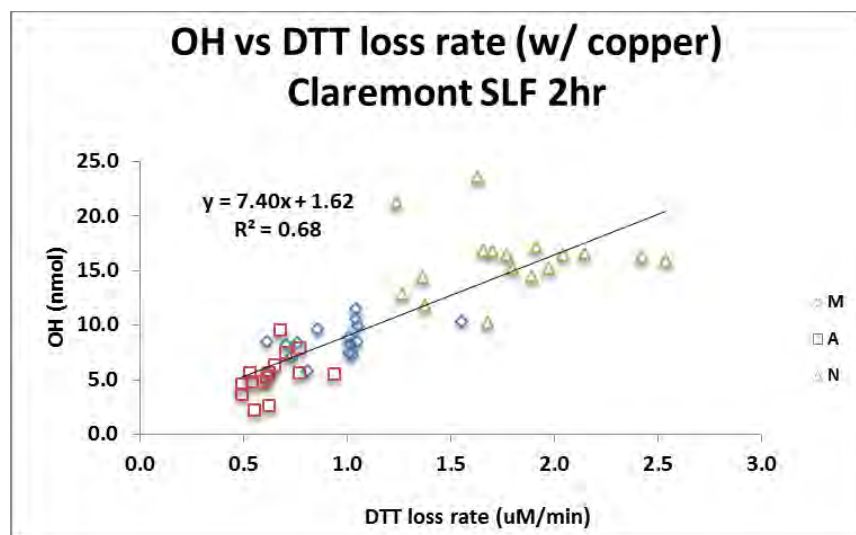
Figure 71. Correlation between •OH and DTT formed after 2 hours extraction in SLF for Claremont samples collected during morning (blue diamonds), afternoon (red squares), and night (green triangles). These DTT data include the non-linear correction for copper in the sample discussed in section III.C. Night samples were collected for approximately twice as long (7 PM – 7 AM) as morning (7AM – 1 PM) and afternoon samples (1PM – 7 PM).
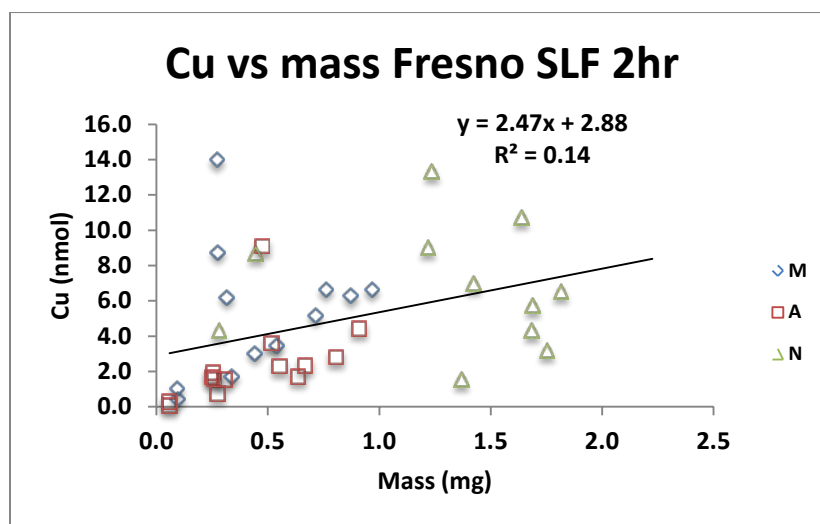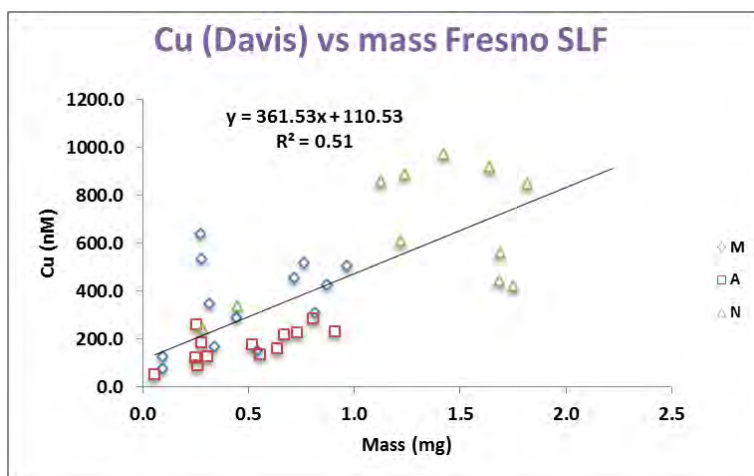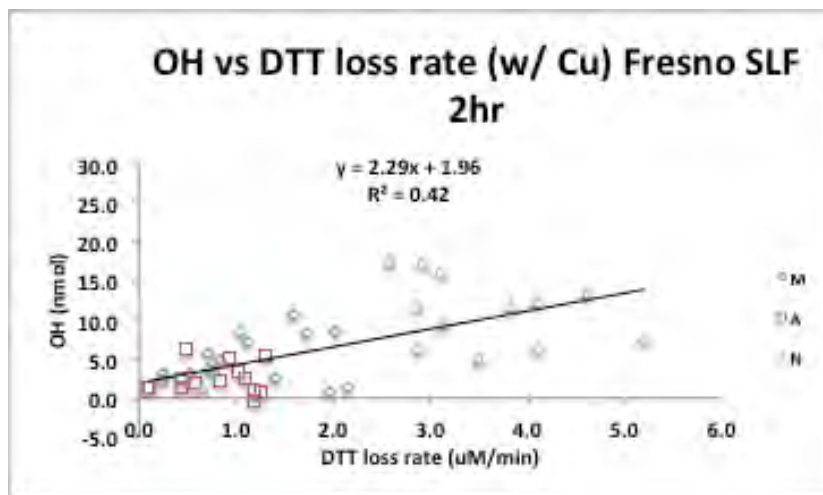

Figure 72. Correlation between •OH and DTT formed after 2 hours extraction in SLF for Fresno samples collected during morning (blue diamonds), afternoon (red squares), and night (green triangles). These DTT data include the non-linear correction for copper in the sample discussed in section III.C. Night samples were collected for approximately twice as long (7 PM – 7 AM) as morning (7 AM – 1 PM) and afternoon samples (1 PM – 7 PM).
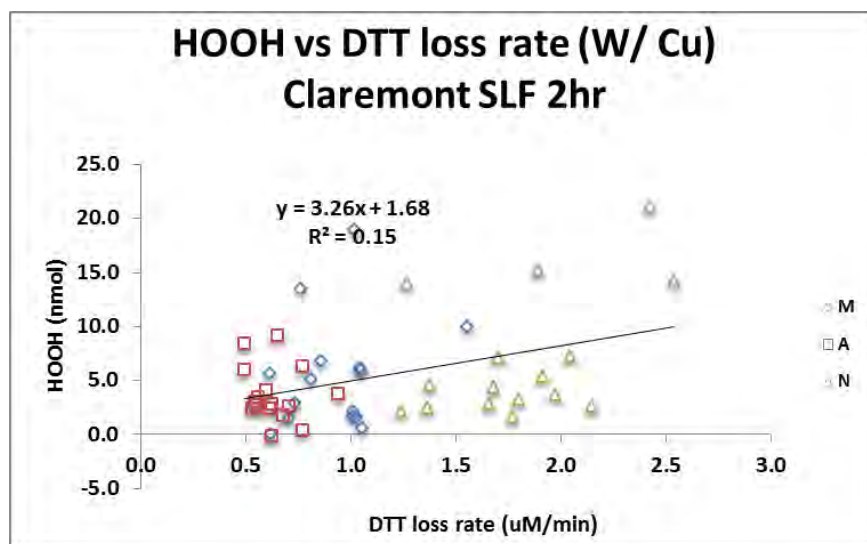
Figure 73. Correlation between DTT consumption rate and H_2O_2 concentration after 2 hours extraction in SLF for Claremont samples collected during morning (blue diamonds), afternoon (red squares), and night (green triangles). The DTT data were corrected for copper concentration in the sample (Section III.C). Night samples were collected for approximately twice as long (7 PM – 7 AM) as morning (7 AM – 1 PM) and afternoon samples (1 PM – 7 PM).
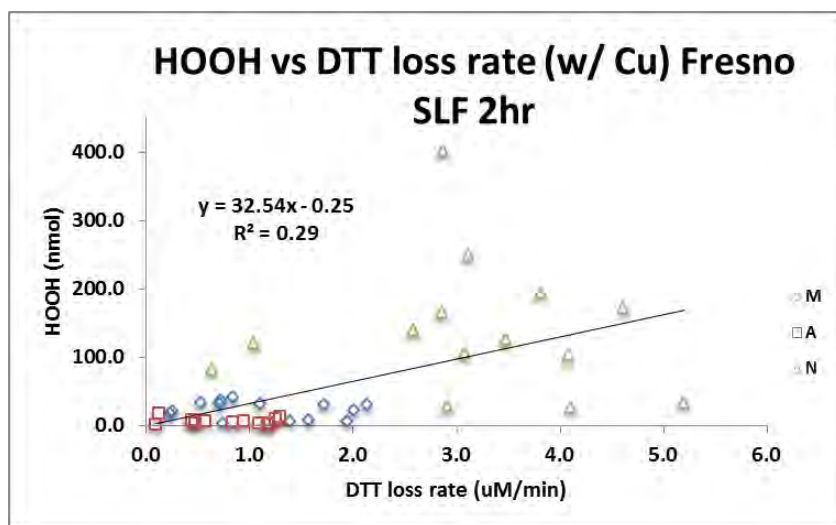
Figure 74. Correlation between DTT consumption rate and H_2O_2 concentration after 2 hours extraction in SLF for Fresno samples collected during morning (blue diamonds), afternoon (red squares), and night (green triangles). Night samples were collected for approximately twice as long (7 PM – 7 AM) as morning (7 AM – 1 PM) and afternoon samples (1 PM – 7 PM).

100

Hydrogen peroxide concentration and hydroxyl radical are essentially uncorrelated in the Claremont (Figure 75) and Fresno samples (Figure 76). However, the samples divided by time of day cluster together, with a characteristic behavior, or range of behaviors for each species.
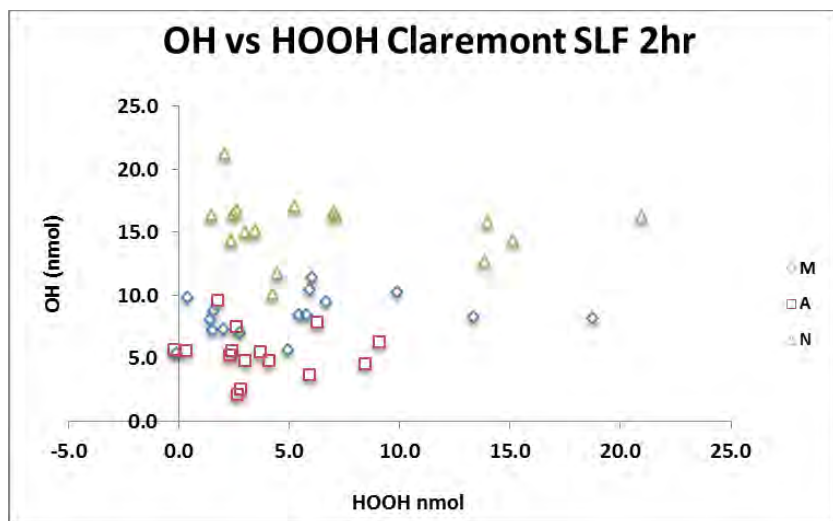
Figure 75. Correlation between •OH formation and H_2O_2 concentration after 2 hours extraction in SLF for Claremont samples collected during morning (blue diamonds), afternoon (red squares), and night (green triangles). Night samples were collected for approximately twice as long (7 PM – 7 AM) as morning (7 AM – 1 PM) and afternoon samples (1P M – 7 PM).
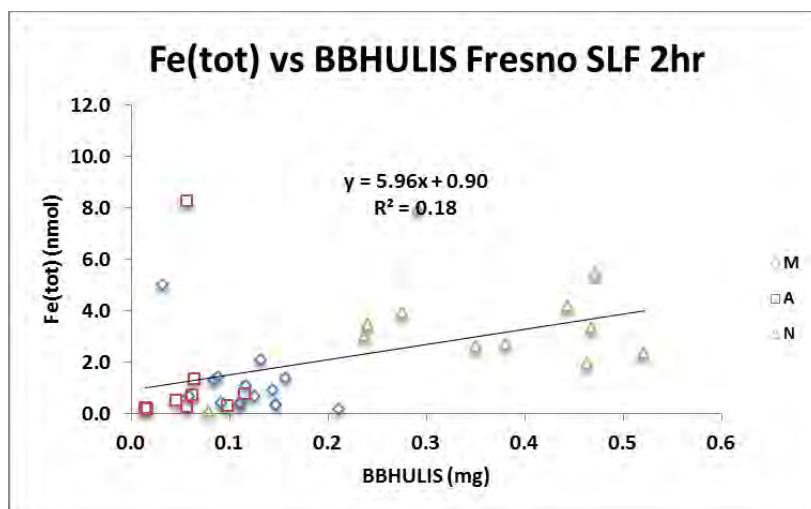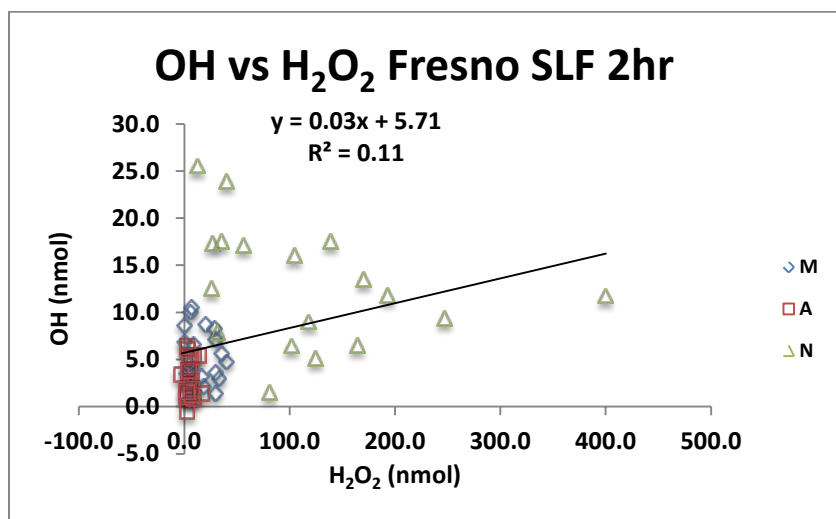

Figure 76. Correlation between •OH formation and H_2O_2 concentration after 2 hours extraction in SLF for Fresno samples collected during morning (blue diamonds), afternoon (red squares), and night (green triangles). Night samples were collected for approximately twice as long (7 PM – 7 AM) as morning (7 AM – 1 PM) and afternoon samples (1 PM – 7 PM).

H_2O_2 in Fresno (and to a lesser degree •OH) is dramatically different over the time of day; H_2O_2 has almost zero activity in the afternoon samples (Figures 78 and 79). While there is much less BBHULIS in the afternoon samples, the absorbing material is still present in significant quantities. Iron content is very low in the afternoon samples (Figure 77). Copper content is also low, but it is not as dramatically absent as is iron.
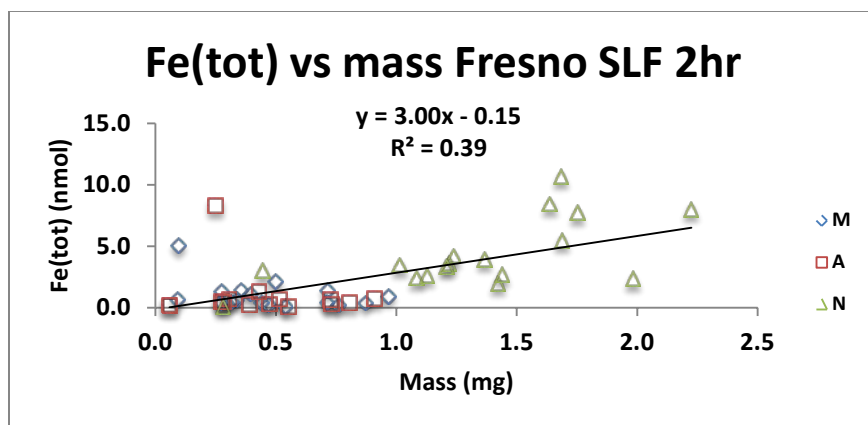
Figure 77. Correlation between aerosol mass (in the sample) and soluble iron after 2 hours extraction in SLF for Claremont samples collected during morning (blue diamonds), afternoon (red squares), and night (green triangles). Night samples were collected for approximately twice as long (7 PM – 7 AM) as morning (7 AM – 1 PM) and afternoon samples (1 PM – 7 PM).
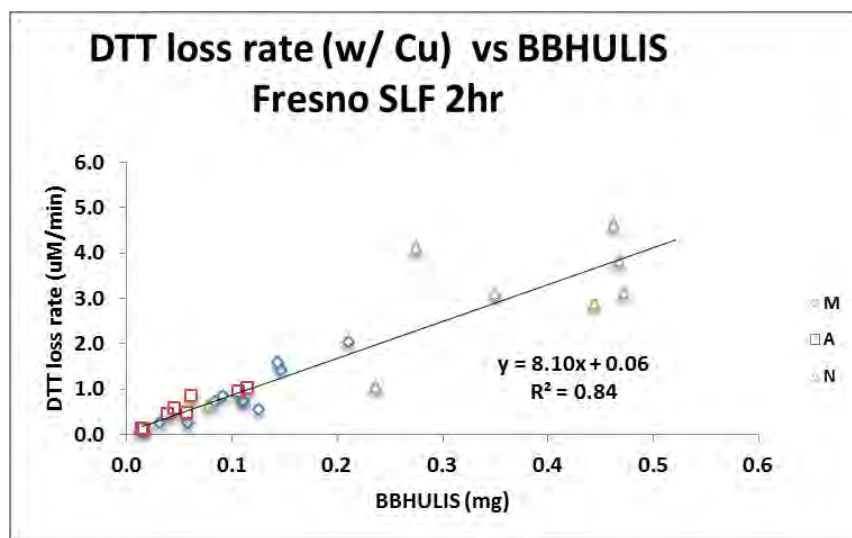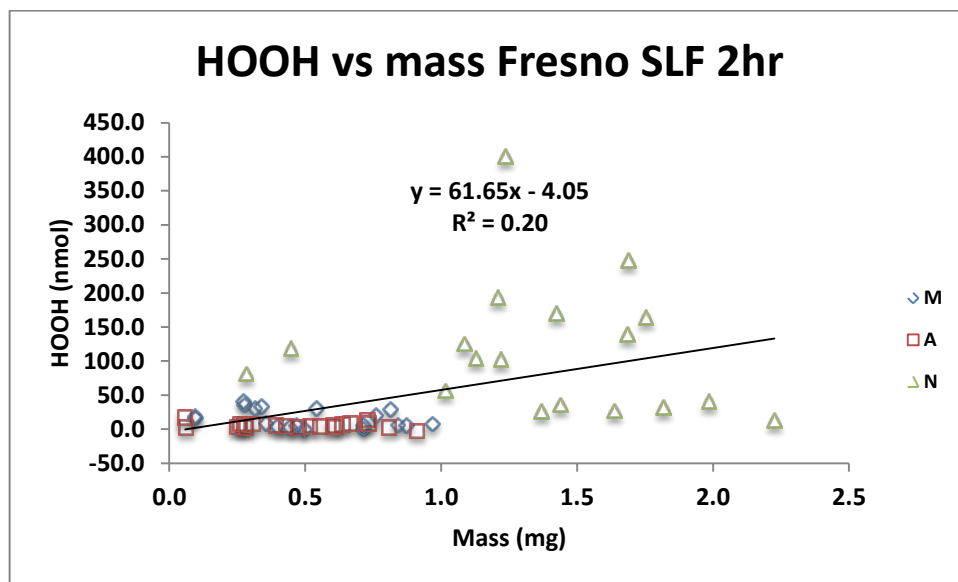

Figure 78. Correlation between aerosol mass (in the sample) and H_2O_2 formed after 2 hours extraction in SLF for Fresno samples collected during morning (blue diamonds), afternoon (red squares), and night (green triangles). Night samples were collected for approximately twice as long (7 PM – 7 AM) as morning (7 AM – 1 PM) and afternoon samples (1 PM – 7 PM).

H_2O_2 vs Fe(tot) Fresno SLF 2hr

H_2O_2 (nmol)

500.0
400.0
300.0
200.0
100.0
0.0
-100.0

Fe(tot) nmol

0.0 2.0 4.0 6.0 8.0 10.0 12.0

$y = 12.16x + 22.59$
$R^2 = 0.17$

M
A
N
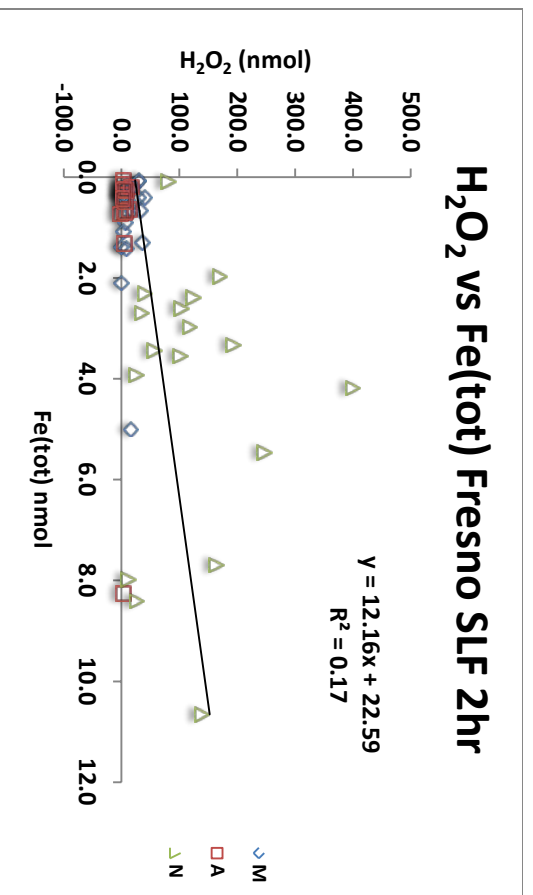
Figure 79. Correlation between aerosol mass (in the sample) and H_2O_2 formed after 2 hours extraction in SLF for Fresno samples collected during morning (blue diamonds), afternoon (red squares), and night (green triangles). Night samples were collected for approximately twice as long (7 PM – 7 AM) as morning (7 AM – 1 PM) and afternoon samples (1 PM – 7 PM).

IV.B.3.2 Temporal variation in ROS production

A striking feature of many of the ROS plots above is the low activity of the afternoon samples at both the Claremont and Fresno sites. For Fresno, •OH production is very low, and H_2O_2 production is almost zero in many afternoon samples. DTT activity is also lower in the afternoon samples. For Claremont, the variation is not quite as dramatic, but it is significant. There are several possible explanations for the behavior of H_2O_2 and •OH, including: differences in concentrations of transition metals, differences in concentrations of other redox active species such as quinones, and in the case of Claremont, addition of photochemical secondary organic aerosol, which may change the activity (presumably reducing it) of transition metals and their ability to generate ROS, and BBHULIS interactions with transition metals, particularly iron, to reduce the activity of Fe, potentially reducing its ability to destroy H_2O_2.

IV.B.3 Multivariate Correlations

Multivariate linear regressions were carried out for each of the three ROS for both field campaigns separately. Multivariate linear regression tools in Excel were used. In most cases linear regressions are appropriate and residuals do not show non-linear trends. The cases for which one or more variables exhibits significant non-linearity are noted.

Most of the independent variables (mass, metals, quinones) have at least some co-linearity, although soluble metals are trace components of aerosols, individually contributing no more than 3% of total mass and usually far less, thus they may be fairly independent of mass. Only in a few cases does the co-linearity reach the level at which it would be expected to be highly problematic (variance inflation factor, VIF >5). High VIF values tend to inflate p values and mask significance. However, many VIF values for our data are moderate, falling in the 1 – 5 range,

and the multivariate regressions exhibit signs of co-linearity as in some cases adding another partly co-linear species to a multivariate regression can substantially change the regression statistics.

Note that units for all chemicals (elements and ROS) in the multivariate regressions are nmoles in the extraction solutions, and mass is in units of mass on a whole 47mm filter collected by UCLA. This means that overnight samples typically have higher masses and concentrations in solutions as they were collected for approximately twice as long as morning or afternoon samples. The concentrations and coefficients do not correspond to mass concentrations in µg/m^3. Additionally, slight changes to some concentrations will be made to the UCLA ICP-MS concentrations due to the observation that the calibration approach need to be adjusted slightly due to some technical difficulties with the Caltech instrument used for the some of the measurements.

IV.B.3.1 Claremont Dataset

For Claremont, the complete set of data (46 samples) included in the regression was aerosol mass, V, Fe, Mn, La, and Se (UCLA ICP), Fe(II), Fe(total), Fe(III) (UCLA Ferrozine assay), Cu, Pb, V and Ni (UCD ICP). Correlations will be updated in future to include CSUF quinones, although significant single variable correlations were only found for Claremont hydrogen peroxide. Data are available for all variables most samples, although a few data are missing for most variables (unfortunately often for different samples), resulting in a complete set for 33 of the samples.

IV.B.3.2 Claremont hydroxyl radical

•OH formation is strongly correlated to several individual variables (above); thus multivariate predictions also produce strong correlations. The whole dataset consists of 46 samples, but the dataset containing all variables contains 33 samples. Regressing on the 33 points produces highly significant correlations with a large set of variables, including transition metals Cu, Mn and Fe(III) (Fe(II) and Fe(total) are also correlated but less so), each with positive coefficients, V with a negative coefficient, and the non-metal Se; each of the five variables has a p value below 0.003 and the adjusted R^2 = 0.87. Using the larger dataset of 44 samples, which requires interpolation of 10 points for Fe, produces essentially the same result but with slightly higher p values and an adjusted R^2 = 0.84. Removing Fe results in a multivariate regression involving only Se, Mn and Cu; without iron the p value for V rose to slightly above 0.05. The coefficients (accounting for average concentrations) suggest a role for Mn and Cu that is about double that of V, Fe and Se. There is no statistical evidence for a role for aerosol mass.

While five independent variables is a large number, all of the variables in this particular set are supported in their impact on ROS by other lines of evidence; laboratory data (Section III.B) shows strong •OH production activity for Cu, Mn and Fe. Se was not assessed but it has known ability to interact with transition metals as an antioxidant in biological systems, by acting as a chelating agent. Vanadium may not have any direct activity, but it may be a tracer for primary organic aerosol which may also act to moderate •OH formation, a possibility that will be further explored.

IV.B.3.3 Claremont DTT Consumption

Multivariate regressions of DTT consumption corrected for the amount of copper in the solution (Section III.C) for the Claremont samples are well-behaved. DTT is predicted well (adjusted R^2 = 0.91, Figure 80) with a combination of total soluble iron measured with Ferrozine (UCLA), soluble copper (measured with ICP by UCD) and manganese (measured with ICP by UCLA). The resulting expression is:

$$\text{DTT consumption} = 0.26 + 0.14 \times [Mn] + 0.26 \times [Fe] + 0.15 \times [Cu] \qquad \text{(R IV.1)}$$

With p values of 0.015, 5×10^{-6}, and 0.00014 for Mn, Fe and Cu respectively. For these coefficients, the average concentrations are 0.98, 1.9 and 1.8 nmoles for Mn, Fe and Cu, respectively, suggesting the contributions to DTT consumption are of similar order, but that Fe plays the largest role. DTT consumption has units of nmol/min.

DTT is even better predicted (adjusted R^2 = 0.96, Figure 80) when mass is added in combination with total soluble iron (measured with the Ferrozine assay), soluble copper and manganese (measured with ICP by UCD). The resulting expression is:

$$\text{DTT consumption} = 0.058 + 0.080 \times [Mn] + 0.105 \times [Fe] + 0.095 \times [Cu] + 1.2 \times \text{aerosol mass}$$

$$\text{(R IV.2)}$$

With p values of 0.03, 0.009, 0.0002 and 2×10^{-6} for Mn, Fe and Cu and mass respectively. The average concentrations associated with these coefficients were 0.98, 1.9 and 1.8 nmoles and 0.53 mg, suggesting the contributions to DTT consumption are similar for Fe, Cu, and Mn, with a much larger role for mass.
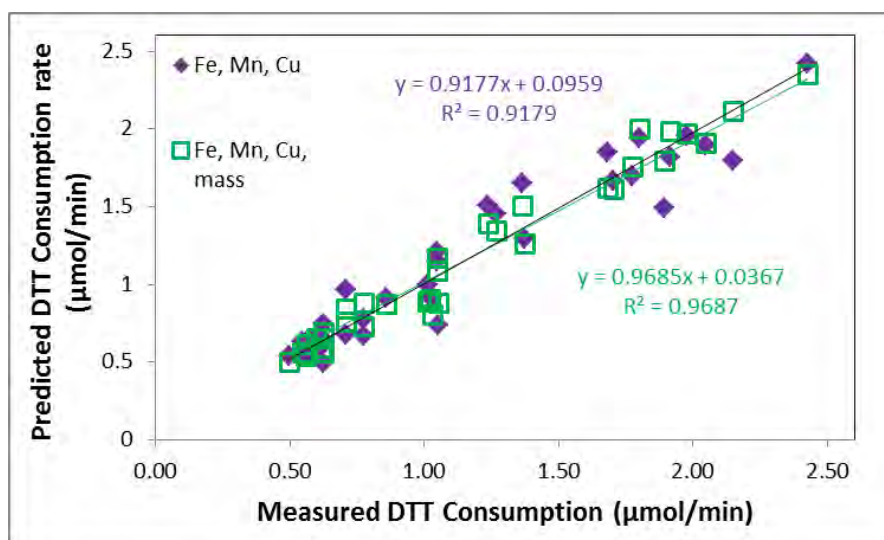
Figure 80. Measured vs. predicted DTT consumption rate vs. predicted using all predictors with p < 0.05; green included mass in the correlation, purple omitted mass.

IV.B.3.4 Claremont hydrogen peroxide

Hydrogen peroxide is much more weakly correlated with the various independent variables; single variables have correlations that generally have R^2 < 0.13 (see Figure 49). Multivariate

regressions resulted in moderately better correlations, but predictability was still weak. The only combination for resulting in all p values < 0.05 is a correlation with Cu, Mn and a large negative coefficient for La; the adjusted R^2 = 0.28.

IV.B.3.5 Fresno Dataset

For Fresno, the complete set of data included in the regression was aerosol mass, Fe, Mn, Cu, Zn and Pb (UCLA ICP), Fe(II), Fe(total), Fe(III) (UCLA Ferrozine assay), Cu, and Pb (UCD ICP). Correlations will be updated in future to include CSUF quinones, although no significant single variable correlations were found for ROS and quinones for the Fresno samples.

While the whole Fresno dataset is larger than the Claremont dataset with 59 samples, it has more gaps. Unfortunately, the CSUF hi-vol sampler stopped working about 2/3 of the way through the campaign, meaning 42 hi-vol samples were available. These were used for ICP analyses by both UCLA and UCD, as well as for the quinone samples. BBHULIS measurements were made on the UCLA filters, of and also have several gaps (18 missing data points), which unfortunately do not overlap well with missing the hi-vol data. The result of all of the gaps is that there are 21 samples with all data available.

IV.B.3.6 Fresno hydroxyl radical

Multivariate linear regressions were performed for •OH formation. Biomass burning HULIS was the most powerful predictor of •OH formation. While for the whole dataset, R^2 = 0.61, (41 points, see also Figure 63), and mass has R^2 = 0.62 (59 points, Figure 46), in a multivariate regression, BBHULIS combined with one or more of the transition metals (especially iron) or H_2O_2 were much more predictive than aerosol mass. Iron is not as strongly correlated with •OH (R^2 = 0.19 – 0.38, not shown) as was either BBHULIS or aerosol mass, but it has the pronounced feature of very low values in the afternoon samples, a feature it shares with •OH formation (e.g., Figure 77). With only iron and BBHULIS in the dataset, the dataset contains 31 samples, and addition of Fe(III) results in an adjusted R^2 = 0.74 (compared to R^2 = 0.59 for BBHULIS alone), with p values << 0.05 for both BBHULIS and Fe(III). Addition of both Fe(III) and H_2O_2 results in an adjusted R^2 = 0.84, with H_2O_2, BBHULIS and Fe(III) all highly significant. Fe(total) is also correlated, but regression statistics are best for Fe(III).

If H_2O_2 was excluded from the multivariate regression, independent variables other than BBH did not have significant correlations at the 95% confidence interval. This situation may arise because of the strong non-linearity in •OH production as well as the non-linearity of iron; multivariate nonlinear regressions might produce somewhat different relationships and will be explored in future.

IV.B.3.7 Fresno DTT consumption rate

Multivariate linear regressions were performed for DTT consumption using data both corrected (Figure 81) and uncorrected (not shown) for the non-linear response of copper discussed in section III.C. In all cases, biomass burning HULIS was the most powerful predictor of DTT behavior. In a single variable regression, it is the most strongly correlated to DTT (R^2 = 0.845, see also Figure 63 and discussion above), although other variables, such as Cu are also strongly

correlated to DTT consumption (R^2 = 0.67, see also Figure 66). Additional predictive power was obtained from either aerosol mass (adjusted R^2 = 0.88, p = 0.003 for BBHULIS and 0.004 for aerosol mass, DTT = -0.135 + 4.34 × BBHULIS +1.32 × aerosol mass) or H_2O_2 if aerosol mass was excluded from the regression (adjusted R^2 = 0.90, p = 7 × 10^{-11} for BBHULIS and 0.0007 for H_2O_2), however for H_2O_2 the coefficient was negative (DTT = -0.1135 + 11 × BBHULIS - 0.00623 × H_2O_2). No other independent variables, including Cu, Mn and Fe, had significant correlations with DTT consumption, unless BBHULIS was excluded from the correlation.
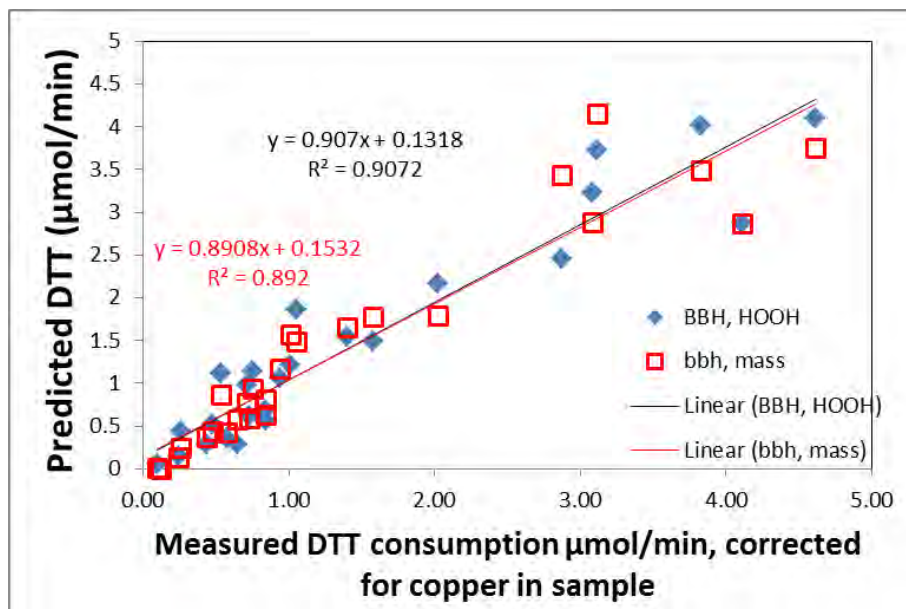
Figure 81. Result of multivariate regression for DTT consumption in the Fresno samples. Red squares indicate prediction of BBHULIS combined with aerosol mass, and blue diamonds indicate prediction of BBHULIS combined with hydrogen peroxide

IV.B.3.8 Fresno hydrogen peroxide

As for •OH formation and DTT consumption, H_2O_2 concentration (H_2O_2 is measured in steady state) is most strongly correlated to biomass burning HULIS. Unfortunately the strength of the correlation with BBH is different for the subset of the data with H_2O_2 and BBH (R^2 = 0.52, N = 39) vs. the subset of points for which all data are available (R^2 = 0.69, N = 24), and the contribution of other species also changes. In the small dataset, while other variables such as copper do improve the R^2 value somewhat (especially if several variables are included) none have p values < 0.1 when other variables are not included in the regression.

Using the larger dataset of 35 points with data for BBH, Fe(II), Fe(III) and Fe(total) measured with the Ferrozine assay, mass, BBH alone has an R^2 = 0.48; and addition of •OH results in an adjusted R^2 = 0.63, and further addition of either Fe(III) or Fe(total) further improves the relationship to yield an adjusted R^2 = 0.67 − 0.68, with p values < 0.03. In both of the latter cases the coefficient for •OH is negative, which is consistent with its formation via H_2O_2

destruction, and the coefficients for both BBH and iron are positive. The observation that copper, iron and H_2O_2 concentrations are close to zero in the afternoon samples is further evidence that these metals play a key role in H_2O_2 chemistry, although it is obviously not addressed by the multivariate regression analysis.

IV.B.3.9 Summary of Multivariate Results

The large differences in chemical composition between the Claremont and Fresno samples produce different relationships. The Claremont samples have relationships that are qualitatively consistent with laboratory results, indicating strong roles for iron, copper and manganese, in decreasing order. These three species can explain about 90% of the variability in the Claremont DTT results; in this case adding mass to the regression does improve the correlation significantly, to an R^2 of 0.96. •OH formation by the Claremont samples is related to manganese and copper, followed by iron, vanadium and selenium; potentially selenium has indirect effects by either changing chelation of the redox active species Mn, Cu and Fe (selenium) or possibly correlating with primary organic carbon which in turn also interacts with the redox active transition metals (vanadium). All five species together predict 87% of the •OH variability, and the first three 84%. Correlations with hydrogen peroxide are much weaker, however the best predictors are copper and manganese.

In all cases, the mass of biomass burning HULIS was by far the dominant variable in all multivariate regressions for the Fresno samples. In several cases, it was the only variable with a significant correlation at the $p < 0.05$ level, although dependencies on the transition metals iron and copper (for the DTT assay, but only significant with 95% confidence if other variables are included) and iron (for the •OH assay, highly significant, especially iron(III)), were evident in some cases. Predictability was high, above 84% for both DTT and •OH. As for Claremont, Fresno H_2O_2 had much weaker relationships with independent variables in the dataset.

Iron was measured by both ICP and with the Ferrozine assay. The Ferrozine assay detects iron that is available for chelation by Ferrozine, while ICP-MS detects all iron that is sufficiently soluble to pass through a 0.2 micron filter. The Ferrozine assay generally results in much lower concentrations than ICP-MS. In all cases, the Ferrozine assay results were much more strongly correlated to ROS activity. This supports the notion that chelation/complexing of transition metals in aerosols plays a significant role in the resulting ROS activity.

VI. Discussion

VI.1. Completion of goals.

The proposed goals were as follows:

VI.1.1. Methods Development

Improve Sensitivity and Accuracy for Quinone and Organic Tracer Measurements [CSUF]. A potential problem with our previous approach was the comparatively small amount of sample that is analyzed by the GC-MS (typically 5 mL). To increase the sensitivity of the technique, the GC-MS was modified to allow introduction of much larger sample volumes using a

programmed temperature vaporizing (PTV) inlet. An improvement in sensitivity was expected to be up to 2-3 orders of magnitude, and was successfully completed.

Adapt Method to Measure •OH in Ambient Aerosols [UCLA]. This was also successfully completed.

VI.1.2 Measurements: Los Angeles and Fresno, CA [UCLA, CSUF,].

1.   Field studies

Field studies were carried out at sites in Los Angeles and Fresno. The Los Angeles measurements took place in summer and were aimed at characterizing SOA as well as other local sources. The Fresno measurements took place in winter when aerosols are dominated with primary organic material, particularly from wood smoke, as well as other partially advected materials during episodic events.

2.   Simultaneous Measurements of Quinones, Elements, •OH and H_2O_2 Generation by Particles was successfully completed.

3.   Quantify the generation of •OH and H_2O_2 by individual and mixed redox-active particle components [UCD, UCLA, CSUF].

SLF composition was used to quantify the amounts of •OH and H_2O_2 that are generated by 10 common transition metals (Fe, Cu, Mn, V, Ni, Zn, Cr, Co, Pb, and Cd) and by the most reactive and/or abundant quinones present in PM. Measurements were made on individual components as well as environmentally relevant mixtures. "ROS calibration curves" (e.g., the amount of H_2O_2 or •OH generated as a function of PM component concentration) were generated to determine the contributions of individual PM components towards •OH and H_2O_2 generation in the ambient and laboratory PM samples. Additionally, non-aromatic SOA generate H_2O_2 and possibly •OH as well. This was planned to be probed by leveraging on-going SOA experiments generated by oxidizing biogenic and anthropogenic hydrocarbons with pure O_3 and high and low NO_x chemistry, with metal salt seed aerosols. Chamber experiments were not completed, however, Instead, more detailed method development was performed for •OH measurements in samples containing high levels of BBHULIS were made. Also, quantification of brown carbon BBHULIS content were added to the analyses.

4.   Probe the sources of quinones in ambient PM [CSUF].

Field measurements of quinones and organic tracers were used to evaluate the relative contributions of different sources to quinone levels.

5.   Compare ROS Generation produced directly by particles vs. that produced as a biological response to PM [UCLA, UCD, CSUF].

We planned continually to put our measurements on a basis that can be compared to ROS related measurements performed in tissues and in animals reported in the literature. We also planned perform the dithiothreitol (DTT) assay on some samples. DTT has been related to expression of heme oxygenase-1, a protein related to oxidative stress [Li et al.], and thus may be an indicator of the oxidative stress related biological response to PM. Our well-characterized ROS production from particles will provide the basis for comparisons in future, when *in vivo* and cell-based assays

109

become quantitative. DTT assay was performed on all Claremont samples and 2/3 of Fresno samples, due to filter availability.

VI.II Discussion of recent literature

The Weber group at Georgia Tech recently published several papers reporting on the DTT response of $PM_{2.5}$ collected in Atlanta and other locations in the southeast U.S. (Bates et al. 2015b; Fang et al. 2015; Verma et al. 2014). They also attempted to identify the important components using linear regressions. Correlations by Verma and co-workers (Verma et al. 2015) suggest that Cu and Mn are each important at only 3 of the 7 sample sites. For example, for the YRK-June samples, linear regressions give R values of 0.64, 0.53, and 0.11 for Mn, Fe, and Cu, respectively (Verma et al. 2015). Cu was considered insignificant in these samples since its correlation coefficient fell below the R threshold, and the authors concluded that Mn and organics each accounted for approximately half of the DTT response. However, as part of the review process for the same data in an earlier paper (Verma et al. 2014), the authors calculated the contributions of metals to measured DTT rates using the mechanistic approach with concentration-response curves from Charrier and Anastasio (Charrier and Anastasio 2012b). While the closure was sometimes poor, Cu generally dominates the DTT response, Mn is significant, and unknown components sometimes contribute. This is an inconsistent picture of the transition metal contribution to DTT loss. Overall for each of their sample sets (approximately six locations in the Southeast U.S.), Cu and Mn generally dominate DTT loss, although there are some exceptions and some samples with poor closure (http://www.atmos-chem-phys-discuss.net/14/19625/2014/acpd-14-19625-2014-AR2.pdf). Thus, while Verma and co-workers link their DTT responses to water-soluble organic compounds (WSOC), and, to a lesser extent, Mn), if the "mechanistic" approach is correct, copper may play a major role. The contrast between the results from laboratory solutions (the "mechanistic" approach) and observed field regressions in this comparison mirrors the somewhat conflicting conclusions found in this project. While the mechanistic approach is clearly helpful, the repeated contradictions with field results indicate that the lab solutions may miss important components that play a substantial role in field samples.

In conjunction with collaborators from Emory University, Georgia Tech researchers also performed historical epidemiological analyses to examine relationships between emergency department (ED) visits (for asthma/wheezing, congestive heart failure (CHF), and other endpoints) and their calculated DTT responses or measured PM2.5 masses (Bates et al. 2015b). They also compared ED visits to calculated ascorbic acid (Asc) responses, another cell-free assay of oxidative potential where the rate of Asc loss is determined in a PM extract, similar to the DTT assay (Fang et al. 2015). They found that DTT is statistically significantly associated with both asthma/wheezing and CHF, but that PM2.5 mass and Asc loss are not (Bates et al. 2015b; Fang et al. 2015). However, there appears to be enormous uncertainty in the DTT (and Asc) rates, which were not measured, but rather estimated for the 1998 – 2009 timeframe of ED data based on regressions from measured data between 2012 and 2013. The regression between measured and estimated DTT rates in the 2012-13 period was modest (R^2 = 0.45), so the determination of DTT rates in the previous decade seems highly uncertain. In addition,

there was no correction for the mass dependence of the DTT rates (which is necessary, as we discuss in this report); this increases the uncertainty. Thus while the questions the authors are addressing are important (and as-yet unanswered), we do not believe that these papers are strong evidence that the DTT assay is linked to human health effects.

This raises the question: Which cell-free assay is the best surrogate for determining ROS generation and oxidative stress *in vivo*? The available data are insufficient to answer this question, but we can give some preliminary responses. First, the relatively small amount of data indicates that the four assays (DTT, •OH, H_2O_2, and Asc) are all generally dominated by copper, with varying, often important, contributions from Mn (for DTT), Fe (for •OH), and unidentified, likely organic, species (for most of the assays). While it appears the assays give broadly similar results, more assay inter-comparisons are needed, especially for particles where ROS generation is not dominated by transition metals. Second, choosing one cell-free assay as the "best" should be based on how well it mimics in vitro or in vivo toxicity responses, but there has been very little work on this front. Thus this criterion can't currently be used. Third, the "best" cell-free assay should also be consistent with epidemiological results identifying which PM components and sources are linked to human health effects. However, as recently summarized by Adams and co-workers (Adams et al. 2015), the epidemiological results do not give a consistent picture, but instead various studies identify different sources (e.g., traffic, coal combustion, oil combustion) and components (secondary sulfate, transition metals, organic carbon) as most significant. Thus it is currently impossible to identify which assay is most strongly linked to health effects.

There is also the issue of the relevance of stored samples and the relative importance of short-lived vs. longer-lived and ROS generated in lung fluid mimic such as SLF. A recent study by Fuller et al. *[2014]* provides evidence for the rapid decay of a large quantity of relatively short-lived ROS species. Organic aerosols generated in the laboratory in oxidized organic model aerosol particles, the majority of ROS in these particles were shown to have a very short lifetime of a few minutes whereas a small fraction was stable for a day or longer (Fuller et al. 2014). This is consistent with earlier examinations of the effect of filter age on H_2O_2 concentrations (Paulson et al. 2009a). As these particles did not contain transition metals, and likely did not contain quinones, there was no direct comparison of the importance of the shorter-lived ROS with the ROS produced via re-dox cycling, so it is not possible to tell at this point the relative importance of the two types of ROS.

VII. Conclusions

While the question of which ROS-related assay (DTT, •OH investigated here, DCFH, Ascorbic Acid or another assay) is the best predictor of health effects is still an open one, the three assays investigated here (•OH, DTT and related H_2O_2 concentration) all point to a small set of aerosol components with the highest activity. All three assays used here on field samples provide strong evidence for the roles of BBHULIS where substantial amounts are present, and there are also indications that soluble iron and copper play a role. Where BBHULIS is not present at high concentrations, strong roles for copper, iron and manganese in ROS formation

are observed. More specifically, the field data indicate that in the presence of BBHULIS (the Fresno winter samples), this component is the primary controlling factor for •OH formation, DTT consumption and H_2O_2 concentration. For •OH formation, the soluble Fe(III) concentration improves the fit of BBHULIS. For DTT, none of the transition metals are statistically significant, however the data produce a better fit after they have been corrected for the non-linear response to soluble copper in the sample in the sample using the method developed in laboratory solutions. For H_2O_2, statistically significant correlations were found only for BBHULIS. For the samples without BBHULIS, transition metals Cu, Fe and Mn have dominant roles, and indeed are able to explain most of the variability in the DTT and •OH assays. For DTT, contributions from soluble copper and iron are similar, and Mn plays a smaller but significant role. For •OH, data indicate roles for soluble copper, Mn and Fe(III), as well as vanadium (a tracer for residual oil burning) and a moderating role for Se, which was present in the samples at fairly high concentrations. For H_2O_2, correlations are much weaker but Cu and Mn also make statistically significant contributions to H_2O_2 concentration. There were no statistically significant correlations with quinones observed. While strong correlations with PM mass were observed especially for the DTT assay, the transition metals or BBHULIS were stronger predictors of DTT behavior than was PM mass. This contrast was even greater for •OH and H_2O_2.

An important result from the trace metal analysis is that Fe measured by the ferrozine assay was much more strongly correlated to the ROS assays than was soluble metals measured by ICP-MS. Both total soluble Fe and Fe measured with the ferrozine assay are a fraction of the total Fe, and Fe measured with ferrozine is much smaller than total soluble metals. This further supports the notion that other components, such as organics, play a large role in transition metal activity. It further points to a need to develop a better understanding of the sources and characteristics of the small fraction of iron that is ROS active in physiologically relevant solutions.

The field data are supported by laboratory studies of individual metals, quinones and mixtures of pairs of some species in SLF. The studies provide strong evidence that copper followed by iron and manganese (depending on the assay) are the primary drivers in the three ROS assays; specifically, Cu and Mn produce most DTT activity, Fe and Cu most •OH activity, and Cu and some quinones, moderated by iron control H_2O_2 concentration. Taken together, the field and laboratory results are largely consistent with each other in the absence of significant BBHULIS, and implicate a strong role for BBHULIS where present, and a strong role for copper, as well as soluble iron and manganese.

Because of the evidence that copper plays a large role in the DTT, •OH, and (probably) H_2O_2assays, it is important that OEHHA evaluate the literature to re-assess the California reference exposure level (REL) for copper. Although the current value of 100 μg m^{-3} may be too high, it is unclear whether ambient levels (generally on the order of 0.01 μg m^{-3} and below) are toxic. If there is insufficient toxicological evidence to set a new REL, funding animal and/or epidemiology studies that can support a revised REL should be a high priority.

There are also several important unanswered questions related to the cell-free assays that we used in this work. The primary question is "How do organic species alter the reactivities of transition metals in the assays?" Based on the comparison of H_2O_2 results in the laboratory and field, it is clear that components in ambient PM extracts – likely organic species such as HULIS – are altering the reactivity of copper and/or iron in the hydrogen peroxide assay. This should be examined. For the DTT and •OH assays the differences between the calculated and measured rates based on laboratory solutions and soluble metal concentrations are smaller, suggesting that PM organics could be less important in these assays, although the dominant role of BBHULIS in the Fresno samples indicates that organics clearly can play a major role in these assays as well, and this should also be examined.

Given the paucity of data linking the cell-free assays to toxicological endpoints, it is also important that future work examine links between cell-free assays and *in vitro* – as well as *in vivo* – endpoints. Together these two types of inter-comparisons will help indicate which of the cell-free chemical assays is the most appropriate surrogate for the more difficult and expensive toxicological assays.

The findings are associated with the DTT assay for ROS generation potential. However, comparing DTT responses among samples requires a robust mass-normalized DTT result. Therefore, a technique should be developed to calculate DTT responses at a standard mass concentration. Additionally, the previous research was performed in cell-free simulated lung fluid. Follow-up research should be conducted using cellular assays. These assays could verify that the following PM components are especially toxic: copper and humic-like substances from biomass burning. Also, research should be conducted to develop a standard technique to calculate dithiothreitol (DTT) responses to standard PM concentrations, for determining the extent of ROS generation. Finally, the relationships between short-lived and longer-lived ROS produced by redox cycling should be placed on a quantitative basis and compared, so that the importance of storing filters can be assessed.

Overall, ROS and related toxicity assay-based investigations have produced results that have significant areas of overlap, as well as significant discrepancies. Given the wide range of assays and their varying sensitivities to different forms of ROS, and in some cases direct interactions with transition metals and other species, this is not surprising. Many of the discrepancies may ultimately be explained with a more fundamental and systematic approach that considers the underlying chemistry and biochemistry more directly.

These results indicate significant public health benefits may accrue from limiting emissions associated with biomass burning, and limiting the copper content in brakes. However, this is based on end-points that are not directly relatable to public health impact. Research in the above areas would enable the ARB to justify emissions regulations to greatly decrease the morbidity and mortality associated with exposure to ambient PM, in a cost-effective manner.

VIII. Acknowledgements

VII. References

Abrams, J., V. Verma, T. Fang, M. Klein, M. J. Strickland, S. E. Sarnat, H. H. Chang, J. A. Mulholland, P.E. Tolbert, and A.G. Russell (2015), Reactive Oxygen Species generation linked to sources of atmospheric particulate matter and cardiorespiratory effects, *Environ. Sci. Technol.,* 49 (22), 13605-13612.

Adams, K., Greenbaum, D. S., Shaikh, R., van Erp, A. M. and Russell, A. G. (2015). Particulate matter components, sources, and health: Systematic approaches to testing effects. *J Air Waste Manage Assoc* 65:544-558.

Alam, M. S., Delgado-Saborit, J. M., Stark, C. and Harrison, R. M. (2013). Using atmospheric measurements of PAH and quinone compounds at roadside and urban background sites to assess sources and reactivity. *Atmospheric Environment* 77:24-35.

Allen, J. O., Dookeran, N. M., Taghizadeh, K., Lafleur, A. L., Smith, K. A. and Sarofim, A. F. (1997). Measurements of Oxygenated Polycyclic Aromatic Hydrocarbons Associated with a Size-Segregated Urban Aerosol. *Environ. Sci. Technol.* 31:2064-2070.

Anastasio, C., Faust, B. C. and Allen, J. M. (1994). Aqueous phase photochemical formation of hydrogen peroxide in authentic cloud waters. *Journal of Geophysical Research, [Atmospheres]* 99:8231-8248.

Anastasio, C. and McGregor, K. G. (2001). Chemistry of fog waters in California's Central Valley: 1. In situ photoformation of hydroxyl radical and singlet molecular oxygen. *Atmos. Environ.* 35:1079–1089.

Anastasio, C. and Newberg, J. T. (2007). Sources and sinks of hydroxyl radical in sea-salt particles. *J. Geophys. Res.-Atmos.* 112.

Andreae, M. O. and Gelencser, A. (2006). Black carbon or brown carbon? The nature of light-absorbing carbonaceous aerosols. *Atmos. Chem. Phys.* 6:3131-3148.

Arellanes, C., Paulson, S. E., Fine, P. M. and Sioutas, C. (2006). Exceeding of Henry's Law by Hydrogen Peroxide Associated with Urban Aerosols. . *Envir. Sci. Tech.* :DOI: 10.1021/es0513786.

Arellanes, C. (2008). Studies of Reactive Oxygen Species Generation by Urban Particulate Matter, in *Department of Chemistry and Biochemistry*, University of California, Los Angeles, 146.

Arnott, W. P., Hamasha, K., Moosmuller, H., Sheridan, P. J. and Ogren, J. A. (2005). Towards aerosol light-absorption measurements with a 7-wavelength Aethalometer: Evaluation with a photoacoustic instrument and 3-wavelength nephelometer. *Aerosol Science And Technology* 39:17-29.

Bates, J. T., Weber, R. J., Abrams, J., Verma, V., Fang, T., Klein, M., Strickland, M., Sarnat, S. E., Chang, H. H. and Mulholland, J. A. (2015a). Reactive Oxygen Species Generation Linked to Sources of Atmospheric Particulate Matter and Cardiorespiratory Effects. *Environmental science & technology*.

Bates, J. T., Weber, R. J., Abrams, J., Verma, V., Fang, T., Klein, M., Strickland, M. J., Sarnat, S. E., Chang, H. H., Mulholland, J. A., Tolbert, P. E. and Russell, A. G. (2015b). Reactive Oxygen Species Generation Linked to Sources of Atmospheric Particulate Matter and Cardiorespiratory Effects. *Environ. Sci. Technol.* 49:13605-13612.

Brown, D., Donaldson, K., Borm, P., Schins, R., Dehnhardt, M., Gilmour, P., Jimenez, L. and Stone, V. (2004). Calcium and ROS-mediated activation of transcription factors and TNF-alpha cytokine gene expression in macrophages exposed to ultrafine particles. *Am. J. Physiol.-Lung Cell. Mol. Physiol.* 286:L344-L353.

Cao, C., Jiang, W. J., Wang, B. Y., Fang, J. H., Lang, J. D., Tian, G., Jiang, J. K. and Zhu, T. F. (2014). Inhalable Microorganisms in Beijing's PM2.5 and PM10 Pollutants during a Severe Smog Event. *Environmental Science & Technology* 48:1499-1507.

Charrier, J. G. and Anastasio, C. (2010). Impacts of antioxidants on hydroxyl radical production from individual and mixed transition metals in a surrogate lung fluid. *Atmospheric Environment*:Submitted.

Charrier, J. G. and Anastasio, C. (2011). Impacts of antioxidants on hydroxyl radical production from individual and mixed transition metals in a surrogate lung fluid. *Atmos. Environ.* 45:7555e7562.

Charrier, J. G. and Anastasio, C. (2012a). On dithiothreitol (DTT) as a measure of oxidative potential for ambient particles: evidence for the importance of soluble transition metals. *Atmos. Chem. Phys.* 12:9321-9333.

Charrier, J. G. and Anastasio, C. (2012b). On dithiothreitol (DTT) as a measure of oxidative potential for ambient particles: Evidence for the importance of soluble transition metals. *Atmos. Chem. Phys.* 12:9321-9333.

Charrier, J. G., Mcfall, A. S., Richards-Henderson, N. K. and Anastasio, C. (2014a). Hydrogen peroxide formation in a surrogate lung fluid by transition metals and quinones present in particulate matter *Environ. Sci. Technol.* 48:7010-7017.

Charrier, J. G., McFall, A. S., Richards-Henderson, N. K. and Anastasio, C. (2014b). Hydrogen Peroxide Formation in a Surrogate Lung Fluid by Transition Metals and Quinones Present in Particulate Matter. *Environmental Science & Technology* 48:7010-7017.

Charrier, J. G. and Anastasio, C. (2015). Rates of hydroxyl radical production from transition metals and quinones in a surrogate lung fluid. *Environ. Sci. Technol.* 4:9317-9325.

Charrier, J. G., Richards-Henderson, N. K., Bein, K. J., Mcfall, A. S., Wexler, A. S. and Anastasio, C. (2015). Oxidant production from source-oriented particulate matter - Part 1: Oxidative potential using the dithiothreitol (DTT) assay. *Atmos. Chem. Phys.* Accepted.

Chen, R. and Pignatello, J. J. (1997). Role of Quinone Intermediates as Electron Shuttles in Fenton and Photoassisted Fenton Oxidations of Aromatic Compounds. *Environ. Sci. Technol.* 31:2399-2406.

Chen, R. and Pignatello, J. J. (1999). Structure-activity study of electron-shuttle catalysis by quinones in the oxidation of aromatic compounds by the Fenton reaction *J. Adv. Ox. Technol.* 4:447-453.

Cho, A., Sioutas, C., Miguel, A., Kumagai, Y., Schmitz, D., Singh, M., Eiguren-Fernadez, A. and Froines, J. (2005). Redox activity of airborne particulate matter at different sites in the Los Angeles basin. *Env. Res.* 99:40-47.

Cho, A. K., DiStephano, E., You, Y., Rodriguez, C. E., Schmitz, D. A., Kumagai, Y., Miguel, A. H., Eiguren-Fernandez, A., Kobayashi, T., Avol, E. and Froines, J. R. (2004a). Determination of Four Quinones in Diesel Exhaust Particles, SRM 1649a, and Atmospheric PM2.5. *Aerosol Science and Technology* 38:68-81.

Cho, A. K., DiStephano, E., You, Y., Rodriguez, C. E., Schmitz, D. A., Kumagai, Y., Miguel, A. H., Eiguren-Fernandez, A., Kobayashi, T., Avol, E. and Froines, J. R. (2004b). Determination of Four Quinones in Diesel Exhaust Particles, SRM 1649a, and Atmospheric PM2.5. *Aerosol Sci. Technol.* 38:68-81.

Chung, M. O. Y., Muthana, S., Paluyo, R. N. and Hasson, A. S. (2005). Measurements of effective Henry's law constants for hydrogen peroxide in concentrated salt solutions. *Atmos. Environ.* 39:2981-2989.

Chung, M. Y., Lazaro, R. A., Lim, D., Jackson, J., Lyon, J., Rendulic, D. and Hasson, A. S. (2006a). Aerosol-Borne Quinones and Reactive Oxygen Species Generation by Particulate Matter Extracts. *Environ. Sci. Technol.* 40:4880-4886.

Chung, M. Y., Lazaro, R. A., Lim, D., Jackson, J., Lyon, J., Rendulic, D. and Hasson, A. S. (2006b). Aerosol-borne quinones and reactive oxygen species generation by particulate matter extracts. *Environmental Science & Technology* 40:4880-4886.

Connell, D. P., Winter, S. E., Conrad, V. B., Kim, M. and Crist, K. C. (2006). The Steubenville Comprehensive Air Monitoring Program (SCAMP): Concentrations and solubilities of $PM_{2.5}$ trace elements and their implications for source apportionment and health research. *J Air Waste Manage Assoc* 56:1750-1766.

CRPAQS (2001). California Regional Particulate Air Quality Study, California Air Resources Board.

De Vizcaya-Ruiz, A., Gutierrez-Castillo, M. E., Uribe-Ramirez, M., Cebrian, M. E., Mugica-Alvarez, V., Sepulveda, J., Rosas, I., Salinas, E., Garcia-Cuellar, C., Martinez, F., Alfaro-Moreno, E., Torres-Flores, V., Osornio-Vargas, A., Sioutas, C., Fine, P. M., Singh, M., Geller, M. D., Kuhn, T., Miguel, A. H., Eiguren-Fernandez, A., Schiestl, R. H., Reliene, R. and Froines, J. (2006). Characterization and in vitro biological effects of concentrated particulate matter from Mexico City. *Atmos. Environ.* 40:S583-S592.

Deguillaume, L., Leriche, M., Desboeufs, K., Mailhot, G., George, C. and Chaumerliac, N. (2005). Transition metals in atmospheric liquid phases: Sources, reactivity, and sensitive parameters. *Chemical Reviews* 105:3388-3431.

Delfino, R. J., Staimer, N., Tjoa, T., Gillen, D. L., Schauer, J. J. and Shafer, M. M. (2013). Airway inflammation and oxidative potential of air pollutant particles in a pediatric asthma panel. *Journal of Exposure Science and Environmental Epidemiology* 23:466-473.

Delhomme, O., Millet, M. and Herckes, P. (2008). Determination of oxygenated polycyclic aromatic hydrocarbons in atmospheric aerosol samples by liquid chromatography-tandem mass spectrometry. *Talanta* 74:703-710.

Dellinger, B., Pryor, W. A., Cueto, R., Squadrito, G. L., Hegde, V. and Deutsch, W. A. (2001). Role of free radicals in the toxicity of airborne fine particulate matter. *Chem. Res. Toxicol.* 14:1371-1377.

Dellinger, B., Lomnicki, S., Khachatryan, L., Maskos, Z., Hall, R. W., Adounkpe, J., McFerrin, C. and Truong, H. (2007). Formation and stabilization of persistent free radicals. *Proceedings of the Combustion Institute* 31:521-528.

Docherty, K. S., Wu, W., Lim, Y. B. and Ziemann, P. J. (2005). Contributions of Organic Peroxides to Secondary Aerosol Formed from Reactions of Monoterpenes with O3. *Environmental Science and Technology* 39:4049-4059.

Eiguren-Fernandez, A., Miguel, A. H., Di Stefano, E., Schmitz, D. A., Cho, A. K., Thurairatnam, S., Avol, E. L. and Froines, J. R. (2008a). Atmospheric distribution of gas- and particle-phase quinones in Southern California. *Aerosol Science and Technology* 42:854-861.

Eiguren-Fernandez, A., Miguel, A. H., Lu, R., Purvis, K., Grant, B., Mayo, P., Di Stefano, E., Cho, A. K. and Froines, J. (2008b). Atmospheric formation of 9,10-phenanthraquinone in the Los Angeles air basin. *Atmospheric Environment* 42:2312-2319.

Eiguren-Fernandez, A., Miguel, A. H., Lu, R., Purvis, K., Grant, B., Mayo, P., Di Stefano, E., Cho, A. K. and Froines, J. R. (2008c). Atmospheric formation of 9,10-phenanthraquinone in the Los Angeles air basin. *Atmos. Environ.* 42:2312-2319.

Eiguren-Fernandez, A., Shinyashiki, M., Schmitz, D. A., DiStefano, E., Hinds, W., Kumagai, Y., Cho, A. K. and Froines, J. R. (2010). Redox and electrophilic properties of vapor- and particle-phase components of ambient aerosols. *Environ. Res.* 110:207-212.

Fang, T., Verma, V., Bates, J. T., Abrams, J., Klein, M., Strickland, M. J., Sarnat, S. E., Chang, H. H., Mulholland, J. A., Tolbert, P. E., Russell, A. G. and Weber, R. J. (2015). Oxidative potential of ambient water-soluble PM2.5 measured by Dithiothreitol (DTT) and Ascorbic Acid (AA) assays in the southeastern United States: contrasts in sources and health associations. *Atm. Chem. Phys. Disc.* 15:30609–30644.

Faust, B. C. and Allen, J. M. (1992). Aqueous-phase photochemical sources of peroxyl radicals and singlet molecular oxygen in clouds and fog. *Journal of Geophysical Research, [Atmospheres]* 97:129,113-129,126.

Faust, B. C., Anastasio, C., Allen, J. M. and Arakaki, T. (1993). Aqueous-Phase Photochemical Formation of Peroxides in Authentic Cloud and Fog Waters. *Science* 260:73-75.

Faust, B. C., Powell, K., Rao, C. J. and Anastasio, C. (1997). Aqueous-phase photolysis of biacetyl (an -dicarbonyl compound): a sink for biacetyl, and a source of acetic acid, peroxyacetic acid, hydrogen peroxide, and the highly oxidizing acetylperoxyl radical in aqueous aerosols, fogs, and clouds. *Atmos. Environ.* 31:497-510.

117

Fels, M. and Junkermann, W. (1993). Occurrence of organic peroxides in air at a mountain site. *Geophys. Res. Lett.* 21:793-796.

Frank, N., Rice, J. and Tikvart, J. (2010). Optical Measurements of PM2.5 Collected on Teflon Filters to Estimate Elemental Carbon, in *Air and Waste Management Association*, U. E. OAQPS, ed., Xi'an China.

Fraser, M. P., Cass, G. R., Simoneit, B. R. T. and Rasmussen, R. A. (1998). Air Quality Model Evaluation Data for Organics. 5. C_6 - C_{22} Nonpolar and Semipolar Aromatic Compounds. *Environ. Sci. Technol.* 32:1760-1770.

Fuller, S. J., Wragg, F. P. H., Nutter, J. and Kalberer, M. (2014). Comparison of on-line and off-line methods to quantify reactive oxygen species (ROS) in atmospheric aerosols. *Atmospheric Environment* 92:97-103.

Haefliger, O. P., Bucheli, T. D. and Zenobi, R. (2000). Laser Mass Spectrometric Analysis of Organic Atmospheric Aerosols. 1. Characterization of Emission Sources. *Environ. Sci. Technol.* 34:2178-2183.

Hannigan, M. P., Cass, G. R., Penman, B. W., Crespi, C. L., Lafleur, A. L., Busby, W. F., Thilly, W. G. and Simoneit, B. R. T. (1998). Bioassay-Directed Chemical Analysis of Los Angeles Airborne Particulate Matter Using a Human Cell Mutagenicity Assay. *Environ. Sci. Technol.* 32:3502-3514.

Hansen, A. D. A., Rosen, H. and Novakov, T. (1984). The aethalometer - an instrument for the real-time measurement of optical absorption by aerosol particles. *Science of the Total Environ.* 36:191-196.

Hasson, A. S., Orzechowska, G. E. and Paulson, S. E. (2001a). Production of stabilized Criegee intermediates and peroxides in the gas phase ozonolysis of alkenes: 1. Ethene, trans-2-butene, and 2,3-dimethyl-2-butene. *J. Geophys. Res.* 106:34,131-134,142.

Hasson, A. S., Ho, A. W., Kuwata, K. T. and Paulson, S. E. (2001b). Production of stabilized Criegee intermediates in the gas phase ozonolysis of alkenes: 2. Assymetric and biogenic alkenes. *J. Geophys. Res.* 106:34,143-134,153.

Hasson, A. S. and Paulson, S. E. (2003). An Investigation of the Relationship between Gas-phase and Aerosol-borne Hydroperoxides in Urban Air. *J. Aerosol Sci.* 34: 459-468.

Heikes, B. G., Lazarus, A. L., Kok, G. L., Kunen, S. M., Gandrud, B. W., Gitlin, S. N. and Sperry, P. D. (1987). Evidence for aqueous phase hydrogen peroxide synthesis in the troposphere. *J. Geophys. Res.* 87:3045-3051.

Hellpointner, E. and Gäb, S. (1989). Detection of methyl, hydroxymethyl and hydroxyethyl hydroperoxides in air and precipitation. *Nature* 337:631-634.

Heo, J., Antkiewicz, D. S., Shafer, M. M., Perkins, D. A. K., Sioutas, C. and Schauer, J. J. (2015). Assessing the role of chemical components in cellular responses to atmospheric particle matter (PM) through chemical fractionation of PM extracts. *Analytical and Bioanalytical Chemistry* 407:5953-5963.

Hewitt, C. N. and Kok, G. L. (1991). Formation and occurrence of organic hydroperoxides in the troposphere: Laboratory and field observations. *J. Atmos. Chem.* 12:181-194.

Holm, B. A., Hudak, B. B., Keicher, L., Cavanaugh, C., Baker, R. R., Hu, P. and Matalon, S. (1991). Mechanisms of H2O2-mediated injury to type II cell surfactant metabolism and protection with PEG-catalase. *Am. J. Physiol.* 261:C751-C-757.

Hung, H. F. and Wang, C. S. (2001). Experimental determination of reactive oxygen species in Taipei aerosols. *Journal of Aerosol Science* 32:1201-1211.

Imlay, J. A. (2003). Pathways of oxidative damage. *Ann. Rev. Microbiol.* 57:395–418.

Jackson, A. V. and Hewitt, C. N. (1999). Atmospheric hydrogen peroxide and organic hydroperoxides: a review. *Crit. Rev. Env. Sci. Tech.* 29:175-228.

Jakober, C. A., Riddle, S. G., Robert, M. A., Destaillats, H., Charles, M. J., Green, P. G. and Kleeman, M. J. (2007). Quinone emissions from gasoline and diesel motor vehicles. *Environmental Science & Technology* 41:4548-4554.

Japar, S. M., Brachaczek, W. W., Gorse, R. A., Norbeck, J. M. and Pierson, W. R. (1986). THE CONTRIBUTION OF ELEMENTAL CARBON TO THE OPTICAL-PROPERTIES OF RURAL ATMOSPHERIC AEROSOLS. *Atmospheric Environment* 20:1281-1289.

Jiang, L., Dai, H., Sun, Q., Geng, C., Yang, Y., Wu, T., Zhang, X. and Zhong, L. (2010). Ambient particulate matter on DNA damage in HepG2 cells. *Toxicology and industrial health*:0748233710387001.

Jimenez, J., Cialborn, C., Larson, T., Gould, T., Kirchstetter, T. W. and Gundel, L. (2007). Loading effect correction for real-time aethalometer measurements of fresh diesel soot. *Journal of the Air & Waste Management Association* 57:868-873.

Jung, H., Guo, B., Anastasio, C. and Kennedy, I. M. (2006a). Quantitative measurements of the generation of hydroxyl radicals by soot particles in a surrogate lung fluid. *Atmos. Environ.* 40:1043-1052.

Jung, H., Guo, B., Anastasio, C. and Kennedy, I. M. (2006b). Quantitative measurements of the generation of hydroxyl radicals by soot particles in a surrogate lung fluid. *Atmos. Environ.* 40:1043-1052.

Kirchstetter, T. W. and Novakov, T. (2007). Controlled generation of black carbon particles from a diffusion flame and applications in evaluating black carbon measurement methods. *Atmospheric Environment* 41:1874-1888.

Koeber, R., Bayona, J. P. and Niessner, R. (1999). Determination of Benzo[a]pyrene Diones in Air Particulate Matter with Liquid Chromatography Mass Spectrometry. *Environ. Sci. Technol.* 33:1552-1558.

Koenig, J. Q., Larson, T. V., Hanley, Q. S., Robelledo, V., Dumler, K., Checkoway, H., Wang, S. Z., Lin, D. and Pierson, W. E. (1993). Pulmonary function changes in children associated with fine particulate matter. *Environ Res* 63:26-38.

Landreman, A. P., Shafer, M. M., Hemming, J. C., Hannigan, M. P. and Schauer, J. J. (2008). A macrophage-based method for the assessment of the reactive oxygen species (ROS) activity of atmospheric particulate matter (PM) and application to routine (daily-24 h) aerosol monitoring studies. *Aerosol Science and Technology* 42:946-957.

Lavanchy, V. M. H., Gaggeler, H. W., Nyeki, S. and Baltensperger, U. (1999). Elemental carbon (EC) and black carbon (BC) measurements with a thermal method and an aethalometer at the high-alpine research station Jungfraujoch. *Atmospheric Environment* 33:2759-2769.

Lee, M., Heikes, B. G. and O'Sullivan, D. W. (2000). Hydrogen peroxide and organic hydroperoxide in the troposphere: A review. *Atmos. Environ.* 34:3475-3494.

Li, N., Wang, M., Oberley, T. D., Sempf, J. M. and Nel, A. E. (2002). Comparison of the pro-oxidative and proinflammatory effects of organic diesel exhaust particle chemicals in bronchial epithelial cells and macrophages. *J. Immunol.* 169:4531-4541.

Li, N., Sioutas, C., Cho, A., Schmitz, D., Misra, C., Sempf, J. M., Wang, M., Oberley, T. D., Froines, J. and Nel, A. (2003). Ultrafine particulate pollutants induce oxidative stress and mitochondrial damage. *Envir. Health Perspect.* 111:455-460.

Lightfoot, P. D., Cox, R. A., Crowley, J. N., Destriau, M., Hayman, G. D., Jenkin, M. E., Moortgat, G. K. and Zabel, F. (1992). Organic peroxy radicals: kinetics, spectroscopy, and tropospheric chemistry. *Atmos. Environ.* 26A:1805-1961.

Ligocki, M. P. (1989). Measurement of the Gas/Particle Distributions of Atmospheric Organic Compounds. *Environ. Sci. Technol.* 23:75-83.

Lind, J. A. and Kok, G. L. (1986). Henry's law determination for aqueous solutions of hydrogen peroxide, methylhydroperoxide and peroxyacetic acid. See also correction in J. Geophys. Res. 99:21,119 (1994). *J. Geophys.s.* 91:7889-7895.

Liousse, C., Cachier, H. and Jennings, S. G. (1993). OPTICAL AND THERMAL MEASUREMENTS OF BLACK CARBON AEROSOL CONTENT IN DIFFERENT ENVIRONMENTS - VARIATION OF THE SPECIFIC ATTENUATION CROSS-SECTION, SIGMA (SIGMA). *Atmospheric Environment Part a-General Topics* 27:1203-1211.

Majestic, B., Schauer, J. and Shafer, M. (2007). Application of synchrotron radiation for measurement of iron red-ox speciation in atmospherically processed aerosols. *Atmospheric Chemistry and Physics* 7:2475-2487.

Marklund, S. (1971). The simultaneous determination of bis. hydroxymethyl-peroxide (BHMP), hydroxymethylhydroperoxide (HMP) and H2O2 with titanium, IV Equilibria between the peroxides and the stabilities of HMP and BHMP at physiological conditions. *Acta. Chem. Scand.* 25:3517-3531.

Marques, M. R. C., Loebenberg, R. and Almukainzi, M. (2011). Simulated Biological Fluids with Possible Application in Dissolution Testing. *Dissolution Technologies* 18:15-28.

Morio, L. A., Hooper, K. A., Brittingham, J., Li, T.-H., Gordon, R. E., Turpin, B. J. and Laskin, D. L. (2001). Tissue injury following inhalation of fine particulate matter and hydrogen peroxide is associated with altered production of inflammatory mediators and antioxidants by alveolar macrophages. *Toxicology and Appl. Pharmacology* 177:188-199.

Ntziachristos, L., Froines, J. R., Cho, A. K. and Sioutas, C. (2007). Relationship between redox activity and chemical speciation of size-fractionated particulate matter. *Particle and fibre toxicology* 4.

Oakes, M., Rastogi, N., Majestic, B. J., Shafer, M., Schauer, J. J., Edgerton, E. S. and Weber, R. J. (2010). Characterization of soluble iron in urban aerosols using near-real time data. *J. Geophys. Res.-Atmos.* 115.

Oakes, M., Weber, R. J., Lai, B., Russell, A. and Ingall, E. D. (2012). Characterization of iron speciation in urban and rural single particles using XANES spectroscopy and micro X-ray fluorescence measurements: investigating the relationship between speciation and fractional iron solubility. *Atmos. Chem. Phys.* 12:745-756.

Oosting, R. S., Bree, L. V., Iwaarden, J. F. V., Golde, L. M. G. V. and Verhoef, J. (1990). Impairment of phagocytic functions of alveolar macrophages by hydrogen peroxide. *Am. J. Physiol.* 259:L87-L-94.

Park, S. S., Hansen, A. D. A. and Cho, S. Y. (2010). Measurement of real time black carbon for investigating spot loading effects of Aethalometer data. *Atmospheric Environment* 44:1449-1455.

Paulson, S. E., Arellanes, C., Kim, H. J., Y.Wang and Curtis, D. (2009a). Particle Phase Peroxides: Concentrations, Sources, and Behavior, California Air Resources Board, 95.

Paulson, S. E., Arellanes, C. and Wang, Y. (2009b). Particle Phase Peroxides: Concentrations, Sources, and Behavior, California Air Resources Board, Sacramento, 93.

Paulson, S. E., Wang, Y. and Curtis, D. (2009c). Generation of Reactive Oxygen Species by Particles: Relationship to Cardiovascular Disease, California Air Resources Board, Sacramento, CA, 39.

Petzold, A., Kopp, C. and Niessner, R. (1997). The dependence of the specific attenuation cross-section on black carbon mass fraction and particle size. *Atmospheric Environment* 31:661-672.

Phousongphouang, P. T. and Arey, J. (2002). Rate constants for the gas-phase reactions of a series of alkylnaphthalenes with the OH radical. *Environmental Science & Technology* 36:1947-1952.

Roginsky, V., Michel, C. and Bors, W. (2000). Reactivity of Semiquinones with Ascorbate and the Ascorbate Radical as Studied by Pulse Radiolysis. *Arch. Biochem. Biophys.* 384:74-80.

Sander, R. (1999). Compilation of Henry's Law Constants for Inorganic and Organic Species of Potential Importance in Environmental Chemistry (Version 3). *http://www.mpch-mainz.mpg.de/~sander/res/henry.html*.

Sauer, F., Schuster, G., Schafer, C. and Moortgat, G. K. (1996). Determination of H2O2 and organic peroxides in cloud- and rain-water on the Kleiner Feldberg during FELDEX. *Geophys. Res. Lett.* 23:2605-2608.

Schafer, M., Schafer, C., Ewald, N., Piper, H. M. and Noll, T. (2003). Role of redox signaling in the autonomous proliferative response of endothelial cells to hypoxia. *Circulation Research* 92:1010-1015.

Schauer, J. J. and Cass, G. R. (2000). Source Apportionment of Wintertime Gas-Phase and Particle-Phase Air Pollutants Using Organic Compounds as Tracers. *Environ. Sci. Technol.* 34:1821-1832.

Schmid, O., Artaxo, P., Arnott, W. P., Chand, D., Gatti, L. V., Frank, G. P., Hoffer, A., Schnaiter, M. and Andreae, M. O. (2006). Spectral light absorption by ambient aerosols influenced by biomass burning in the Amazon Basin. I: Comparison and field calibration of absorption measurement techniques. *Atmos. Chem. Phys.* 6:3443-3462.

See, S. W., Wang, Y. H. and Balasubramanian, R. (2007). Contrasting reactive oxygen species and transition metal concentrations in combustion aerosols. *Environ. Res,* 103:317-324.

Shang, Y., Fan, L. L., Feng, J. L., Lv, S. L., Wu, M. H., Li, B. and Zang, Y. S. (2013). Genotoxic and inflammatory effects of organic extracts from traffic-related particulate matter in human lung epithelial A549 cells: The role of quinones. *Toxicology in Vitro* 27:922-931.

Shang, Y., Zhang, L., Jiang, Y. T., Li, Y. and Lu, P. (2014). Airborne quinones induce cytotoxicity and DNA damage in human lung epithelial A549 cells: The role of reactive oxygen species. *Chemosphere* 100:42-49.

Sharma, S., Brook, J. R., Cachier, H., Chow, J., Gaudenzi, A. and Lu, G. (2002). Light absorption and thermal measurements of black carbon in different regions of Canada. *J. Geophys. Res.-Atmos.* 107.

Shen, H., Barakat, A. I. and Anastasio, C. (2010). Generation of hydrogen peroxide from San Joaquin Valley particles in a cell-free solution. *Atmospheric Chemistry and Physics Discussions*:10, 21323–21356.

Shen, H., Barakat, A. I. and Anastasio, C. (2011). Generation of hydrogen peroxide from San Joaquin Valley particles in a cell-free solution. *Atmos. Chem. Phys.* 11:753-765.

Tobias, H. J., Docherty, K. S., Beving, D. E. and Ziemann, P. J. (2000). Effect of relative humidity on the chemical composition of secondary organic aerosol formed from reactions of 1-tetradecene and O3. *Envir. Sci. Technol.* 34:2116-2125.

Upadhyay, N., Clements, A., Fraser, M. and Herckes, P. (2011). Chemical speciation of PM2. 5 and PM10 in South Phoenix, AZ. *Journal of the Air & Waste Management Association* 61:302-310.

Venkatachari, P., Hopke, P. K., Grover, B. D. and Eatough, D. J. (2005). Measurement of particle-bound reactive oxygen species in Rubidoux aerosols (and Erratum). *J. Atmos. Chem.* 50, 52:49-58.

Venkatachari, P., Hopke, P. K., Brune, W. H., Ren, X. R., Lesher, R., Mao, J. Q. and Mitchel, M. (2007). Characterization of wintertime reactive oxygen species concentrations in Flushing, New York. *Aerosol Sci. Technol.* 41:97-111.

Venkatachari, P. and Hopke, P. K. (2008). Characterization of products formed in the reaction of ozone with alpha -pinene: case for organic peroxides. *Journal of Environmental Monitoring* 10:966-974.

Verma, V., Ning, Z., Cho, A. K., Schauer, J. J., Shafer, M. M. and Sioutas, C. (2009a). Redox activity of urban quasi-ultrafine particles from primary and secondary sources. *Atmos. Environ.* 43:6360-6368.

Verma, V., Polidori, A., Schauer, J. J., Shafer, M. M., Cassee, F. R. and Sioutas, C. (2009b). Physicochemical and toxicological profiles of particulate matter in Los Angeles during the October 2007 Southern California wildfires. *Environ. Sci. Technol.* 43:954-960.

Verma, V., Fang, T., Guo, H., King, L., Bates, J. T., Peltier, R. E., Edgerton, E., Russell, A. G. and Weber, R. J. (2014). Reactive oxygen species associated with water-soluble PM2.5 in the southeastern United States: spatiotemporal trends and source apportionment. *Atmos. Chem. Phys.* 14:12915-12930.

Verma, V., Fang, T., Xu, L., Peltier, R. E., Russell, A. G., Ng, N. L. and Weber, R. J. (2015). Organic Aerosols Associated with the Generation of Reactive Oxygen Species (ROS) by Water-Soluble PM2.5. *Environ. Sci. Technol.* 49:4646-4656.

Vidrio, E., Jung, H. and Anastasio, C. (2008a). Generation of hydroxyl radicals from dissolved transition metals in surrogate lung fluid solutions. *Atmos. Environ.* 42 4369-4379.

Vidrio, E., Jung, H. and C., A. (2008b). Generation of hydroxyl radicals from dissolved transition metals in surrogate lung fluid solutions. . *Atmos. Environ.* 18:4369-4379.

Vidrio, E., Phuah, C. H., Dillner, A. M. and Anastasio, C. (2009). Generation of hydroxyl radicals from ambient fine particles in a surrogate lung fluid solution. *Environ. Sci. Technol.* 43:922-927.

Virkkula, A., Makela, T., Hillamo, R., Yli-Tuomi, T., Hirsikko, A., Hameri, K. and Koponen, I. K. (2007). A simple procedure for correcting loading effects of aethalometer data. *Journal of the Air & Waste Management Association* 57:1214-1222.

Wang, L., Atkinson, R. and Arey, J. (2007). Formation of 9,10-phenanthrenequinone by atmospheric gas-phase reactions of phenanthrene. *Atmos. Environ.* 41:2025-2035.

Wang, Y., Arellanes, C., Curtis, D. and Paulson, S. E. (2010a). Concentrations and Sources of Coarse Mode Aerosol H_2O_2 in Southern California. *Env. Sci. Tech.* **44:** 4070-4075. DOI: 10.1021/es100593k.

Wang, Y., Arellanes, C., Curtis, D. B. and Paulson, S. E. (2010b). Probing the source of hydrogen peroxide associated with coarse mode aerosol particles in Southern California. *Env. Sci. Technol.* 44:4070-4075.

Wang, Y., Arellanes, C. and Paulson, S. E. (2012). Hydrogen Peroxide Associated with Ambient Fine Mode, Diesel and Biodiesel Aerosol Particles in Southern California. *Aerosol Sci. Tech.* 46:394–402.

Weingartner, E., Saathoff, H., Schnaiter, M., Streit, N., Bitnar, B. and Baltensperger, U. (2003). Absorption of light by soot particles: determination of the absorption coefficient by means of aethalometers. *Journal Of Aerosol Science* 34:1445-1463.

Wilson, N. K., McCurdy, T. R. and Chuang, J. C. (1995). Concentrations and Phase Distributions of Nitrated and Oxygenated Polycyclic Aromatic Hydrocarbons in Ambient Air. *Atmos. Environ.* 29:2575-2584.

Yassaa, N., Meklati, B. Y., Cecinato, A. and Marino, F. (2001). Organic Aerosols in Urban and Waste Landfill of Algiers Metropolitan Area: Occurrence and Sources. *Environ. Sci. Technol.* 35:306-311.

Zhou, Y. M., Zhong, C. Y., Kennedy, I. M., Leppert, V. J. and Pinkerton, K. E. (2003). Oxidative stress and NF kappa B activation in the lungs of rats: a synergistic interaction between soot and iron particles. . *Toxicol. & Applied Pharmacol.* 190:157–169.

Ziemann, P. J. (2002). Evidence for Low-Volatility Diacyl Peroxides as a Nucleating Agent and Major Component of Aerosol Formed from Reactions of O3 with Cyclohexene and Homologous Compounds. *Journal of Physical Chemistry A* 106:4390-4402.

Zuo, Y. G. and Deng, Y. W. (1997). Iron(II)-catalyzed photochemical decomposition of oxalic acid and generation of H_2O_2 in atmospheric liquid phases. *Chemosphere* 35:2051-2058.